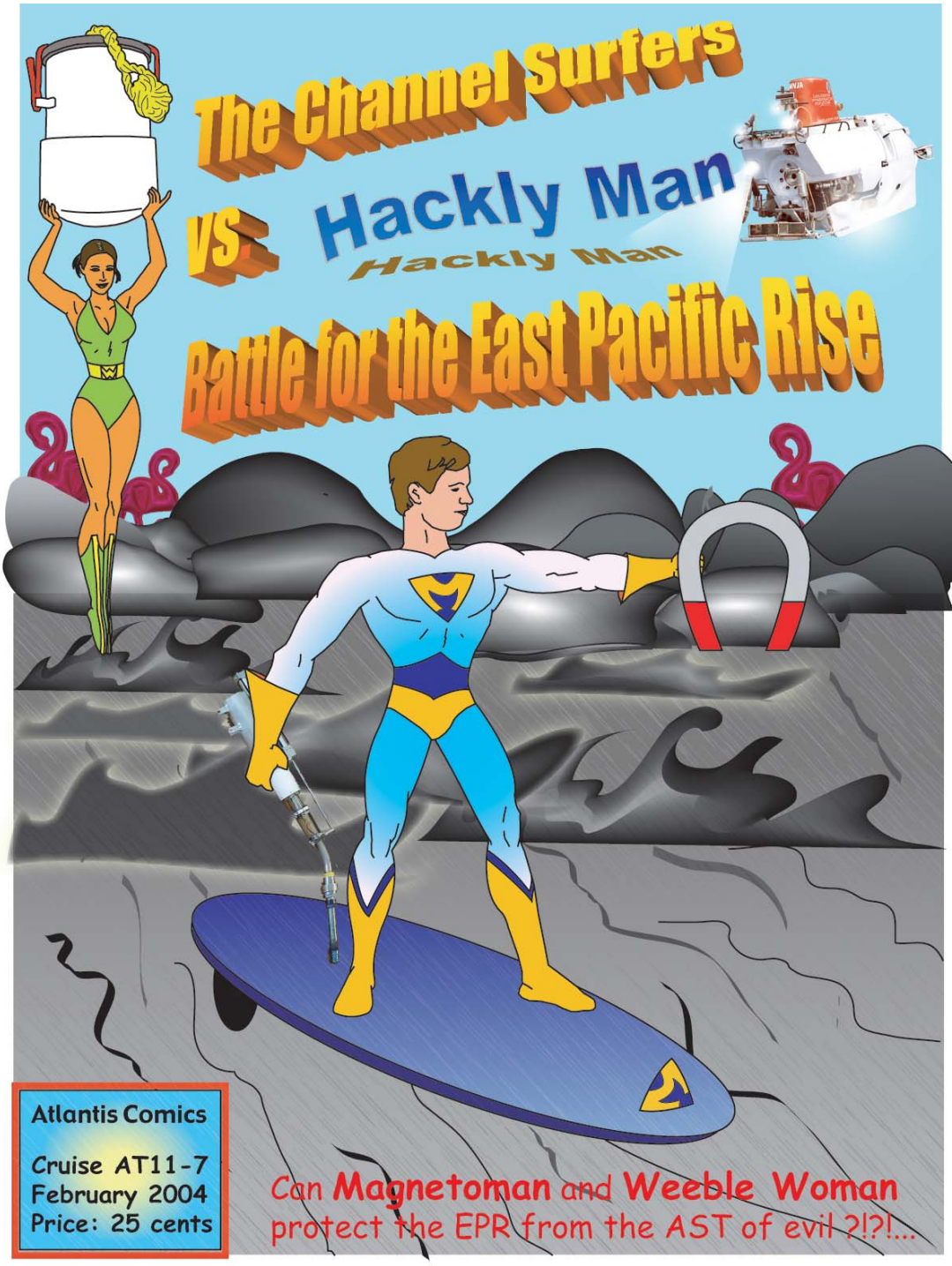
The Channel Surfers
vs.
Hackly Man
Hackly Man
Battle for the East Pacific Rise
Atlantis Comics
Cruise AT11-7
February 2004
Price: 25 cents
Can Magnetoman and Weeble Woman
protect the EPR from the AST of evil ?!?!...

Cruise Report

Atlantis/*Alvin* Voyage 11 Leg 7 (AT11-7)

San Diego, CA to Puntarenas, Costa Rica
January 26 to February 24, 2004

Hans Schouten – Chief Scientist
Maurice Tivey, Dan Fornari and Bill Seyfried – Co-Chief Scientists

March 30, 2004

1. Introduction

Two research programs were carried out during this cruise. The scientific party represents two primary research groups with extensive collaboration between many individuals from various universities and institutions (Table 1). The group from Woods Hole Oceanographic Institution (WHOI) [Schouten, Tivey, Fornari] is investigating processes related to construction of fast-spreading oceanic crust at the East Pacific Rise (EPR) in the 9° 20'-55'N area (Figure 1) using a combination of near-bottom magnetic data, side-scan sonar imagery, digital bottom photography using a towed camera system and microbathymetry acquired using the AUV ABE (Autonomous Benthic Explorer) [Yoerger et al., 1996]. The first field program for the WHOI group, conducted in November 2001, included the DSL-120A side scan sonar acquisition and ABE microbathymetry and near-bottom magnetics, and digital seafloor photography using a prototype camera system [Schouten et al., 2002; Fornari et al., in press]. The current fieldwork represents the culmination of the data acquisition effort to directly observe and sample specific seafloor sites identified in the side scan, microbathymetry and magnetics data. The second research group, from the U. of Minnesota [Seyfried and Ding] is investigating the physical chemistry of hydrothermal vent fluids and developing novel instrumentation to monitor deep-sea vents over a range of temperatures and physical conditions.

Wolfgang Bach – Woods Hole Oceanographic Institution
Stace Beaulieu – Woods Hole Oceanographic Institution
Javier Escartin – Univ. of Paris, France
Kang Ding – Univ. of Minnesota
Vicki Ferrini – SUNY-Stony Brook
Daniel Fornari – Woods Hole Oceanographic Institution, Co-Chief Scientist
Dionusios Foustoukos – Univ. of Minnesota
John Maclennan – Univ. of Edinbrough
Antoine Page – Portland State Univ.
Michael Perfit – Univ. of Florida
Ryan Perfit – Univ. of Florida
W. Ian Ridley – US Geological Survey - Denver
Yuri Rzhanov – Univ. of New Hampshire
Cara Santelli – Woods Hole Oceanographic Institution
Hans Schouten – Woods Hole Oceanographic Institution, Chief Scientist
Jeffrey Seewald – Woods Hole Oceanographic Institution
William Seyfried, Jr. – Univ. of Minnesota, Co-Chief Scientist
Kenneth Sims – Woods Hole Oceanographic Institution
S. Adam Soule – Woods Hole Oceanographic Institution
Maurice Tivey – Woods Hole Oceanographic Institution, Co-Chief Scientist
Rhian Waller – Southampton Oceanography Centre, UK
Clare Williams – Woods Hole Oceanographic Institution
Canjun Yang - Zhejiang Univ., China

Table 1. AT11-7 scientific personnel.

1.1 Central Anomaly Magnetic High and Volcanic Processes on Fast-spreading Mid-Ocean Ridges

This field and laboratory research addresses fundamental processes in the creation of young ocean crust including: volcanic accretion of ocean crust, the rapid thickening of layer 2A, and the nature of the layer 2A/B boundary. Geophysical surveys and sampling programs

were designed to investigate the relationship between the shape of the near-bottom magnetic field and the volcanic history of the mid-ocean ridge (MOR). Recent data suggest that young MOR crust evolves (thickens) rapidly and acquires its geophysical characteristics within a narrow zone along the axis. However, the identification of the processes by which upper crustal accretion takes place, i.e. by relatively focused on-axis lava deposition, or more broadly distributed lava deposition both on and off-axis, remain important questions to be resolved. Understanding how magma is supplied to the crust at a MOR and the mode of its emplacement are questions of primary importance if we are to understand the history of crustal accretion and volcanic stratigraphy. We suggested in our proposal for this work that high-resolution magnetic data offer important constraints on both the lateral and vertical dimension of crustal accretion. The map-based field data we have collected to date support this contention.

The primary hypothesis to be tested by our field and laboratory studies is that the Central Anomaly Magnetic High (CAMH), as recorded in near-bottom magnetic data, reflects both the width of the neovolcanic zone and the spatial distribution of lava emplacement on the fast spreading East Pacific Rise (EPR) between 9° and 10°N (Figure 1). The Central Anomaly Magnetization High is a zone of high crustal magnetization centered on the spreading axis of the EPR and is a common feature of many other MOR systems [Klitgord, 1976]. Near-bottom magnetic measurements of the CAMH indicate that the width of this zone is roughly 4-6 km and is not dependent on spreading rate (e.g. Tivey, 1988), which argues against an exclusively geomagnetic source for this anomaly. The CAMH is thought to reflect the presence of recently emplaced and highly magnetic lavas, which record the recent doubling of the geomagnetic field intensity from 40 kyr to the present [Guyodo and Valet, 1999]. Rapid low temperature alteration of the exrusives was originally thought to contribute to the decrease in magnetization from the present to ~ 20 kyr [Klitgord, 1976; Klitgord et al., 1975; Gee and Kent, 1994; Schouten et al., 1999]. Recent microscopic studies now reveal that alteration of magnetic grains does not occur over these short time scales suggesting that recent history of the earth's magnetic field is the primary source of the CAMH [Zhou et al., 2001]. The width of the CAMH is thus a first-order estimate of the width of the axial neovolcanic zone, and the structure of the CAMH provides important insight into the processes of upper crustal accretion at a fast-spreading MOR and its neovolcanic architecture.

The research program is located at a well-studied segment of the EPR between 9°N and 10°N [e.g. Detrick et al. 1987; Macdonald et al., 1992; Haymon et al., 1991, 1993; Harding et al., 1993; Carbotte and Macdonald, 1993; Toomey et al., 1994; Kent et al., 1993a,b; Perfit et al. 1994; Wright et al., 1995; Lee et al., 1996; Fornari et al. 1998a,b; Cochran et al., 1999; Kurras et al., 2000; Engels et al. 2003] (Figure 1). Our research is focused on two areas within this segment, 1) near 9°28'-29'N, and 2) 9°50'N. These two areas represent fast-spreading segments with contrasting styles of volcanic construction and seismic layer 2A thickening and different near-bottom magnetic character [Schouten et al., 1999].

Information on the vertical structure of ocean crust comes from seismic data collected over the study area. These data show that seismic layer 2A doubles in thickness within 1 to 2 km of the rise axis, which strongly suggests the possibility of lava deposition off-axis [Christeson et al., 1994; 1996; Hooft et al., 1996; Carbotte et al., 1992]. Because young lava is highly magnetic, off-axis lava deposition has important consequences for the magnetic character of the CAMH. Forward models show that the complicated structure of the near-bottom CAMH can be successfully reproduced by the convolution of a lava deposition distribution model convolved with a lava magnetization function that describes the variation in lava magnetization with age. The success of the forward modeling suggests that the inverse process is also possible i.e. a deconvolution of the magnetic data to infer the lava distribution, which can then be integrated for layer thickness.

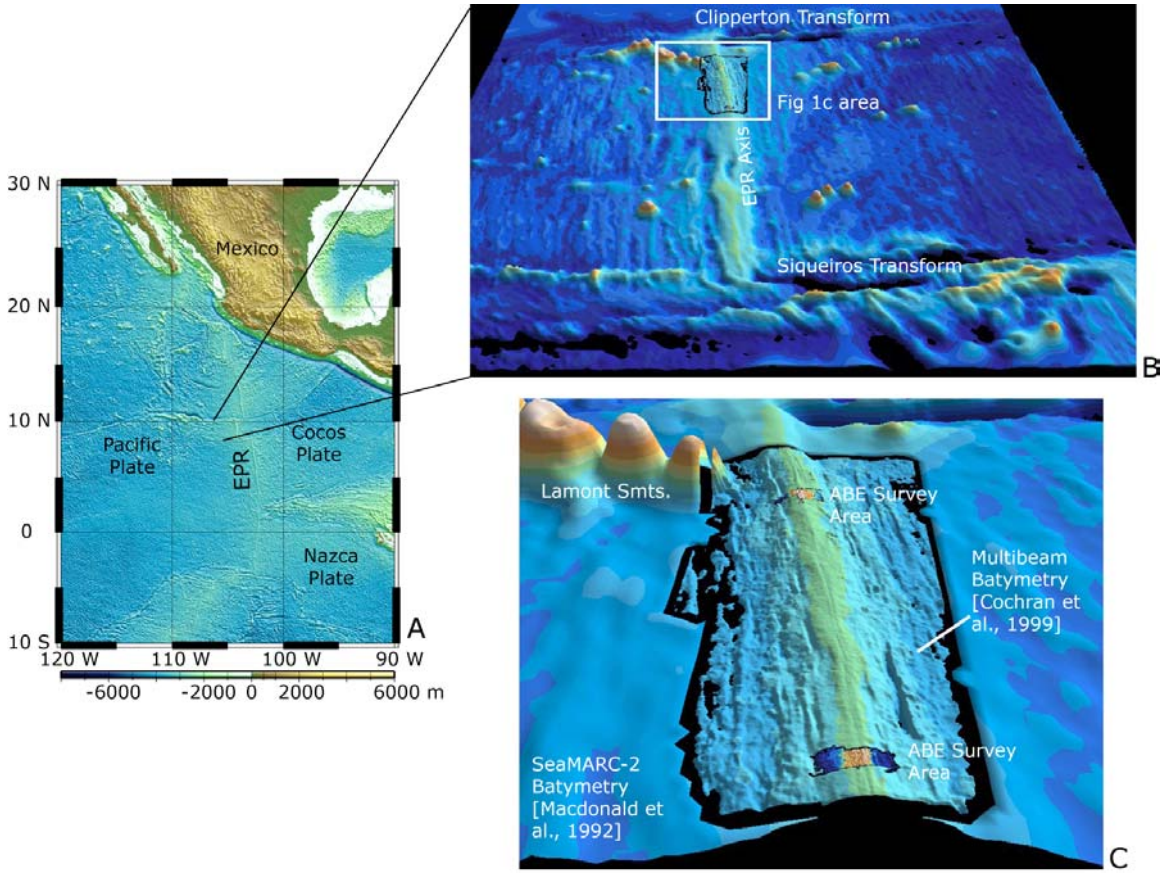

Figure 1. a) Regional location map of the eastern Pacific showing EPR axis and plate boundaries. b) Location map of the EPR based on SeaMARC2 bathymetry [*Macdonald et al.,* 1992] and multibeam sonar data [*Cochran et al.*, 1999] between the Clipperton and Siqueiros transforms. Gridded data (300 m) were visualized with Fledermaus software [http://www.ivs.unb.ca/products/fledermaus/]. c) Close-up view of area shown by white box in 1b, with multibeam data gridded at 80 m imbedded within the coarser resolution SeaMARC2 bathymetry. Multibeam data show details of axial and off-axis terrain along the EPR between ~ 9° 25'N and 9° 55'N. Inset multi-color areas are sites of ABE micro-bathymetry surveys near 9° 28'N and 9° 50'N collected on the AT7-4 cruise in 2001 and AT7-12 cruise in 2002.

This approach was initially tested using two near-bottom magnetic profiles across the EPR axis collected in 1994 using *Alvin's* magnetometer. Using those data, we were able to estimate the relative thickness of the magnetic lava layer which is remarkably consistent with existing multichannel seismic estimates of layer 2A thickness [Schouten et al., 1999]. Our primary objective for this research is to verify the presence of off-axis lava transport and depocenters through analysis of the sidescan sonar data, and to establish the correlation between the shape of the CAMH and the distribution of lava emplacement. In addition, a petrological and geochemical program is planned for the recovered basalts in order to place them within the local and regional context of geochemical variations and melting processes, and to assess the ages of the lava flows using a variety of U-series geochemical and isotopic techniques [e.g. Langmuir et al., 1986; Perfit et al., 1994; Perfit and Chadwick, 1998; Sims et al., 2003; Smith et al., 2001].

1.2. Hydrothermal Fluid Chemistry and in situ Monitoring

It is well known that redox components and pH of hydrothermal vent fluids can provide fundamental constraints on phase relations at depth in the ocean crust. Moreover, these species can also be linked to metabolic pathways of microbial communities inhabiting near vent environments, underscoring further the need to develop technologies that allow redox and pH measurement and monitoring at a wide range of temperatures and pressures. Since the discovery of deep-sea hydrothermal vents more than 25 years ago, numerous efforts have been made to determine the pH and redox components of the hot venting fluid. In almost all cases, however, this has required quenching fluid samples and then correcting for temperature and pressure using available thermodynamic data. Unfortunately, the dearth of thermodynamic data in the near-critical region of seawater have effectively precluded unambiguous interpretation of these geochemical critical parameters. Thus, hydrothermal alteration processes that control vent fluid chemistry in sub-seafloor reaction zones are difficult or impossible to interpret quantitatively. Moreover, it is becoming increasingly clear that the dynamic nature of geologic, geochemical and biologic processes at MORs can result in large changes in vent fluid chemistry during relatively short intervals underscoring the need to develop new technologies to both measure and remotely monitor key chemical components in deep-sea vent fluids. Motivated by this need, the Univ. of Minnesota group have designed and developed a series of solid-state electrochemical sensors for hydrothermal application. Lab tests using hydrothermal reactors at elevated temperatures and pressures have demonstrated the robustness and accuracy of the sensors for pH and redox determination. Moreover, in the last year we have advanced the technology from spot measurement capabilities to longer term monitoring configurations. Deployment of the chemical data-loggers at high and low temperature hydrothermal vents at EPR 9° 50'N, and comparison of the data from the loggers with the on-board chemistry of fluid samples collected by Jeff Seewald of WHOI, will allow field testing of material properties, quantification of signal response characteristics, and examination of newly designed electronics packages and system software. Although the present study permits unattended deployments for as long as approximately ten days in a variety of chemical and physical environments, the data we obtain will allow us to assess better design modifications necessary to enhance the success of even longer term monitoring studies.

1.3. Ancillary and Collaborative Studies

1.3.1. Basalt Glass Weathering and Microbial Activity

Three additional experiments/programs were accommodated during the cruise. The first concerns processes related to basalt glass weathering and microbial activity being studied by Katrina Edwards, Wolfgang Bach, Cara Santelli and Dan Rogers at WHOI. This involved deployment of groups of incubation chambers containing polished chips of basalt glass and other naturally occurring seafloor materials (sulfides, oxides, silicates) for in situ incubation studies at various locations on the EPR axis and upper flanks. The materials will be recovered during an *Alvin* cruise later in 2004 (November) and examined for initial colonization of mineral surfaces by micro-organisms. The WHOI group also were provided sub-samples of lava collected for geochemistry and U-series dating, to study the development of basalt glass alteration, the deposition of Fe-oxyhydroxides and clays, and the relation of microbial bio-films to the development of alteration fronts in seafloor lava.

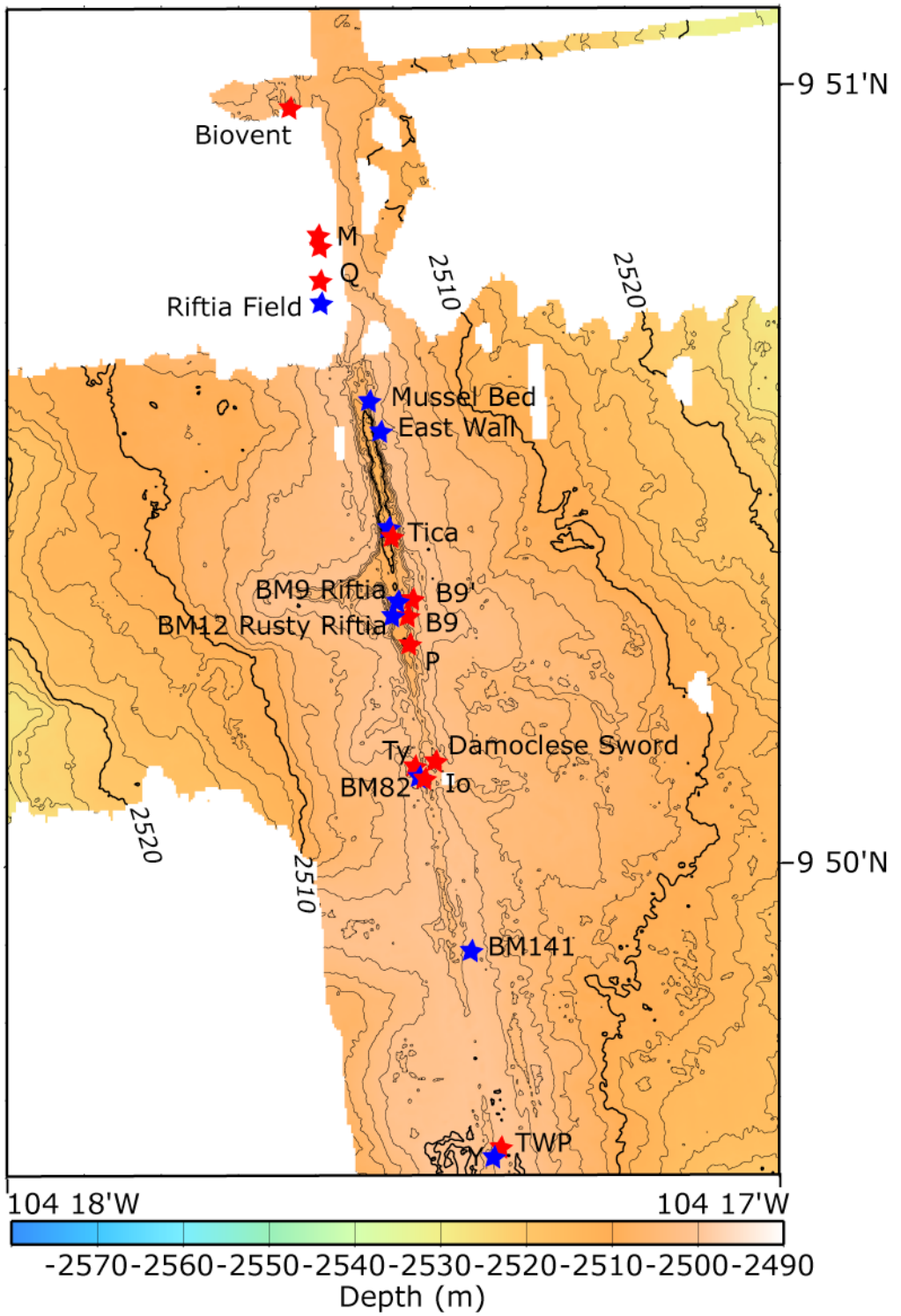

Figure 2. Microbathymetry map (2 m contour interval) derived from ABE 675 kHz scanning altimetric sonar surveys conducted on the AT7-4 cruise in Nov. 2001 [from Fornari et al., 2004]. Locations of all high- (red labels) and low-temperature (blue labels) hydrothermal vents along the EPR axis between 9° 46'-51'N are shown. *ABE* data over the study area are gridded at 5 m horizontal and contoured at 2 m.

Previous investigations revealed that the oxidation of sulfides is strongly controlled by Fe and S oxidizing microorganisms that cover the mineral surface [Edwards et al., 2003]. The

microorganisms produce bio-films to regulate the oxygen level at the mineral-water interface such they can control the kinetic rates of oxidation. This process allows the microorganisms to utilize the chemical energy associated with various weathering reactions to fuel their metabolic activities. Unlike the majority of microorganisms that thrive in surface waters of the oceans by consuming organic matter (heterotrophs), these newly discovered deep-sea microorganisms are autotrophs, i.e., they can use inorganic CO_2 as a sole carbon source. Like plants, these microorganisms are primary producers of biomass, and a significant fraction of organic carbon in the deep sea may be related to chemoautotrophic activity. Additionally, seafloor weathering of basalt releases calcium to the oceans, which reacts with CO_2 from the atmosphere to form limestone. If weathering of seafloor basalt is catalyzed by microbial activity, microorganisms could play a significant role in controlling long-term storage of CO_2 in sediments and weathered crust, which may have consequences for long-term climate regulation.

1.3.2. Basalt Colonization Panels

Hydrothermal vents provide ephemeral habitats for chemosynthetic deep-sea fauna. Biologists have long proposed that the chemical compositions of vent fluids along MORs serve as settlement cues for vent-dependent fauna; however, this hypothesis remains largely untested. In addition, microbial community composition in vent fluids and the development of microbial biofilms at vent openings would be expected to vary in response to vent fluid chemistry, and may facilitate or inhibit the settlement of invertebrate species. A major objective of the research undertaken by Stace Beaulieu, Tim Shank and Stephan Sievert of WHOI, with shipboard assistance by Rhian Waller of Southampton Oceanography Centre, is to understand biological/geochemical interactions during initial colonization of basalt at deep-sea hydrothermal vents through time-series studies that combine molecular genetic characterization of colonists and in situ measurements of fluid chemistry. One of the ancillary projects conducted during the cruise was an interdisciplinary pilot study of the microbial and invertebrate species colonization of basalt panels in conjunction with co-located, in situ, time-series detection of pH, temperature, and dissolved H_2, H_2S at a hydrothermal vent on the EPR. This study involved deploying and recovering a series of settlement panels in close proximity to the Univ. Minnesota in situ chemical sensor at Tica vent (Figure 2) for 4- to 12-day time periods. Bacterial and archaeal species diversity will be studied in developing bio-films on the panels. Small, recovered colonists that are not amenable to species identification based on morphology will be identified using molecular methods developed at WHOI. The experiment will evaluate the notion of chemical environment as a settlement cue for initial colonization of basalt. This may provide insights into how hydrothermal fluid chemistry and microbial bio-films affect larval settlement on basalt substrates, the first step in larval recruitment, and ultimately development of megafaunal assemblages at vent sites.

1.3.3. Microbiology

Four samples of high temperature chimneys were collected from three vent sites (P Vent, Bio 9', Q Vent, Figure 2). Onboard the ship, DNA was extracted from sub-samples of each chimney and PCR amplifications were conducted with primers specific to Bacteria, Archaea, and the archaeal lineage DHVE2. In addition, chimney material was collected for enrichment culturing and fixed for fluorescent in situ hybridization (FISH).

Our main objective is to describe the phylogenetic diversity within the microbial communities that colonize the sampled structures. Information obtained through this analysis will be correlated with chemistry analysis performed by the Univ. of Minnesota group. In parallel, high pressure culturing experiments will be conducted in Dr. Seyfried's lab (University of Minnesota), in an effort to obtain new isolates of interest. Samples preserved for

FISH will be analysed in Reysenbach's lab at Portland State University, using a variety of domain- and lineage-specific probes.

2. Cruise Logistics and Operational Summary

R/V Atlantis departed San Diego, CA at mid-day on Jan. 28. Departure was delayed by ~4 hours to wait for needed engineering parts for the ship's sewage system. Transit to the EPR was shorter than normal owing to following current for most of the time and good speed over the ground that averaged better than 12 knots. A short, ~3-4 hour stop was made during the third transit day to deploy the TowCam to 1500 m depth to test it, the CTD winch and new wire that was installed in San Diego, and also to test some of the remote chemical sensors that were strapped onto the TowCam frame. The tests were all successful and the transit resumed.

Diving operations commenced on Feb. 3, one day ahead of schedule, and it was decided to dive at the 9° 50'N vents to initiate the chemical sensing program of the Univ. of Minnesota group so that their time-series experiments could extend for as long a period as possible during the cruise. Navigation of that dive (D3961) used the preexisting network of two transponders located west of the EPR axis (Figure 3). Operational logistics, navigation information and locations of *Alvin* dives and camera tows during AT11-7 are detailed in Tables 2-4.

2.1. R/V Atlantis Operations

Overall, shipboard and diving operations were successful during this cruise. The night surveying consisted exclusively of camera tow work using the CTD wire. The starboard hydro-boom and the sheave block worked well with no problems. The winch had a few minor problems that were corrected quickly by the ship's engineering department and SSSG technicians. Specifically, the winch control joystick in the computer lab was not performing well (ie. sticking and with large jumps despite small movements of the stick). It was replaced with a spare that was also found to be unsatisfactory. It was finally swapped with the one in the main doghouse. Spares for the winch controls should be checked and refurbished as needed.

Other issues that came up are related to two main topics. First, the waste-line drains in the main lab and in several of the science rooms were not functioning properly. It is recommended that at the next US port stop, the drains in ALL the staterooms and the labs throughout the ship get 'roto-rooted' by a commercial outfit –so that the engineering department is not overtaxed with this chore. The ship's drainage system is poorly designed. Routine commercial cleanout of the drains every 6 months, at a minimum, should help minimize what is already a nagging problem. This should have been done in San Diego during the January in-port period. Second, the air conditioning in the main lab, hydro lab and bio-analytical lab is much too strong, with directed flow from the overhead ducts going straight onto people working at benches or desks. Two suggestions for improvement are: 1) replace the overhead ducts with louvers that direct the air outwards at the ceiling level, rather than down, and 2) install a multi-speed control on the fan so that the flow is not so strong. These two improvements would significantly improve the 'liveability' in the main lab area. The improvements made earlier to the A/C and air handling in the library and mess deck were substantial and we note that the types of ducts we suggest using were adopted in those areas. Replacing the ducts should be done immediately as it represents a relatively low cost improvement that could easily be implemented.

The ship's officers and crew provided excellent support throughout the cruise and their dedication and high level of proficiency contributed to the overall success of our field program. We thank them sincerely for their help in making our cruise a success.

2.2. Alvin Operations

Alvin operations were hampered by a variety of electrical and hydraulic problems that we believe stemmed from inadequate engineering dive time after the submarine was laid up for the January in-port period of *Atlantis*. The problems included: 1) electrical failures requiring replacement of some of the inverters, 2) problems with the Kraft manipulator, 3) connectivity problems with the ICL links to the Seewald gas-tight water samplers and chemical sensors, 4) hydraulic problems related to the port manipulator, 5) problems with the *Alvin* magnetometer- both data recording and sensor functionality (see section 3.6.1.), and 6) intermittent data from the Imagenex scanning altimeter. The *Alvin* operations group worked tirelessly to repair the problems and resume diving as soon as possible. Overall, 1 dive was lost to electrical problems and 1/2 dive lost to mechanical/hydraulic problems. An additional 1/2 dive (D3972) was considered lost in terms of key science capabilities because the ICL connector had been disconnected to the boot, thereby preventing water samples to be taken with the Seewald gas tight bottles. 1/2 dive was lost to weather (D3966).

Some additional, minor problems included grounding issues with the new Insite external digital camera and difficulty in downloading the images. The Insite camera was just installed in San Diego; this was the first science cruise to work out the bugs in it (Figure 3b). More experimentation is needed to settle on optimal acquisition parameters, especially when *Alvin* is traversing the seafloor. With the normal lighting configuration, there is usually not enough light for good imaging; the camera is set on "P" so the shutter speed is predetermined by the camera- it was often too low so many of the images are blurry. When *Alvin* is sitting on the seafloor, the images are quite good.

The group also experimented with a 1200 watt HMI light head loaned by DeepSea Power & Light (DSPL) (http://www.deepsea.com). Three 50 watt Xenon lights were also loaned to be used for observer and fill-in lights. The most significant result of the lighting tests was the vast improvement in visibility while using the 1200 watt light, without any other light turned on (see Figure 4). This light provides a dramatic improvement on the area that can be observed, even from altitudes of 5-6 m, which with the normal *Alvin* lighting is usually quite dim. The power consumption while using the 1200 watt HMI was monitored semi-quantitatively during the dive program. It was used on nearly every dive, and some dives that used the light as the only source of illumination, traversed the seafloor for ~ 2-3 km and collected as many as 10 samples and the dive time was still ~4.5 to 5 hours.

The *Alvin* Expedition Leader, *Alvin* pilots, and seagoing technical group provided excellent support throughout the cruise. Their dedication and high level of proficiency contributed to the overall success of our field program. We thank them sincerely for their help in making our cruise a success.

While one engineering dive was made off San Diego on Jan. 26, prior to the start of our cruise, it was only to ~500 m depth and was short. Some equipment was tested, but we believe that in the future several engineering dives are required to fully test all *Alvin* operational and science systems prior to commencing science operations. It has been a recurring problem over the past few years that inadequate engineering dive time has been planned for by the operator and provided for by the federal funding agencies. While the National Deep Submergence Facility (NDSF) is 'success oriented' and has a high rate of success in operating *Alvin* effectively for science with rigorous safety guidelines, we believe that in the future a more comprehensive approach to engineering dive scheduling, planning and funding should be implemented by both the operator and the funding agencies to help avoid the types of vehicle and sensor problems we experienced.

We also fully acknowledge and thank the operator and NSF for agreeing to extend the cruise by 3 days to help make up for the lost dive time. This was essential to help us meet our research objectives.

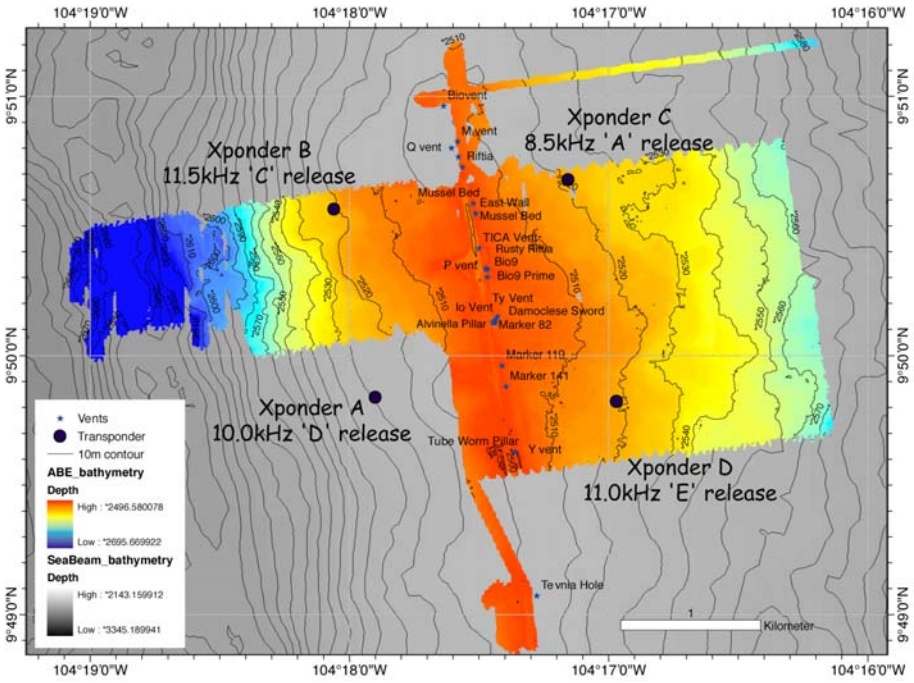

Figure 3. Map showing surveyed-in positions of acoustic transponders in the 9° 50'N area of the EPR. ABE microbathymetry in color; multibeam bathymetry in gray. See Table 2 for details of transponder locations and depths.

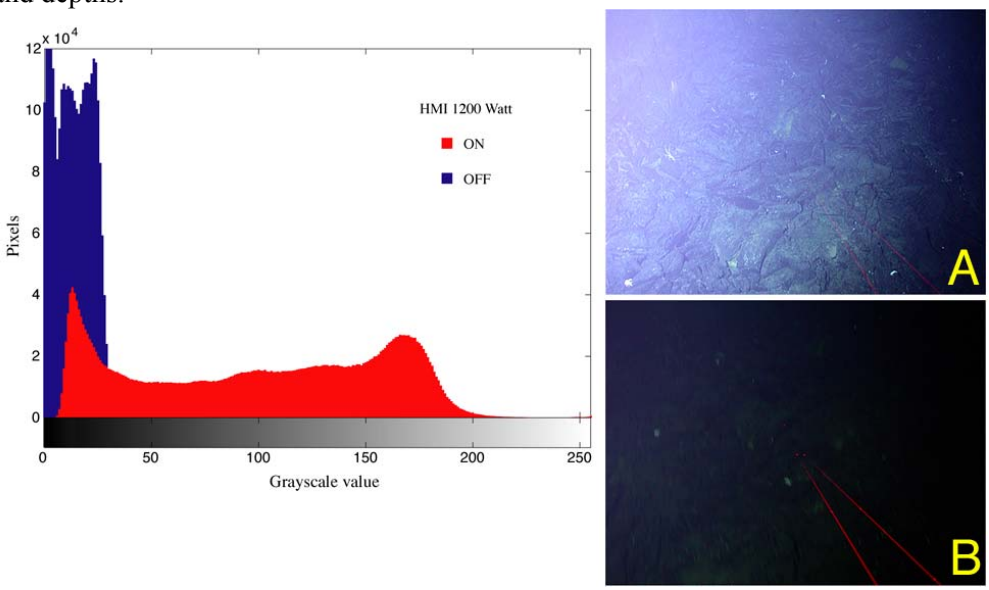

Figure 4. Plot (left) shows dramatic difference in dynamic range of images taken with the 1200 watt HMI on (red field) and off (blue field). Lighting for image when 1200 watt HMI was off was by two 400 watt HMIs as is normally used for *Alvin* traverses. Photos at right show examples of sequential *Alvin* Insite external digital camera images taken ~30 s apart during dive 3972. The 1200 watt HMI light was turned on in image A (19:21:47) and off in image B (19:21:19).

3. Shipboard Data Processing and Navigation

3.1. Alvin Long Baseline (LBL) Acoustic Navigation

Long baseline (LBL) navigation was used primarily for dives in the 9° 50'N area that utilized the ABE microbathymetry to plan the dives. Details of the transponder network and local x/y origin used are shown in Figure 4 and Tables 2-3. A full survey of all 4 transponders in the 9° 50'N permanent network resulted in small (1-4 m) shifts of the positions of the two transponders deployed in Nov. 2003 (Table 3). Dive locations are shown in Figures 5-8.

3.2. Alvin Navigation Processing

During all dives, *Alvin* navigation data were acquired using the bottom-lock Doppler navigation DVLNAV software [Whitcomb et al., 2003]. When within the network of transponders deployed near 9° 50'N, the Doppler navigation was supplemented with long baseline (LBL) acoustic navigation. When LBL was available, it was used to "renavigate" the Doppler navigation by matching the mean of the Doppler track to the mean of the LBL track (Figure 9). 'Navplot', a suite of MATLAB programs developed by D. Yoerger, L. Whitcomb, and J. Howland, which allow the user to manually remove bad LBL data points, was used to

Xpdr Freq (kHz) Xmit/Rec.	S/N	Net ID	Release Code	Latitude	Longitude (*Alvin* Y/X)	Depth (meters)
9.0/11.5	68266	A	D	9° 49.839'N (Y=77120)	104°17.900'W (X=3849)	2340m
9.0/10.0	68234	B	C	9° 50.564'N (Y=78461)	104° 18.060'W (X=3558)	2341m
(NB- 2 transponders above deployed in Nov. 2003)						
9.0/8.5	54180	C	A	9° 50.678'N (Y=78668)	104° 17.156'W (X=5210)	2335m
9.0/11.0	67311	D	E	9° 49.824'N (Y=77093)	104° 16.970'W (X=5551)	2330m

Table 2. Transponder locations surveyed during AT11-07. Corrected Positions for ABCD transponders (see Figure 4) based on a full circle survey of each transponder carried out on Feb. 3, 2004. Circle diameters were ~2 km. Origin for net is: 09° 08.0'N 104° 20.0'W. Magnetic variation is 8° East. UTM Zone 13, Time Zone +6. Survey Calculations had RMS <2m). 10.0 and 11.5 were deployed during the Voight/Von Damm/Fisher AT11-03 cruise on 9 Nov. 2003. The old transponders, released by *Alvin* and recovered in Nov. 2003, were sent to Benthos for refurbishment and to convert them to recoverable transponders. The units deployed on AT11-7 were loaned from the *Alvin* group and will be replaced with the refurbished units. The transponder drops on AT11-7 occurred on 3 Feb, 2004.

A 9.0/11.5 s/n 68266 rel D x=3848 y=77124 z=2340 November 2003
A 9.0/11.5 s/n 68266 rel D x=3849 y=77120 z=2340 February 2004
B 9.0/10.0 s/n 68234 rel C x=3554 y=78462 z=2341 November 2003
B 9.0/10.0 s/n 68234 rel C x=3558 y=78461 z=2341 February 2004

Table 3. Comparison between Nov. 2003 and Feb. 2004 surveyed positions (**bold** text) of transponders A and B in the 9° 50'N permanent transponder network. See Figure 4 for final locations.

apply the renav horizontal shift to the Doppler navigation data. This shift, usually on the order of 10s of meters, improves navigational accuracy by including LBL navigation, and compensates for drift within the Doppler navigation that occurs over the course of the dive. If LBL was not used, the raw Doppler navigation data ('*.csv' files saved by DVLNAV) were used as *Alvin* navigation. These have less absolute accuracy than LBL or LBL-Doppler 'renavigated' navigation. However, it was found that if *Alvin* was surveyed in at the start of the dive, the navigation agreed very well with the expected terrain features imaged by the side scan sonar or previously run camera tows. All *Alvin* navigation data were binned at 1Hz to create text files and MATLAB ('*.mat') files containing time, position in local XY, UTM, Lat/Lon, water depth, altitude, pitch, heading, roll and altitude. Observer transcripts for *Alvin* dives are available online at <http://www.whoi.edu/atlantis117> under 'Cruise Data'. Individual, time annotated maps for each *Alvin* dive are shown in Appendix 9.1, and in Figures 5-8.

Table 4. AT11-7 *Alvin* Dive and TowCam Operational Logistics.

Dive #	Date	Pilot/Port Obs./Stbd Obs.	Objective
TowCam#	Date	Area/Objective	
TowCam#1	Feb. 3	9° 53.55'N traverse west to east across crestal plateau to investigate eastern trough and pillow mounds	
Dive 3961	Feb. 3	Hickey/Ding/Beaulieu	Pvent/hiT sniffing Tica low-T remote sensor deployments
		Deploy 2 transponders east of EPR axis and survey-in all 4 EPR- ISS transponders in permanent net.	
TowCam#2	Feb. 4	9° 49.5'N east to west tow across off-axis scarp (east of axis) and across lava channel at AST	
Dive 3962	Feb. 4	Tarantino/Tivey/Sims	Off-axis, ~ 2km east of AST- 9° 50.5'N, flow fronts, sampling, mapping, imaging
		DIVE ABORTED	
TowCam#3	Feb. 4-5	9° 48-48.5'N traverse EPR crest for magnetic profile and to cross prominent scarp ~2km east of axis	
NO DIVE	**Feb. 5**	***Alvin* BEING REPAIRED**	
TowCam#4	Feb. 5	9° 43.5'N W-E traverse EPR crest and across the large lava flow on east side of axis	
TowCam#5	Feb. 5-6	9° 51.4'N traverse EPR crest for magnetic profile, traverse across some pillow mounds and a lava channel near AST	
Dive 3963	Feb. 6	Strickrott/Tivey/Sims	Off-axis, ~ 2km east of AST- 9° 50.5'N, flow fronts, sampling, mapping, imaging
TowCam#6	Feb. 6-7	9° 49.7'N traverse EPR crest for magnetic profile on west side of axis and then traverse back to axis near 9° 49.5'N to join up with TowCam#3 profile, also crossing some lava channels.	
Dive 3964	Feb. 7	Hickey/Seyfried/Seewald	Seyfried Dive #2
TowCam#7	Feb. 7-8	9° 37'N traverse EPR crest for magnetic profile across ridge crest. Also cross some pillow mounds	
Dive 3965	Feb. 8	Tarantino/Schouten/Ridley	Off-axis, ~2km east of AST – ~9° 49'N, fault scarp and lava flow contacts

Table 4. (continued) AT11-7 *Alvin* Dive and TowCam Operational Logistics.

Dive #	Date	Pilot/Port Obs./Stbd Obs.	Objective
TowCam#	Date		Area/Objective
TowCam#8	Feb. 8-9	9° 43.5'N - AST transition from fissure swarm to paved over new flows with very narrow, enechelon fissures representing nascent AST.	
Dive 3966	Feb. 9	Strickrott/ Perfit/Escartin	Dive #1 on large lava flow east of axis near 9° 43.5'N
DIVE CUT SHORT DUE TO WEATHER – 1.5 HRS ON BOTTOM			
TowCam#9	Feb. 9	9° 43.5'N - AST transition from fissure swarm to paved over new flows with very narrow, enechelon fissures representing nascent AST – S to N slalom track over axis fissures and flow lobes.	
Dive 3967	Feb. 10	Hickey/Tivey/Rzhanov	2nd lava flow mapping dive at 9° 43.5'N east of axis
TowCam#10	Feb. 9-10 full	9° 30'N traverse for magnetic profile across ridge crest. Also cross pillow mound on east side of axis and some lava channels.	
Dive 3968	Feb. 11	Tarantino/Fornari/Soule	9° 28'N lava channels, AST and western trough
TowCam#11	Feb. 11-12	9° 50'N lava channel - detailed survey	
Dive 3969	Feb. 12	Strickrott/Ding/PIT	
TowCam#12	Feb. 12-13	~9° 26.5'N traverse of EPR crest for magnetic profile across ridge crest. Also cross lava channels and western trough south of ABE box	
Dive 3970	Feb. 13	Hickey/Perfit/Maclennan	Off axis pillow mounds at ~9° 30'N
TowCam#13	Feb. 13-14	9° 32'N, traverse across tectonic/volcanic contacts and en-echelon fissured portion of AST	
Dive 3971	Feb. 14	Tarantino/Ding/Foustoukous	9° 50'N vent chemical sensing
TowCam#14	Feb. 14-15	9 37'N overlapper propagating tip traverses across line of pillow mounds just east of axis south of.	
Dive 3972	Feb. 15	Strickrott/Ridley/Williams	9° 43.5 lava flow, off axis, distal end of flow
TowCam#15	Feb. 15-16	9° 49-50'N traverse to fill in near bottom magnetics south of ABE survey area	
Dive 3973	Feb. 16	Hickey/Fornari/PIT	9° 28'N flow fronts west of AST
TowCam#16	Feb. 16-17	9° 51.2 'feathery' lava flow and channel and contacts with lobate flow fronts east of AST	
Dive 3974	Feb. 17	Tarantino/Perfit/PIT	9° 50'N flow fronts west of axis
TowCam#17	Feb. 17-18	9° 39'N across axis survey along CDP seismic line for magnetic profile and pillow mound samples	
Dive 3975	Feb. 18	Strickrott/Tivey/Bach	9° 28'N flow fronts west of axis
TowCam#18	Feb. 18-19	E-W transects of 'Cement Pond' east of AST near 9° 28.5'N	
Dive 3976	Feb. 19	Hickey/Ferrini/Seyfried	9° 50'N AST and lava channel mapping/imaging and chemical sensing a P and Bio9 vents
		Depart for Puntarenas, Costa Rica after dive 3976.	

3.3. Imagenex Scanning Altimeter Data Processing

Final navigation tracks for *Alvin* are shown in Figures 5-8. Appendix 9.1 contains detailed navigation and bathymetry maps for each dive track. After processing navigation data, Imagenex (675 kHz scanning altimetry) data were processed using a set of MATLAB scripts to calculate the position and corrected depth soundings for each ping ('go_vlf.m'). These

soundings ignore the effects of tidal fluctuation. The depth data were filtered using offsets declared in a filter file called 'imagenex_filter.dat'. This file dictates the maximum allowable horizontal range (10 m) and the maximum depth range (25 m) as well as the number of standard deviations (7) about the mean outside of which data are considered unacceptable. Since this method does not remove all 'bad' depth data (i.e. when incorrect depth values are reported over time periods of many seconds), an additional step was included to allow the user to remove bad depth data. This was done by plotting depth as a time series of points that can be edited by drawing rectangles around bad depth points. The final xyz data were saved into two text files in the directory with the raw Imagenex data: one in Lat/Long ('*.llz') and the other in local XY ('*.xyz'). Figure 10a shows an example of Imagenex data acquired on several dives flying at altitudes of ~3-6 m with ~ 10 m line spacing, and processed to a 1 m grid. These data provide substantial improvement over the ABE data acquired in 2001 where the AUV was flying at ~40 m altitude and with 60 m line spacing (Figure 10b).

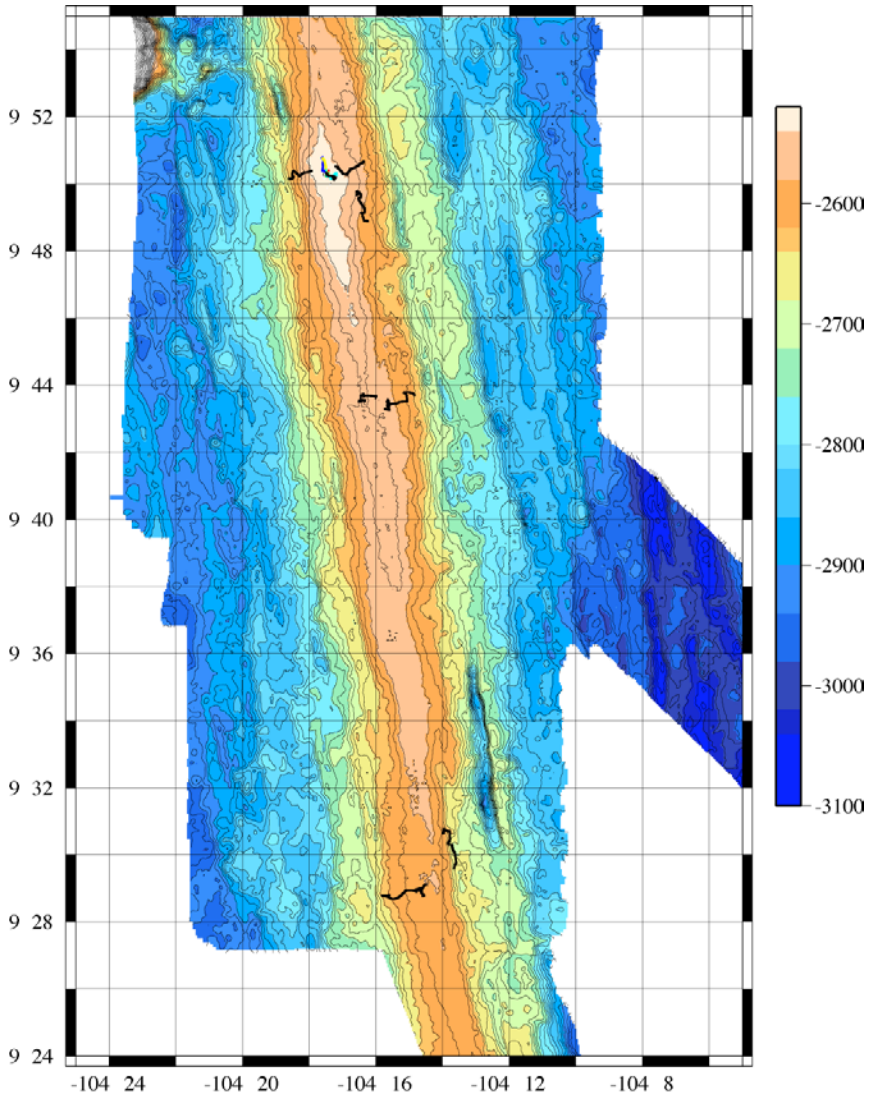

Figure 5. General location map of 15 *Alvin* dives conducted during AT11-7. Multibeam bathymetry in meters based on 80m gridded data from Cochran et al. [1999]. See Appendix 9.1 for detailed dive maps.

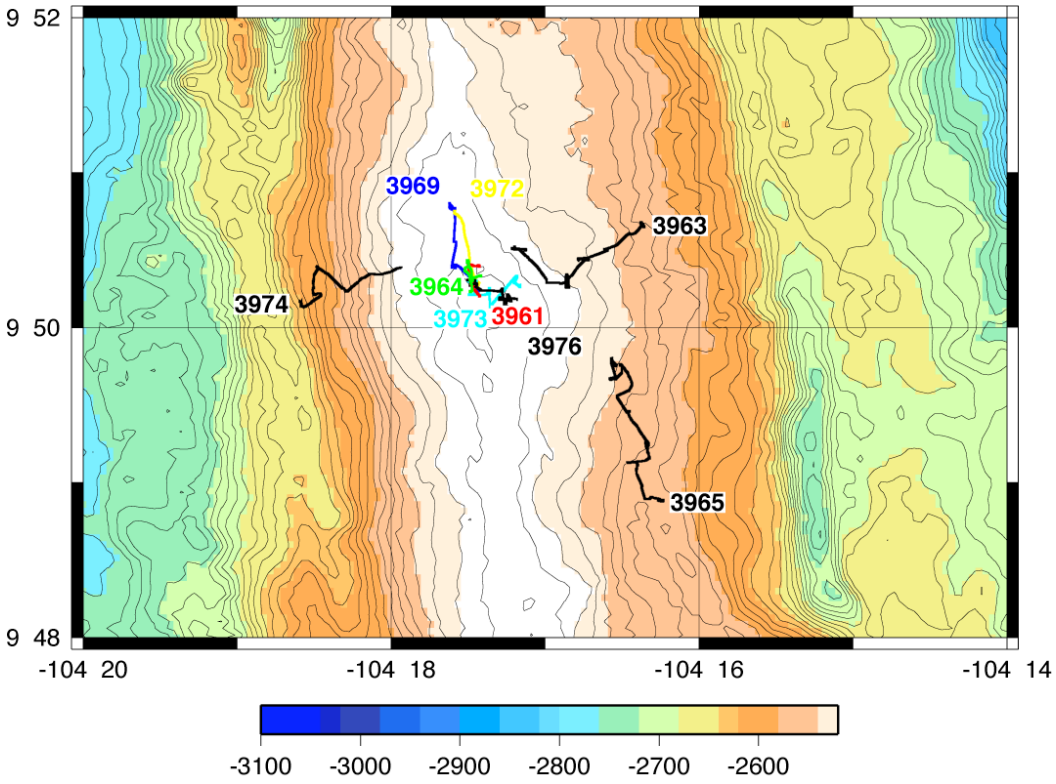

Figure 6. Location map of *Alvin* dives conducted in the 9° 50'N area during AT11-7. Multibeam bathymetry in meters based on 80m gridded data from Cochran et al. [1999].

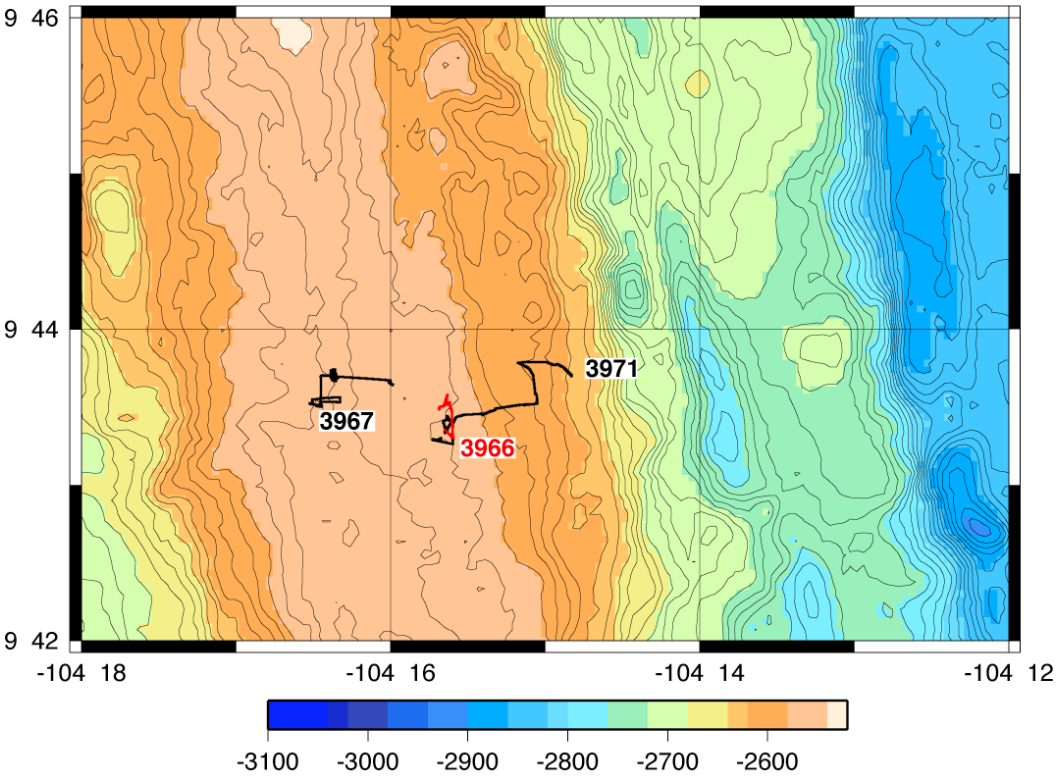

Figure 7. Location map of *Alvin* dives conducted in the 9° 43'N area during AT11-7. Multibeam bathymetry in meters based on 80m gridded data from Cochran et al. [1999].

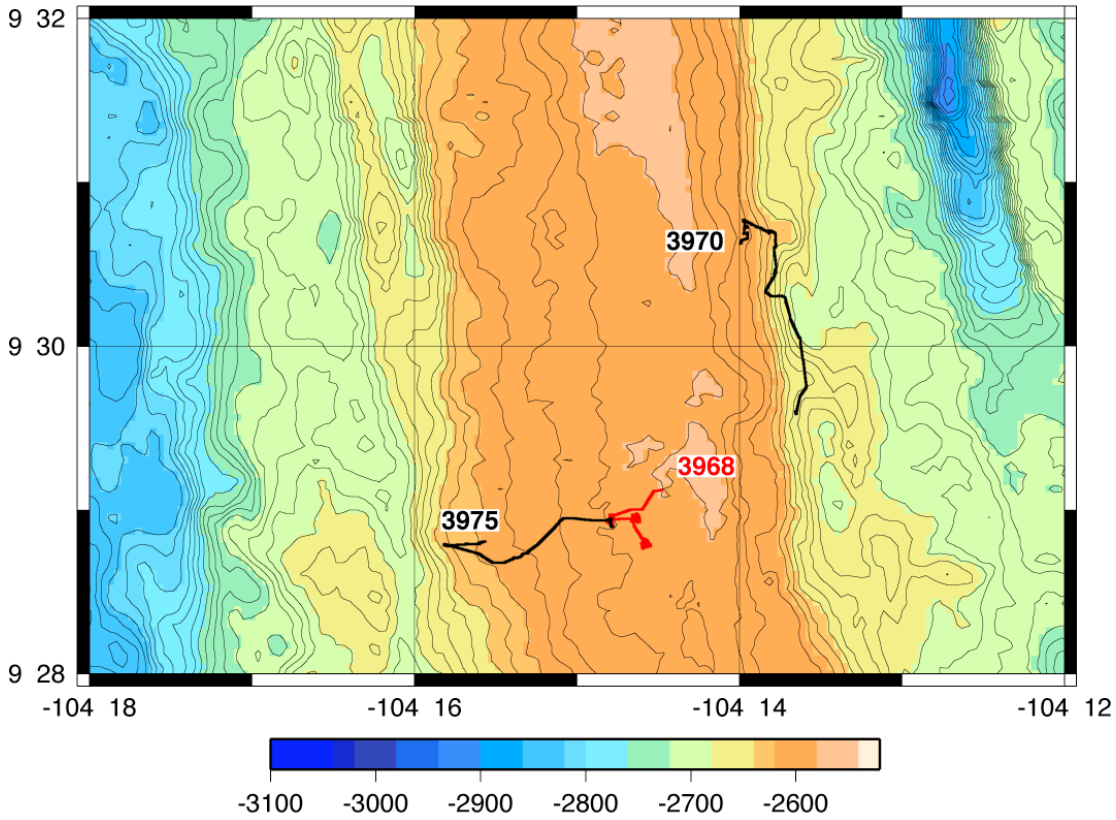

Figure 8. Location map of *Alvin* dives conducted in the 9° 28'-30'N area during AT11-7. Multibeam bathymetry in meters based on 80m gridded data from Cochran et al. [1999].

3.4. Layback Navigation for Camera Tows

Towed camera surveys were conducted with the ship using Dynamic Positioning (DP) at speeds ranging from 0.5 to 0.7 knots. Because of the generally easterly direction of the wind and seas during the cruise, the ship was usually pointed in the NE to SE quadrant to optimize operations in DP. Most of the survey lines ran from west to east across the EPR axis. However, numerous tows also had multiple lines that were run generally E-W with the starting point to the south so that the ship would not tend over the CTD wire that over-boards mid-ship on the starboard side. In many cases, during camera traverses to the west, the ship was actually pointing east under DP so that it could head into the wind/seas. In those cases, the ship's heading was ~180° different from the TowCam's actual direction of motion. Figure 11 shows the locations of all the TowCam surveys. Correlation between ship's heading and TowCam orientation based on processed magnetometer data was within $\pm$5° of course over ground. Detailed maps for each tow plotted over multibeam, ABE microbathymetry (when available) and side scan sonar are shown in Appendix 9.2.

The ship's navigation for the duration of the camera tows was extracted from the daily ship's '.dat' files. After shipboard analysis of wire out and TowCam depth during initial tows, the mean layback of the TowCam was determined to be ~250m and the position of the system behind the ship was calculated using a Perl script, 'RunLaybackNav.pl', originally written by Dan Scheirer and modified by Yuri Rzhanoz. The script requires the subroutine 'bin_dsl_data', and outputs both the ship location and the layback location at a sampling rate of 0.067Hz (every 15 seconds) for this cruise. The sampling rate can be changed as desired but the '.dat' file for this cruise has a sampling rate of ~0.1Hz.

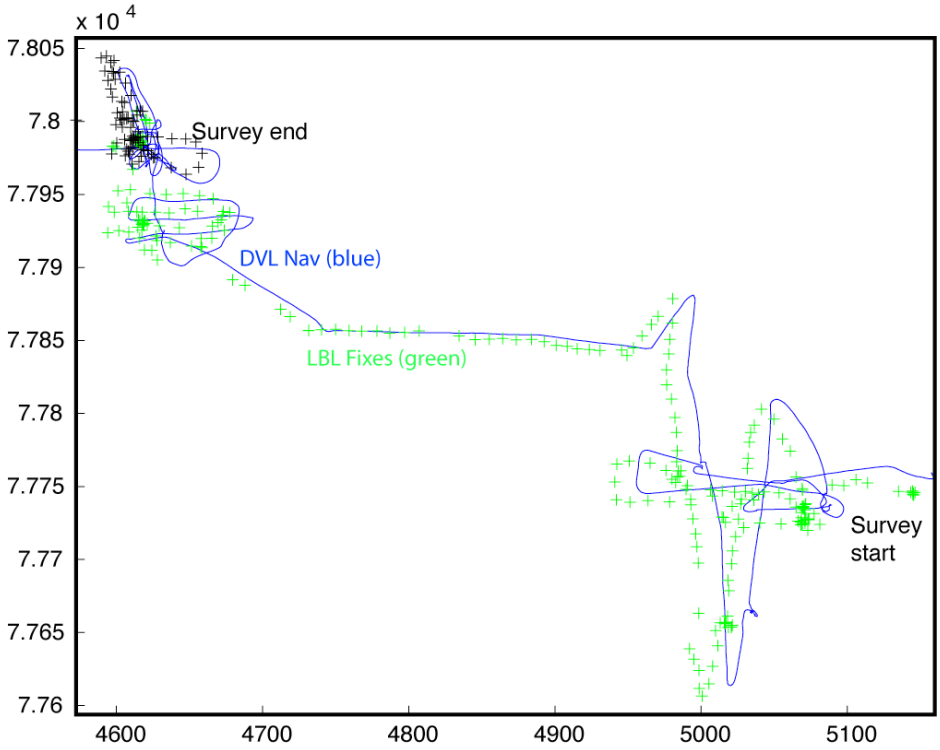

Figure 9a. Example plot showing *Alvin* LBL (green) and DVL (blue) navigation data for dive 3976.

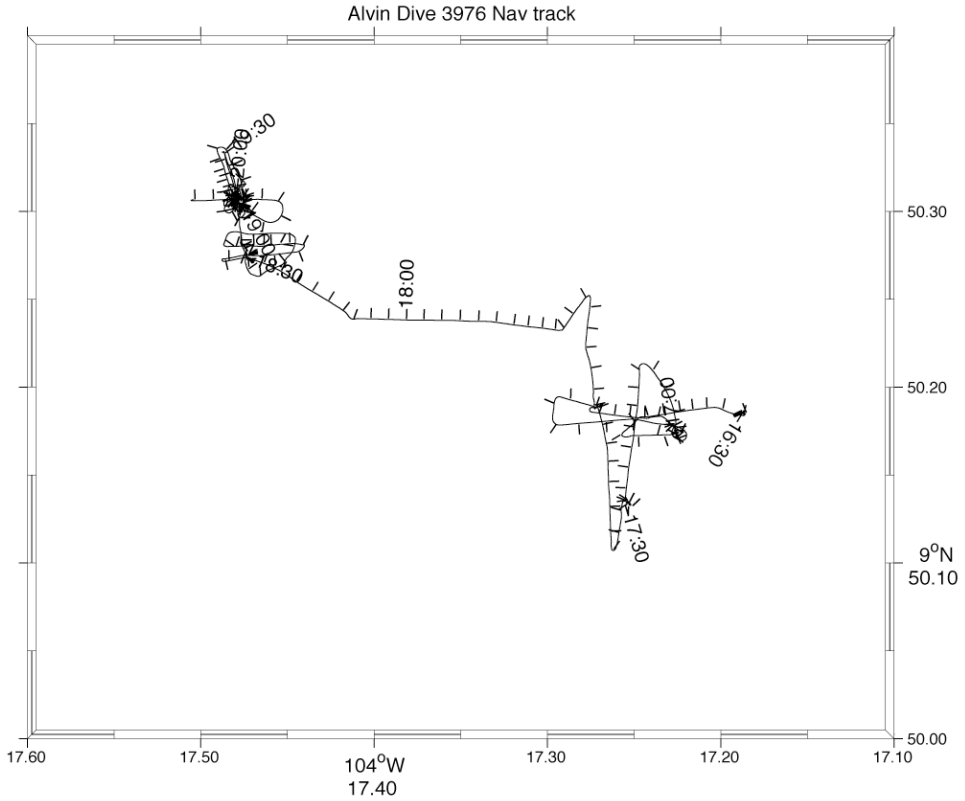

Figure 9b. Example plot showing final re-navigated and merged *Alvin* LBL and DVL data for dive 3976.

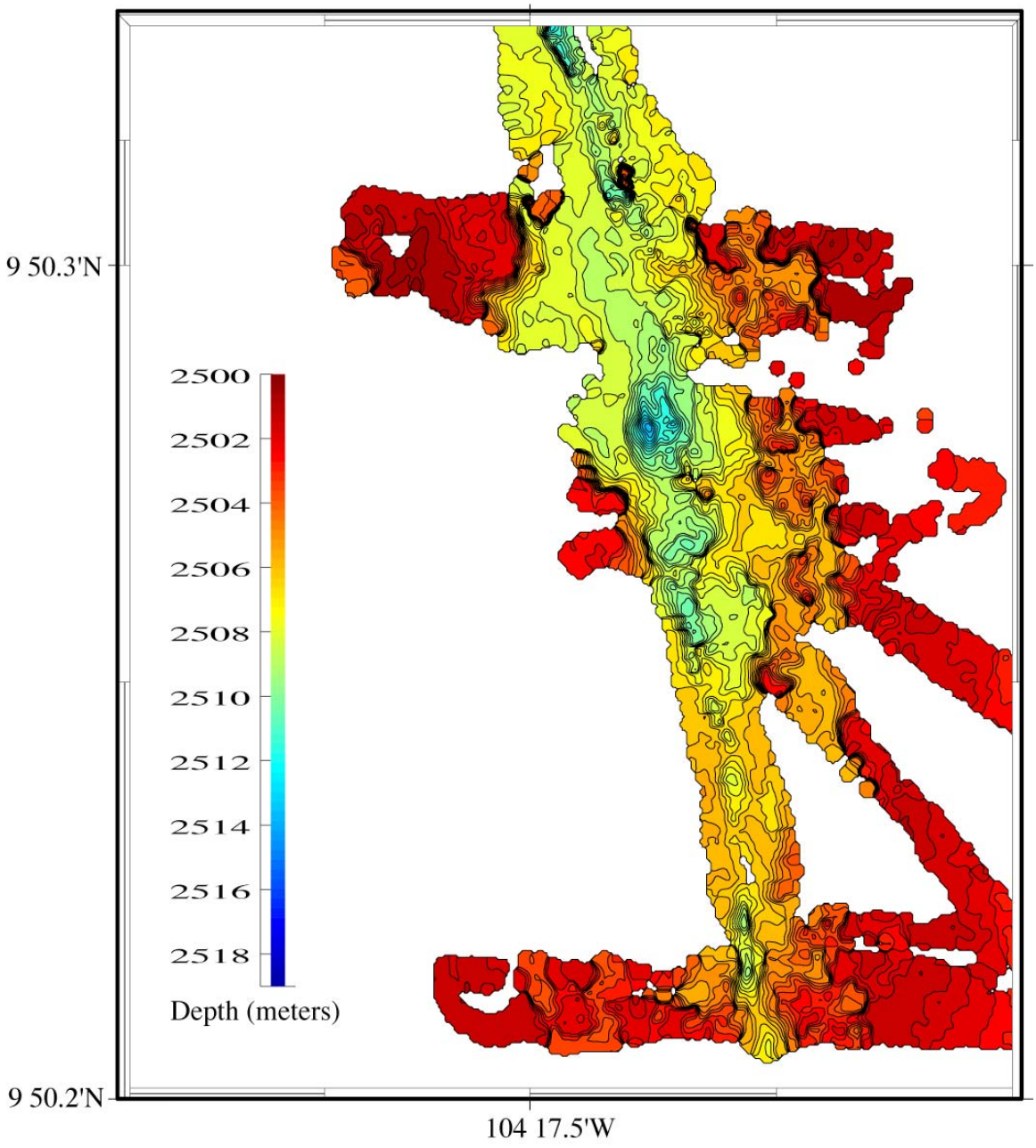

Figure 10a. Imagenex micro-bathymetry acquired on primarily 3 dives that traversed and mapped the AST in the 9° 50'N area. Data are gridded at 1 m and contoured at 0.5 m.

The Matlab script 'Interppos', written by Clare Williams, was used to perform a linear interpolation on the layback navigation to produce a layback latitude and longitude for each of the CTD (sampling rate 1Hz), magnetic (sampling rate 1Hz) and flash (sampling rate either 0.067-0.1Hz) data points. The script also checks for any altitude data >30m or unreasonable latitude/longitude values and replaces them with NaN's. Layback latitude and longitude were added to the original CTD ('ct**ctd.dat'), mag ('ct**mag.dat') and flash ('ct**flash.dat') files as the last two columns of data. Latitude, longitude, depth and altitude from the CTD data are

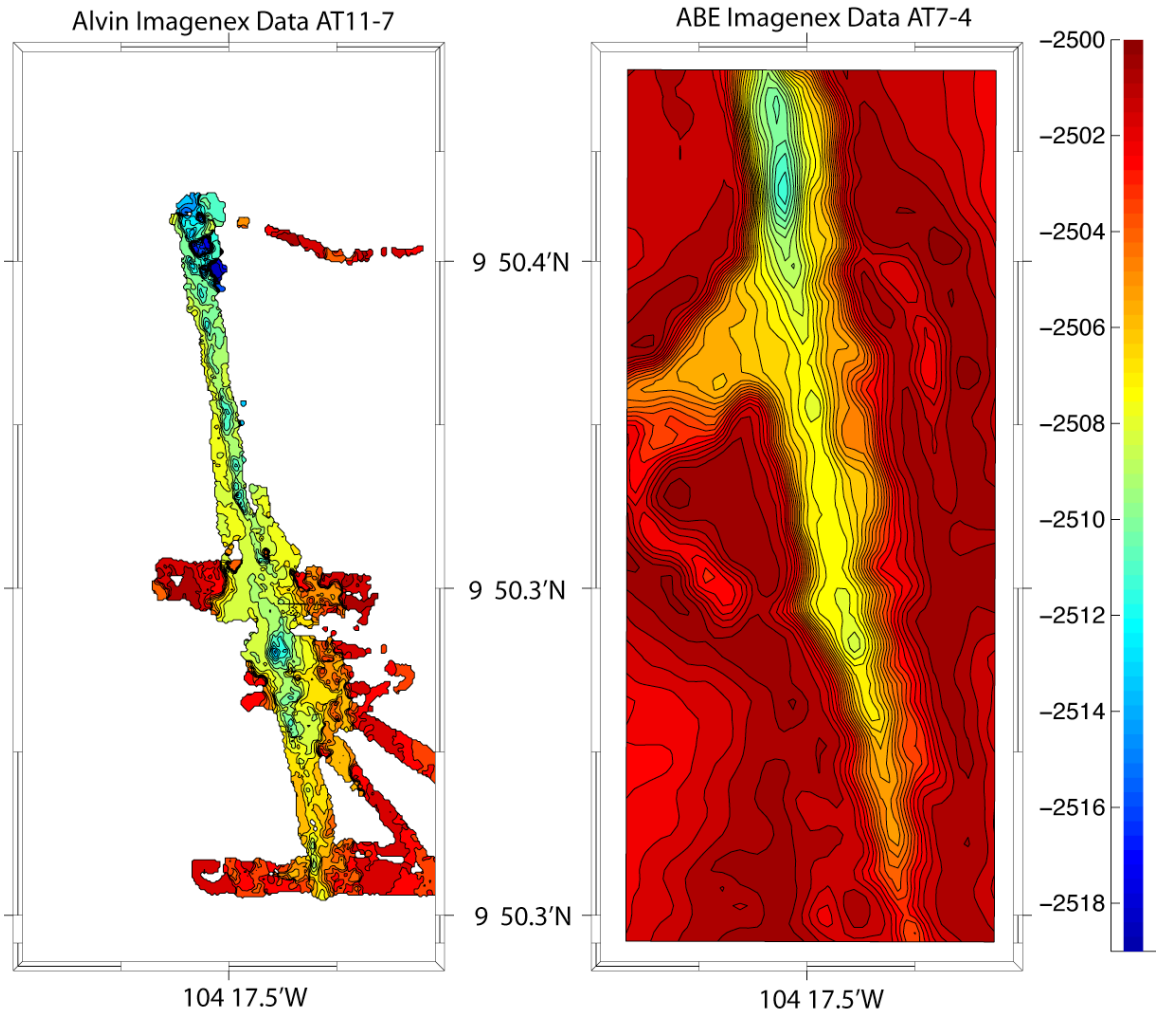

Figure 10b. Comparison between 5m gridded Imagenex micro-bathymetry data collected by ABE on the AT7-4 cruise in 2001 and *Alvin* Imagenex data collected on this cruise (Figure 10a) over the AST in the 9° 50'N area.

also added to the magnetic data files. A 'readme.txt' file is included in the digital data for the Camera Tows that identifies the headers for each type of data. The headers are shown below in Table 5. The layback locations of the wax core balls were extracted based on the time of their deployment. A navigation file 'ct**nav.dat' contains time, and both ship position and layback position at a sampling rate of 0.067Hz (15 seconds) for the duration of the camera tow.

Ship's navigation problems experienced during the cruise were minor. During Tow 2 the ship lost GPS navigation around 07:30Z and wandered off course, to the south. During Tow18 the GPS used for the logged navigation '.dat file' failed around 7:20Z. The ship did not go off course and the data gap was filled by linear interpolation.

3.5. TowCam Vehicle Data

The WHOI TowCam (Figure 12) employs a Seabird SBE25 CTD to acquire and record depth and altitude data at 1 Hz update rate to facilitate real-time monitoring of camera altitude and provide a capability to construct a near-bottom profile of the seafloor along the camera traverse. In addition, a forward-looking altimeter provided obstacle avoidance and was found to be very effective at range of ~ 50 m. It permitted flying towards scarps with known

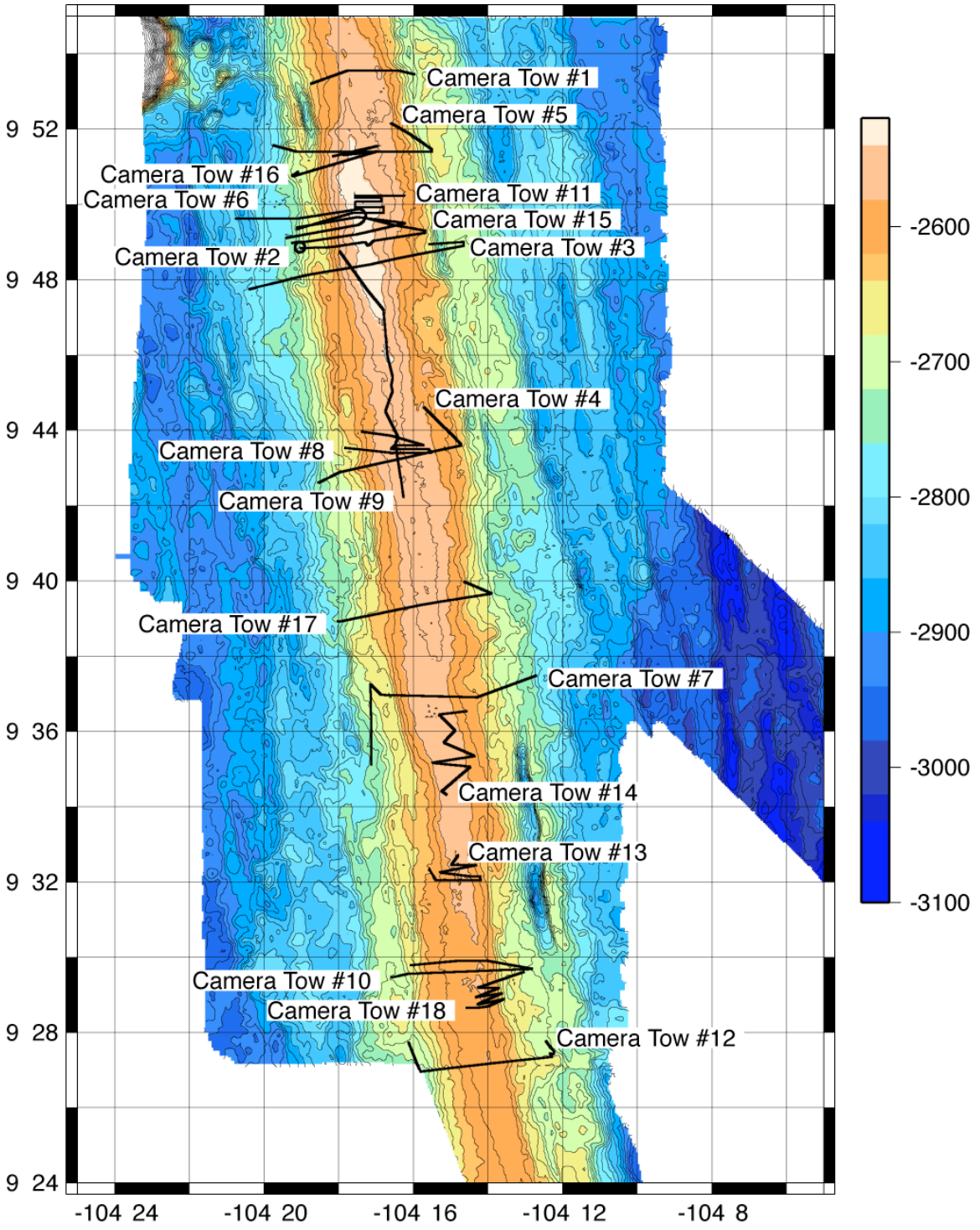

Figure 11. Location map of WHOI TowCam camera tows conducted during AT11-7. Multibeam bathymetry in meters based on 80m gridded data from Cochran et al. [1999]. See Appendix 9.2 for detailed maps.

throws of tens of meters by hauling in at a known rate to keep the scarp face a fixed distance in front of the camera while maintaining a ~ 6 m altitude for optimal imaging. A three-axis magnetometer was also mounted on the TowCam to provide near-bottom magnetic data as well as vehicle heading to help in orienting the photographs (see Figure 12).

More information is available for the WHOI TowCam at: (http://www.whoi.edu/marops/support_services/list_equip_towed_camera.html), and in Fornari [2003].

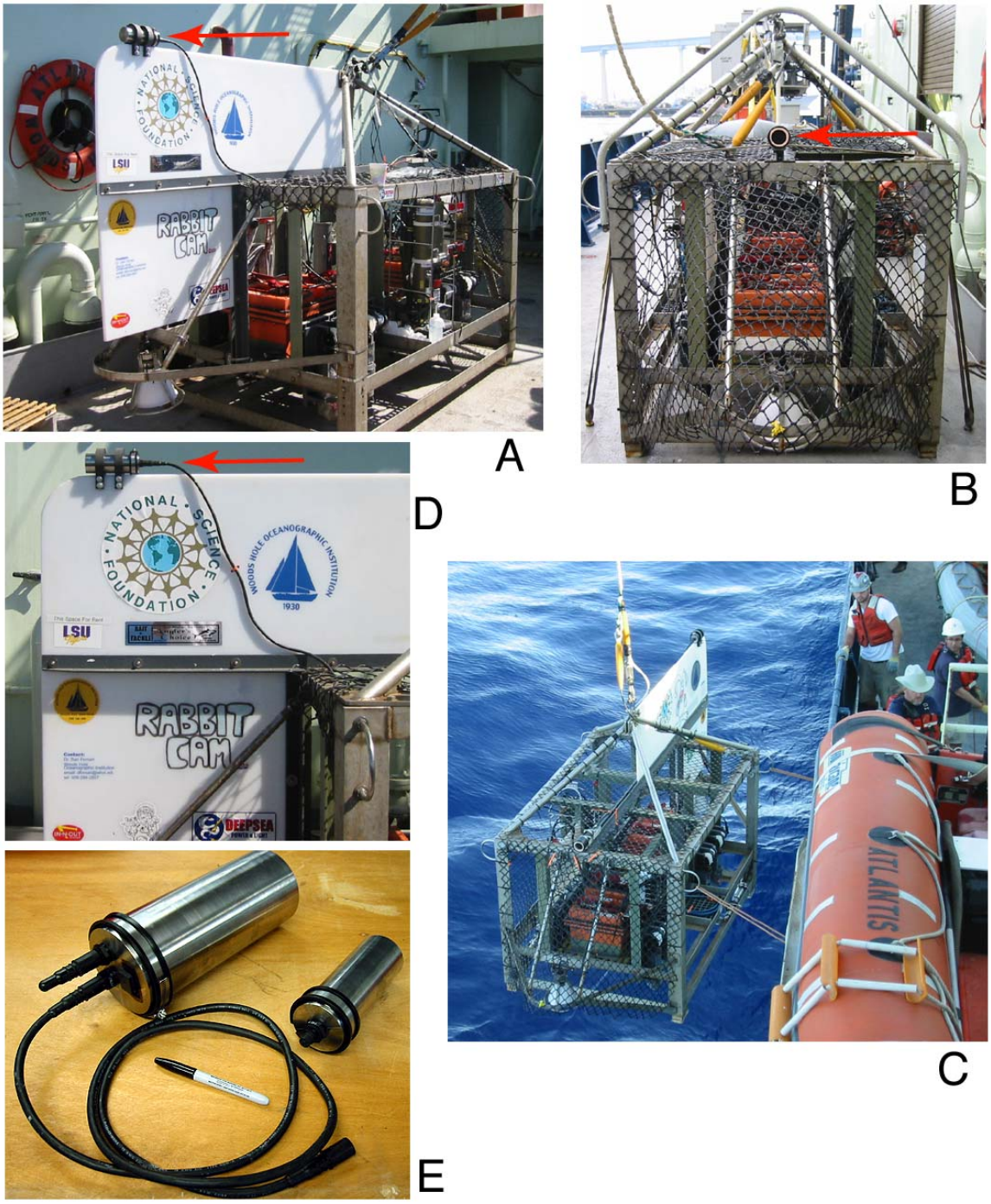

Figure 12. Photographs of the WHOI TowCam as configured for the AT11-7 cruise. A- View from the aft end of the Towcam, rear strobe head is below the white tailfin. Orange boxes are batteries. Red arrow points to the magnetometer sensor. CTD is visible in the middle of the right frame. B- View from the front of the TowCam. Red arrow points to forward-looking obstacle avoidance altimeter. C- Top view as the TowCam is lowered into the water, rock core winches are visible on the right side of the frame. D- Tailfin; showing placement of the magnetometer sensor. E- Magnetometer data logger pressure housing (left) and sensor housing (right) and interconnect cable in the lab.

3.6.1. Near-Bottom Magnetics- Alvin

The *Alvin* magnetometer was operational for all 15 dives for which the submersible reached the bottom (Figure 13). The magnetometer was mounted to the sample basket along the port side with the long axis of the sensor housing oriented fore and aft with X positive up (Z forward, Y positive to port) so as to be somewhat protected from hydrothermal vent work. This position results in a rather large ambient field effect of the submersible of ~4000 nT. The sensor was mounted with 3 stainless hose clamps for the first two dives but this was changed to 6 plastic tie wraps for dive 3965 to try and help reduce ambient field effects. The magnetometer had intermittent behavior during the dives with several channels (Y and Z2, particularly) spuriously maxing out at +/-90000 nT. Dives 3963, 3966, and 3968 were severely impacted by this problem resulting in only half of the dive or less providing usable magnetic data. The sensor cable was replaced with a short cable for dive 3969 and the problem seemed to go away after that. Throughout the dive program the magnetic data were plagued with a spiky noise problem that affected all four-sensor channels. This spike problem showed a sharp increase (less than a second) followed by a slower decay (over 4 s). No obvious repetition time was noted and the spikes occurred at all times of the dive. For all the *Alvin* dives, the 'CSV' file was missing many data points that were simply substituted by zeros, which contributed to an extremely noisy record. This was also the case for other quantities such as depth and altitude. The magnetometer data files from the 'CSV' records were essentially not usable. The magnetometer '*.dat' files were therefore used exclusively in the data processing and merged with the raw DVLnav files after being "grepped" - using standard UNIX command language - for depth, altitude, heading, pitch, and roll.

The processing steps for the *Alvin* magnetic data included parsing the data files as described above and merging into a 1 s record in MATLAB. The data were then calibrated using the spin data at the beginning and end of the dives. The calibration technique used the vector approach of Isezaki [1986] as modified by Korenaga [1995] to use the attitude of the plaform (pitch, roll, heading) and a predicted field from the IGRF. A least squares inversion was used to minimize the difference between the observed and predicted fields producing a correction coefficient matrix that accounts for the permanent and induced field of the platform. In this way, the 5000 nT ambient field effect of the submersible can be effectively reduced to less than 300 nT. Once the data have been calibrated, the magnetic field data are merged with processed navigation and projected along a track into equally spaced data points. The data are then continued upward to a level plane and inverted for crustal magnetization.

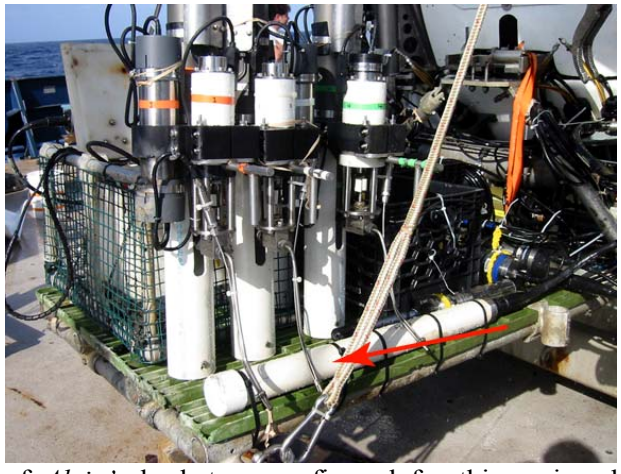

Figure 13. Photograph of *Alvin's* basket as configured for this cruise showing placement of the magnetometer (red arrow pointing to long white tube laying on the basket), and Seewald gas-tight water samplers (vertical cylinders with colored tape).

NAV header
Date Time(GMT) ShipnavLat(dec.deg) ShipnavLong(dec.deg) LaybackLat(dec.deg) LaybackLong(dec.deg)

CTD header
Date Time(GMT) Depth(m) Alt(m) T90(oC) Turb(ftu) Sal(psu) Lat(dec.deg) Long(dec.deg)

Flash header (time of each TowCam photograph)
Date Time(GMT) Depth(m) Alt(m) T90(oC) Turb(ftu) Lat(dec.deg) Long(dec.deg)

Magnetometer header
Date Time(GMT) Battery xf(nT) yf(nT) zf(nT) Tot.Field(nT) Heading(deg) Lat(dec.deg) Long(dec.deg) Depth(m) Alt(m)

Table 5. Header formats for TowCam data collected on AT11-7.

3.6.2. Near Bottom Magnetics - TowCam

A small, self-contained magnetometer system was built to record magnetic data during the deep-tow camera operations (Figure 12). The magnetic sensor is a Honeywell model HMR2300 digital 3-axis magnetoresistor that produces a digital RS232 output. This is the same type of sensor as used on ROV Jason. A separate pressure housing containing a datalogger and battery pack was built using a "Persistor" brand datalogger and compact flashcard memory storage (64 Mb). Only two battery packs were required for the entire 18 camera tow program of the cruise. Data is collected at a 1 Hz rate and the hourly files log elapsed time, battery voltage and the three vector components of the magnetic field. A simple Perl script reads the ascii files and converts the elapsed time to GMT time and the raw millivolt readings to magnetic field units (6.667 nanoTesla per millivolt). The magnetic data were merged with ship navigation data as described earlier to produce a composite of camera tow depth, altitude, position and magnetic value. The three-component magnetic data can also be used to calculate a magnetic heading. A calibration circle of the magnetometer on the camera tow system was completed during CamTow15. The result confirmed that the magnetic effect of the camera tow frame is negligible recording less than 82 nT for a magnetic effect, which is substantially less than the observed magnetic anomalies of several thousand nanoTesla (Figure 14).

3.7. Digital Imaging from Alvin and the WHOI TowCam and Shipboard Mosaicing

Digital still images were collected using various sources during the cruise. The primary imaging sensor was the DeepSea Power & Light (DSPL) DigiSeacam camera described by Fornari [2003]. The sensor consists of a Nikon 995 consumer grade camera mounted in a specially designed housing with water corrected optics providing 3.3 megapixel images with minimal distortion. Field of view of the camera from 5 m altitude (the average altitude used for TowCam and *Alvin* down looking imaging) is ~ 27 m^2 (6 m x 4.5 m, ~45°, Table 6). DSPL DigiSeacams were mounted on *Alvin* in a down-looking mode and on the TowCam. In both cases, illumination for down-looking images was provided by two 300 watt/s Benthos strobes. *Alvin* images were recorded every 10 s, TowCam images were recorded either at 10 s or 15 s repetition rates. A secondary digital still camera (Insite Scorpio model) was mounted on the starboard pan/tilt of *Alvin*. That camera has a forward view at varying angle depending on the orientation of the pan/tilt during image acquisition. Lighting for this camera was provided only by the HMI lights on the submarine. Table 7 contains the number of digital images acquired by the various imaging systems on *Alvin* and the TowCam during the cruise.

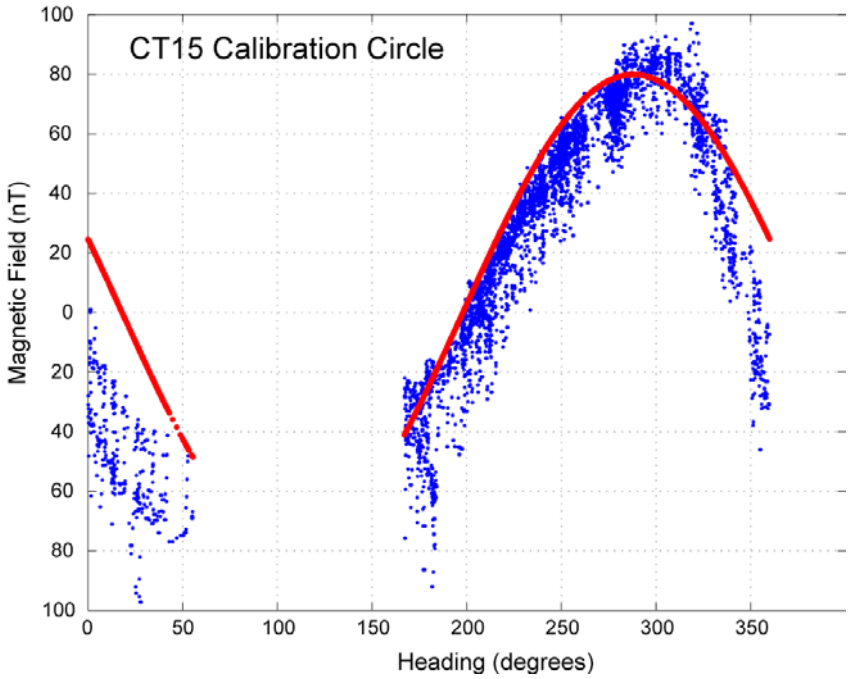

Figure 14. Plot showing total magnetic field versus ship's heading for the 360° calibration turn during Camera Tow 15. The total magnetic effect is about 80 nT. Blue dots are observed data; red line is theoretical effect of the TowCam frame.

Image processing of *Alvin* digital imagery and video data was carried out primarily by Yuri Rzhanov of the Center for Coastal and Ocean Mapping at the Univ. of New Hampshire (http://www.ccom-jhc.unh.edu/). Imagery was acquired from three sources: 1) a digital down-looking still camera on *Alvin*, 2) 1- and 3-chip video cameras with tilt and pan capabilities mounted on the front of *Alvin*, and 3) a digital still camera on the TowCam. Images from the TowCam were not mosaiced on board.

The repetition rate of images from the DSPL digital camera (10 s) are limited by the strobe recharging process which takes a minimum of 8 s. The strobes are sufficient to adequately illuminate the seafloor from an altitude of 6-7 meters. Images taken from higher altitudes are not good enough for identification of essential features to permit automated processing. The camera's vertical (along *Alvin's* axis) field of view is about 45 degrees, hence for consecutive images to have overlap, *Alvin* should not move faster than 0.83 times the altitude in 10 seconds. For an altitude of 6 meters that equates to a speed of <0.5 m/s. For overlap of 30 percent, the speed would have to be limited to 0.35 m/s, and to be able to employ automatic methods for image registration, the speed should not be greater than 0.175 m/s (65% overlap). For lower altitudes the restrictions are proportionally lower. All missions were time-critical, and it was not always possible to satisfy the above conditions optimally. Consequently, only about 10 percent of all images were suitable for assembling in photo mosaics. However, image quality for all acquisition using the DSPL cameras is excellent.

A Windows application PatchMap was developed by Rzhanov (unpublished data) to serve two purposes; a) real-time control/assessment of digital still image coverage during a dive, and b) off-line stitching of acquired imagery on the basis of DVL and LBL navigation. In the first case, the application provides visual feedback, allowing the observer and pilot to make corrections for the speed and altitude in order to maintain optimal conditions under which the imagery can be mosaiced automatically. In the second case, it allows one to assess spatial relationship between various images and helps to develop a mosaic-building strategy for any particular sequence.

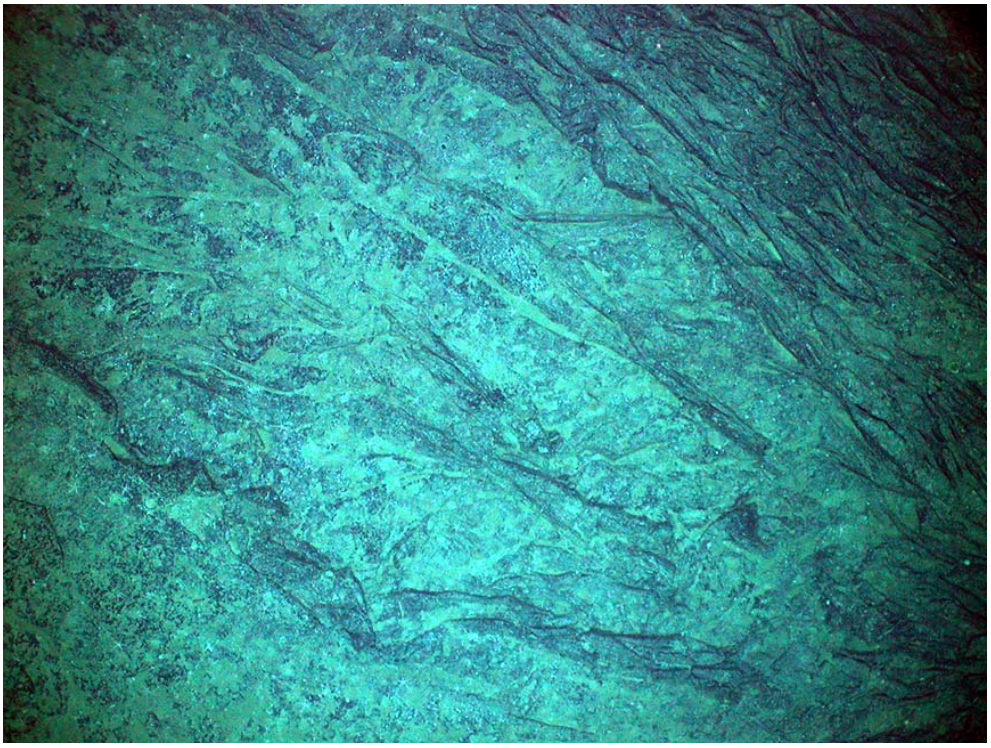

Figure 15. Example of a TowCam photograph from tow#16 showing curtain folded lava from ~ 3 m altitude (see Figure 12 for location of tow).

WHOI TowCam **Field of view in seawater for DSPL DigiSeacam**
2m altitude = 2.10m x 1.57 m= 879 pixels/meter
3m altitude = 3.49m x 2.62 m= 586 pixels/meter
5m altitude = 6.06m x 4.54 m= 352 pixels/meter
7m altitude = 8.03m x 6.02 m= 255 pixels/meter

Table 6. Calculated field of view for optics on WHOI TowCam using the Nikon 995 cameras installed in the DSPL DigiSeacam housings.

Typical screenshots of preliminary mosaics from post-dive processing of imagery collected during dive 3976 and compiled using Patchmap are shown in Figures 16-18. The frames are positioned on the map according to navigation and attitude recorded during the dive. This information was extracted from 1 Hz merged navigation file for *Alvin* data. Figure 16 shows a straight run, with altitude varying from 3.5 to 6 meters. Images overlap only when the altitude is at its highest. Figure 17 shows an attempt to make a survey of a ~40 by 50 meter area during dive 3976 around P vent (see Figure 2 for vent location). Images taken from higher altitude are darker and cover bigger footprints which makes it difficult to make a direct comparison. Right side of the picture clearly corresponds to sharp rise in the seafloor, as footprints are significantly smaller there. Figure 18 shows another photo-survey conducted around the Bio9 vent area with reasonably high overlap between consecutive images, except for the loop in the bottom right corner (see Figure 2 for vent location).

***Alvin* Downlooking**		**TowCam**		***Alvin* Video Clips**		**Insite Fwd. Looking**	
Dive	No. Photos	Lowering	No. Photos	Dive	No. Clips	Dive	No. Photos
3961	242	1	1001	3961	36	3961	2
3962	0	2	1925	3962	0	3962	0
3963	0	3	1819	3963	20	3963	205
3964	0	4	1805	3964	29	3964	0
3965	1820	5	1794	3965	14	3965	0
3966	148	6	1580	3966	10	3966	0
3967	1555	7	1551	3967	17	3967	324
3968	1999	8	1651	3968	18	3968	0
3969	942	9	1899	3969	14	3969	0
3970	0	10	1820	3970	14	3970	757
3971	1489	11	1738	3971	10	3971	642
3972	1111	12	1558	3972	19	3972	927
3973	1602	13	1554	3973	12	3973	699
3974	0	14	1881	3974	15	3974	1180
3975	1329	15	1490	3975	21	3975	0
3976	1434	16	1906	3976	9	3976	528
Total	13671	17	1851	Total	258	Total	5264
		18	1874				
		Total	30697				

Table 7. Number of digital images acquired on AT11-7 using *Alvin*, the WHOI TowCam, and Insite Scorpio camera. Also included is the number of digital video clips duplicated from the digital video recorded by *Alvin* cameras for use in constructing video mosaics.

Video cameras generally provided a better source of imagery for mosaicing, with guaranteed very high percentage of overlap, although at the cost of reduced resolution relative to DSPL camera imagery. It was sufficient to down-sample video sequences to 1 Hz to have consecutive overlap above the level of 80%; this guaranteed robust automatic registration. After sub-sampling, frames were cropped to a size of 688x376 pixels, to remove overlay from the top part of the screen and black padded margins (a result of conversion from DVCam tapes to video files in AVI format). For fast processing, frames were then resized using Lanczos filtering to 344x188 pixels. If illumination was insufficient, images were also enhanced using adaptive histogram equalization. Automatic registration of two frames took around 5 seconds on a PC with an Intel4 3 GHz processor and 1 Gb RAM. Typical sequences of 500 frames (~8 min of footage) took around 40 min to process. The co-registration program (YuriSoft) employs an AI scheme (based on a Support Vector Machine) to assess the quality of registration, which significantly reduces manual work of checking correctness of found transformations. Typically, bad co-registrations were detected when video channels were switched ("cut"), imaged terrain had exceptionally strong 3D content, or a moving object (with respect to the background) appeared in the camera's field of view. Human intervention was required to resolve split sequences (in the first case), approve the transformation marked as bad (second case), or cut off footage that could not be mosaiced (third case). Video cameras were usually mounted with a significant pitch (and sometimes roll) owing to their presence on the

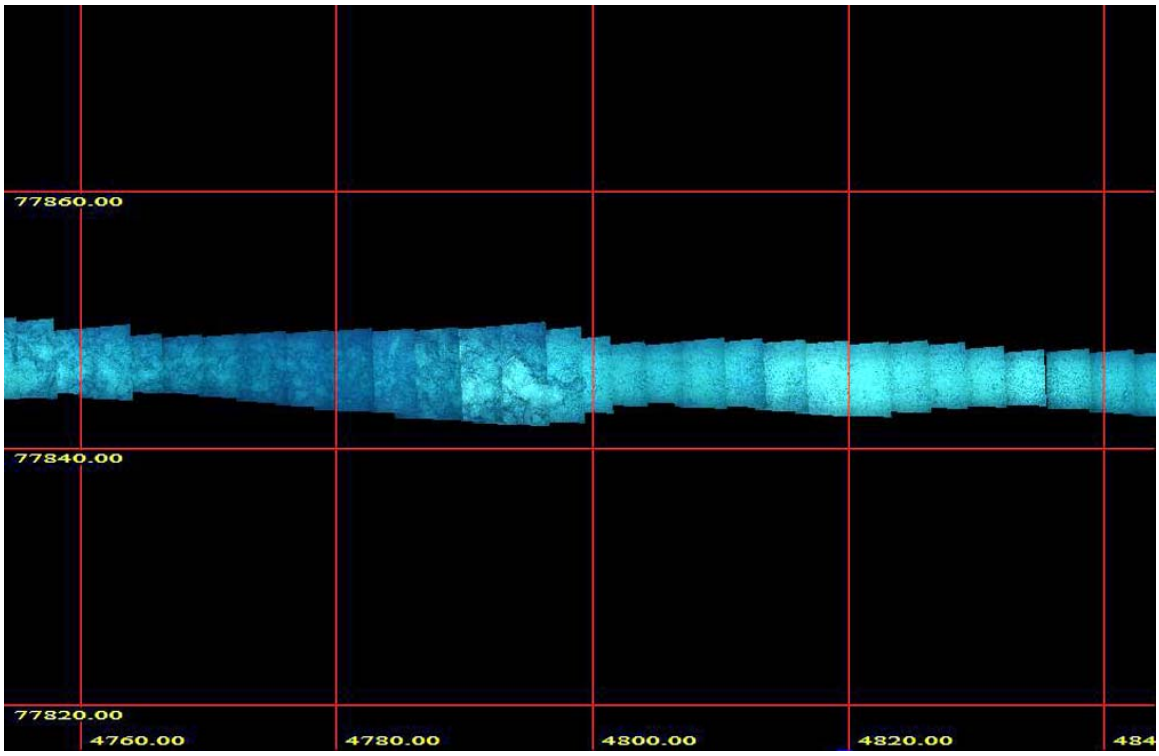

Figure 16. DSPL down-looking photos mosaiced using Patchmap program during a straight segment of track along *Alvin* dive 3976 (Figure 7). Positions are in local x/y. See Table 2 for origin.

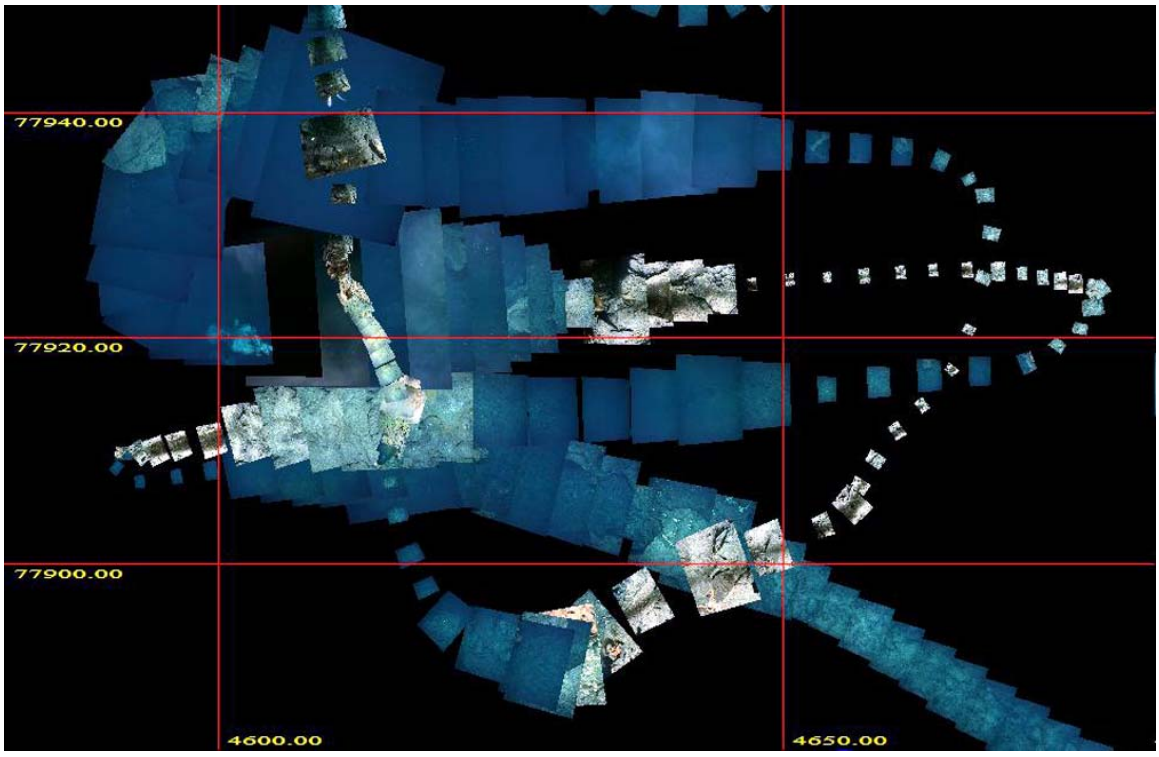

Figure 17. DSPL down-looking photos mosaiced using Patchmap program during a survey of the P vent area (Figure 2) within the AST during *Alvin* dive 3976 (Figure 6). Positions are in local x/y. See Table 2 for origin.

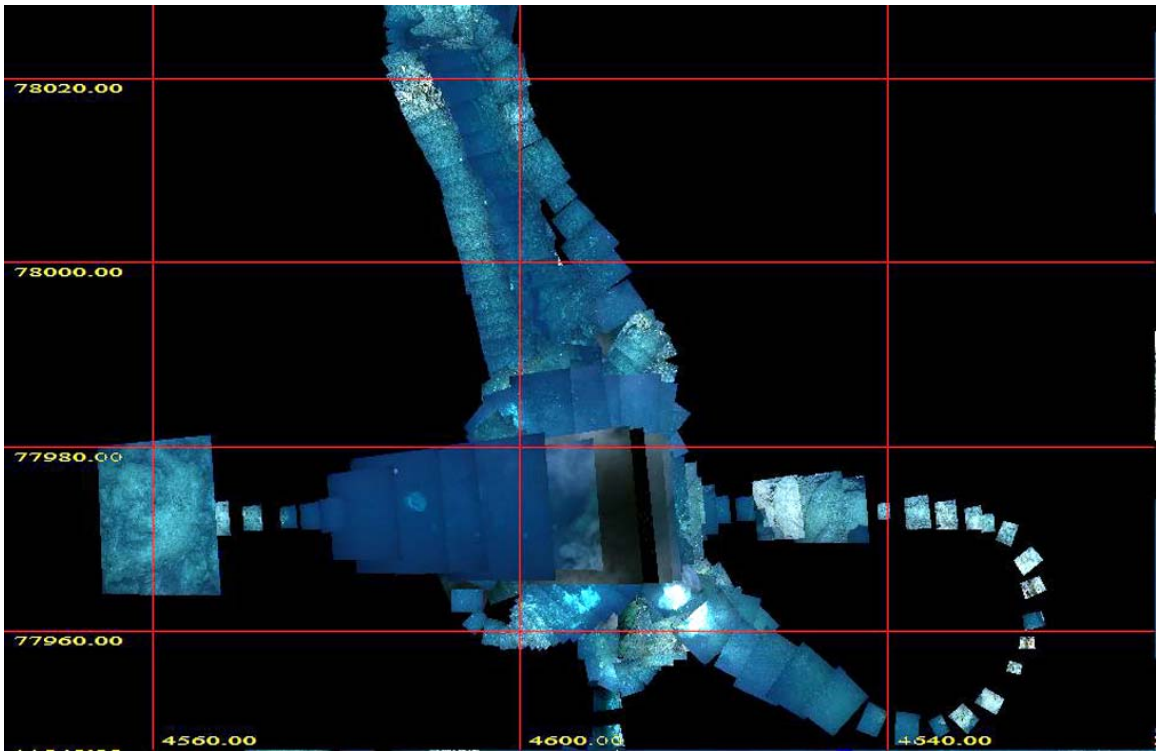

Figure 18. DSPL down-looking photos mosaiced using Patchmap program during a survey of the Bio9vent area (Figure 2) within the AST during *Alvin* dive 3976 (Figure 6). Positions are in local x/y. See Table 2 for origin.

pan/tilt units on the front of *Alvin*. Moreover, illumination was found to be inhomogeneous, with pronounced directional shadows. This did not complicate mosaic construction; however, if the path loops back, it cannot be combined with the previous pass without strong artifacts. This effect is similar to one in mosaicing of side scan sonar records and can be avoided only by a normal-incidence looking camera with inhomogeneous illumination. Camera attitude is not measured at present on *Alvin*. However, even if it is measured and recorded, there is a little chance that the imagery can be ortho-rectified to improve mosaic quality due to strong parallax effects. Suggestions for an improved image acquisition for mosaicing would include a video camera (to guarantee high sequential overlap and hence robust automatic registration) with a dynamic range of at least 12 bits per pixel. This would permit significant reduction of required illumination and still obtain quality data after suitable enhancement procedures. The camera would need to be carefully calibrated underwater in its housing, to compensate for lens distortions, which are almost negligible in the DSPL digital still camera.

4. *Alvin* Dive Summaries

Summary sample listings for all dives are presented in Appendices 8.4 and 8.5. The following summaries were written largely by the port (lead) observer for each dive, with input from the other observer's notes and post-dive reconciling of sample information and other pertinent data.

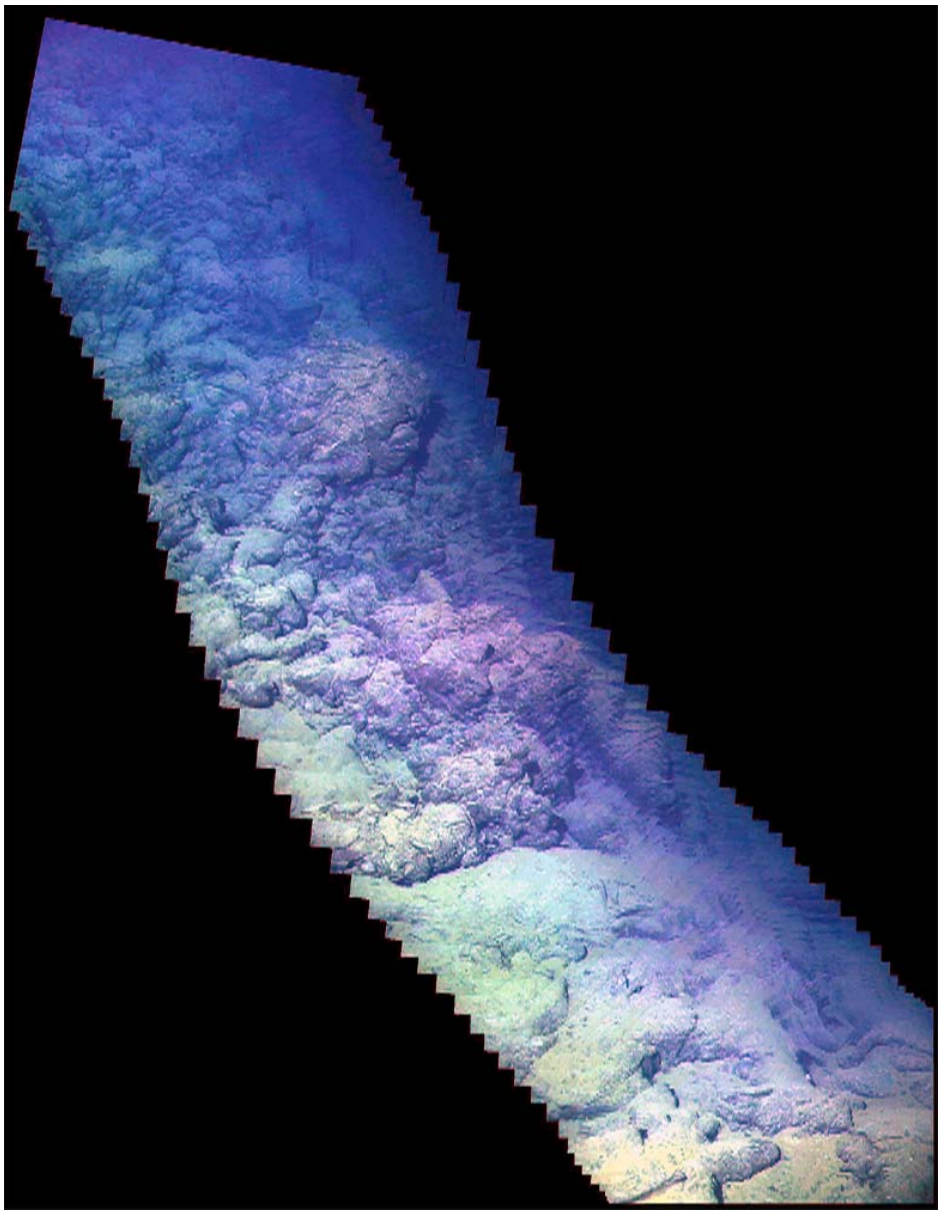

Figure 19. Video mosaic of a flow front compiled from video still images collected during dive 3963. Approximate scale across the image area is 4 m.

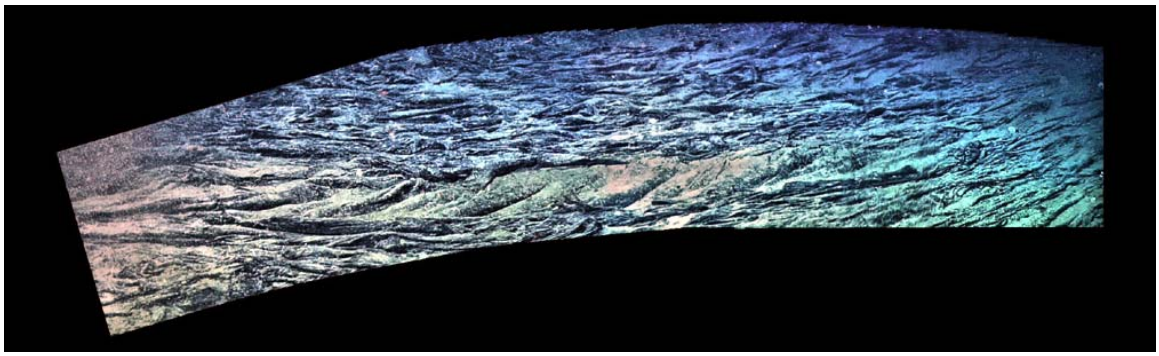

Figure 20. Video mosaic of a panorama across a folded sheet flow compiled from video still images collected during dive 3968. Approximate scale across the image area is 3 m.

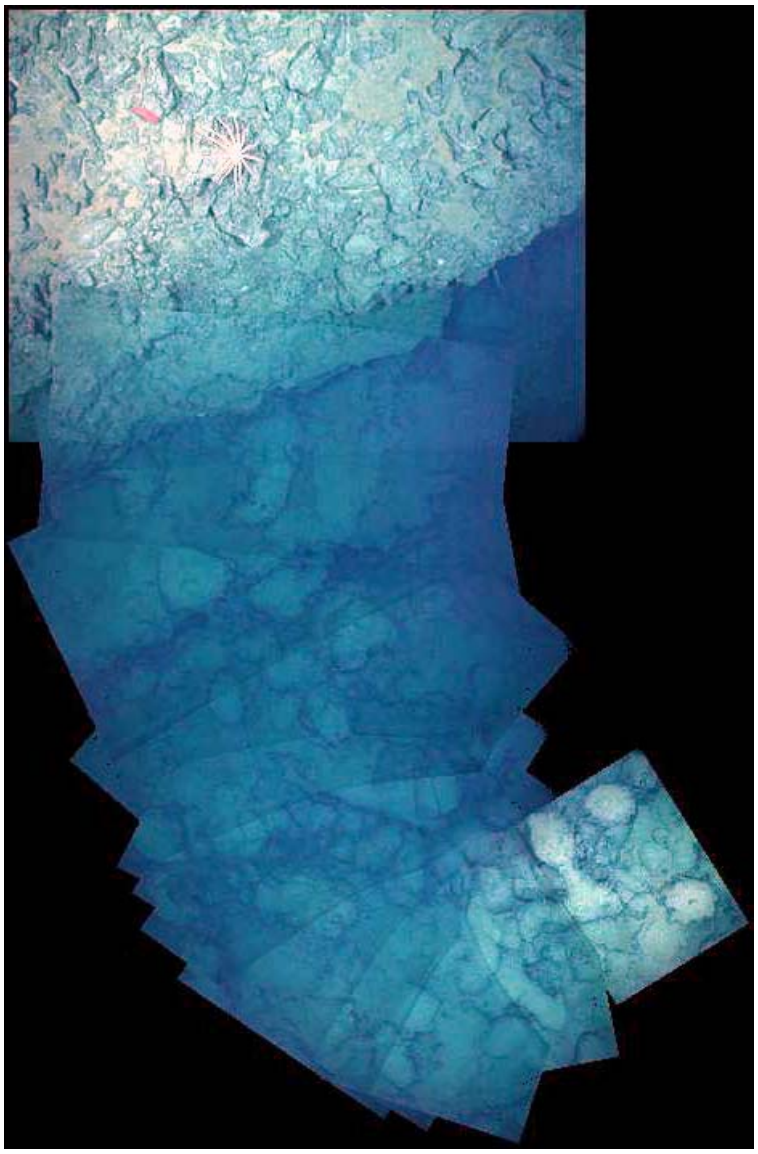

Figure 21. Mosaic of a scarp with lobate and pillow lava at the base, imaged during dive 3965 using down-looking digital images collected by the DSPL DigiSeacam camera on *Alvin* using strobes for illumination. Approximate scale across top of image is 2 m. Approximate horizontal scale from bottom to top of mosaic is 5 m.

Dive 3961

The primary objective of this dive was to perform chemical sensor measurements at high (P and Bio-9) and low temperature (Tica) hydrothermal vents. In addition to in-situ chemical sensor measurements (pH, H_2, H_2S), fluid samples using both major pairs and gas-tight samplers were also carried out at these vent sites. In cooperation with Tim Shank and Stace Beaulieu, basalt panels were deployed at Tica in the same general area as chemical sensor deployment. Panels were also deployed in a control site away from the Tica Riftia patch. Chimney material was recovered from P-vent to assist groups involved in vent microbial studies and as a means of providing sulfide samples to more indirectly assess vent geochemistry. At Tica vent, we first collected a gas-tight sample and then deployed two low temperature chemical data loggers in a healthy Riftia patch along with two sets of basalt settlement panels. We deployed a third set of basalt panels and the Edwards/Bach/Santelli

baskets on bare rock about a meter from the Riftia patch. We finished the dive with a video reconnaissance of the beehive at Tica. Virtually all objectives were met.

Dive 3962

Aborted

Dive 3963

Dive 3963 was located in the 9° 50N area of the EPR. Our objectives were to: 1) examine and map (using imagenix) several apparent flow fronts and a lava channel, previously imaged by side-scan sonar and ABE during the 2001 Schouten et al cruise; 2) survey magnetics using the 3 component magnetometer; 3) deploy Cara and Wolfgang's in-situ incubation experiments; and 4) investigate the condition of the RatCAM elevator and release it for recovery. At our start location, we deployed the in-situ incubation experiments and collected two samples of older ropey lavas, which protruded through the sediments as if they were remnants of pressure ridges (*Samples 1 and 2*). We proceeded in a southwesterly direction over ropey, lobate and sheet textured flows covered by a thin (a few cms thick) veneer of sediments. Approximately 200 meters along the dive transect, the slope steepened significantly and the lava textures changed from lobate to pillows. We interpreted this change in slope and texture as a flow front, and collected a pillow sample along this front (*Sample 3*) (e.g., see Figure 19 for an example of the flow fronts encountered during this dive). Beyond this pillow front were more ropey, lobate and sheet textured flows, which were again covered by a thin veneer of sediments. Occasionally, some of these lobate textured flows had breakout pillows, and in a few areas there were broken up sheet textured flows and collapsed lobates. At WP2, we encountered a second lava front several meters high and characterized by large pillows. Two samples were collected from this pillow front (*Samples 4 and 5).* Sample 4 appears to have come from alluvium along this pillow front; sample *5* came from an "in place" pillow. We then turned around and collected a sample of the older lobate flows underlying this pillow front (*Sample 6*). Note that samples *5* and *6* will make an ideal conjugate pair for evaluating age relations. At the top of this second pillow front, the terrain was relatively level and consisted of lobate flows, which were lightly sediment covered (< cm). The "apparent age" of these flows was perhaps younger, but essentially indistinguishable from the other lobate textured flows we had encountered along the dive transect. The third pillow front was even more distinctive and another sample was collected *(Sample 7)*. We then used sonar imagenix to survey this front for the next 25 minutes. After the survey, we collected a sample of the lobate flows underneath the pillow front *(Sample 8)*, which is presumably older than sample *7*; samples *7* and *8* will make another ideal conjugate pair for evaluating age relationships. From this flow front we proceeded toward the "channel" observed on the ABE bathymetry. This channel was located on a flat plateau within lobate and sheet textured flows. In addition to the main channel, there were several additional smaller collapse features/skylights in the immediate vicinity. We landed in the main channel, which was ~1 meter deep; its walls were laminated, and the bottom was flat and covered with sediment. In some places you could see sheet flow textures beneath the sediment. After collecting a sample from the wall of the main channel (*Sample 9*), we surveyed the area for the next twenty minutes. We then followed the northern edge of this channel upstream toward the axis. At its terminus we emerged onto lobate and sheet textured terrain. A few hundred meters from the channels end, we came to the fourth pillowed flow front. After taking two samples from this pillow front (Samples 10 and 11), we turned northward toward the RatCAM location. After finding the RatCam, we released it and then headed home. The lavas in the vicinity of the RatCam were glassier and had less sediment

covered than previous flows, but we were unable to collect a sample because of power limitations.

Dive 3964

A key objective of this dive was to deploy a high-temperature chemical and temperature data logger in a hydrothermal vent. This was accomplished at the base of P-vent, which issued fluid at approximately 365°C (*Alvin* high-T probe). ICL communication with the data-logger corroborated the 365°C temperature, and even reported temperatures as high as 372°C. The data-logger was left in place at P-vent for recovery on a subsequent dive. The dive included a return to Tica where data from both of the two low-temperature data-loggers were retrieved by ICL communication. One of the units (blue) was allowed to remain at Tica, while the other (yellow) was temporarily re-positioned in a control environment and then deployed for a short time (~15 minutes) in Riftia patch near Bio9 vent. Basalt panels for microbial studies at Tica were retrieved and exchanged with new panels for time series investigation. Fluid samples were obtained at Bio9 (double prime) and Bio9 (prime) (384°C). In-situ chemical sensor data were acquired from both vent sites. Virtually all objectives were achieved, with the minor exception of the Hobo temperature probe deployment at P-vent. This will be carried out on a subsequent dive.

Dive 3965

The objective of this dive was to examine a linear N-S feature imaged on side scan sonar at ~9° 50'N. To the north the linear feature is a fault spatially associated with the sharp edge of the central magnetic anomaly high. The dive traversed N to S following the side scan trace. At the northern end, the fault is not observed; and is assumed to be resurfaced by younger flows. An area of N-S trending tension fractures may represent its surface expression. There is an increasing surface throw of the fault southward, which may represent a gradual decrease in lava infilling in front of the fault southward. This is consistent with older flows observed on the footwall. The total movement on the fault is estimated to be ~ 20meters. Ten lava samples were collected for chemical analysis.

Dive 3966

The goal of this dive was to: a) explore the continuity of lava channel (dark reflective sonar areas), b) the transition from the lava channel to adjacent areas and determine the associated lava morphologies and possible contact relationships, c) explore the head/source of the lava channel, d) follow the associated lava flow to its distal end and e) observe the interaction of the flow with inward-facing faults near its end. Due to deteriorating weather at the surface the dive was aborted and only objectives a) and b) were partially addressed. The rest of the objectives were pursued in Dive 3971 (Ridley/Williams). The dive started in a low-relief area with mixed lava morphologies with light sediment cover. It was primarily flat sheet and lobate flows exhibiting some collapse (Sample 1). In a few places, pillows seemed to overlie the lobates. There was a rapid transition to folded and jumbled sheetflows to hackley terrain just south of the channel. There are small areas within the hackly terrain that are flat but do not appear to extend very far. The hackly and folded sheets are commonly piled up in small ridges with 1-2 m relief. The transition from hackly to sheet flow that comprises the channel occurs over a short distance <2 m) and there is a corresponding 1-2 m drop in topography into the channel. The lava channel is >100 m wide (crossed S to N), and is characterized by flat sheet flows (Sample 2) with areas of curtain folds terrain elongated in the easterly direction of flow within the channel. Some chevron folds in the flow also point "down stream". The northern boundary of the flow is transitional into hackly (Sample 3) and then

lobate flows. In one place at the N edge of the sheet flow it is covered by pillow lava (Sample 3) that seem to pour out of the hackly terrain. Further to the north the terrain becomes mostly lobate flows. Turning back to the south, the dive followed the northern edge of the lava channel where there was a clear contact of pillows over the sheet flow. The dive ended at the edge of a hackly mound transitioning to lobate flows (Sample 5) that appeared to be connected to the channel locally, but was not determined to be at the head of the channel. A total of 5 samples were recovered.

Dive 3967

The initial launch dive position requested was 9° 43.535'N and 104° 16.451'W located near a small offset (~200 m) in the Axial Summit Trough. The southern limb of the trough appears to be older and more tectonized in the DSL-120 side scan while the northern limb has apparent younger flows with an "incipient" trough just beginning to form in the recent flows. The primary objectives of the dive were to investigate the "older" southern AST and then drive north and east to investigate the newer flow and young AST. We then planned to drive east to a near-axis fault/scarp within 1 km of the axis to see if flows were dammed at this fault. We landed in the old AST and proceeded west to the western wall which was offset from the map coordinates by ~125 meters west. We deployed the in situ basalt baskets of Wolfgang and Cara and took a sample at this wall (Sample 1). We then proceeded east for a complete AST crossing reaching a minor collapse area, which we presumed was the eastern extent of the AST. We then drove west to the middle of the AST and then north to find the young flow. We crossed lobate flows and a gradual morphological gradient into what appeared to be more pillows. We encountered very glassy lava, which we interpreted as being the young flow. We sampled this (sample 2) glassy flow then moved east to the young AST axis. The young AST was a remarkable 5-m deep trough with many lava pillars and bath tub rings in the walls and collapsed material at the base of the trough. We took Sample 3 from the top of a pillar and then proceeded with a sonar and photo mosaic of the AST. After the sonar survey we decended into the trough and took a sample that had remarkable drips ~10cm long extending from the underside of the lobate shell crust. We then proceeded east, rapidly covering ground, crossing the edge of the glassy young lava about 200 m east of the AST. We then continued crossing lobate collapse, which became almost exclusively collapse with lava pillars and caverns. This then almost immediately gave way to a sheet flow and then hackly sheet flow, which continued east until we reached the scarp about 1.2 km from the AST. The scarp was a small west-facing fault (~3 m high), which we sampled on the top (Sample#5) and then retraced our path to sample the presumably younger hackly sheets (Sample#6). That was the end of the dive.

Dive 3968

The objective of this dive was to examine features presumed to be lava channels west of the AST at 9° 29'N, 104° 15'W. The channels were previously mapped high-resolution bathymetry where they appeared as sinuous depressions oriented normal to the AST and side scan sonar where they were delineated by continuous areas of low reflectivity. Upon landing the Santelli/Bach incubation chamber experiments were deployed on a collapsed lobate flow, where we collected a sample of lobate crust and fired four Niskin bottles. We transited to the southerly of the two channel systems examined on this dive. We conducted a Imagenix/photomosaic survey over the channel. The channel was characterized by a flat central sheet bound on either side by parallel regions of lineated sheets, within parallel margins of jumbled lava that graded into lobate lavas. There was 1-2 m of relief from the surrounding lobates to the central portion of the sheet. Samples were collected in the lobate, jumbled, and lineated lavas encountered during the transect across the channel. Next we traversed across

collapsed lobate lavas to the northerly of the two channels examined. We conducted another imagenix/photomosaic survey and collected another pair of intra- and extra-channel samples. We transited west along the channel to the eastern wall of the western graben. We concluded that the graben wall was tectonic in origin and traversed along the upper surface of the wall to the south. We collected a sample of lobate lava from within the graben and a sample lineated sheet from the westernmost extent of the channel where it was truncated by the graben. Finally we transited to the north and collected a final sample from what we presume to be the northern, near-axis, region of the channel. Ten lava samples were recovered.

Dive 3969

The primary objective of this dive was to recover the high temperature chemical data-logger from the base of "P-vent" as well as move the non-Tica low-temperature chemical logger to a control site to test electronics stability in fluids unaffected by hydrothermal emissions. Spot measurements using the high-temperature chemical sensor (Ghostbuster) were also a key objective. Unfortunately, the ICL communication from the submersible to the sensors and samplers was not established. It was subsequently determined that the ICL connector in the "boot" of the submersible had become disengaged during maintenance following one of the previous dives. Thus, much of the dive plan could not be carried out. In spite of this, data-loggers were effectively off-loaded, uploaded and re-positioned for subsequent studies. The Hobo temperature probe was deployed at P-vent.

Dive 3970

The aim of this dive was to study a series of off-axis mounds that had been identified on the sonar images. These mounds lie about 1.5 km to the east of the ridge axis at 9° 30'N. We wanted to determine the character of the mounds, to examine what their contacts with surrounding flatter and less sonar-reflective material are like, and to focus on areas where the sonar showed that fissures had been covered over by the mounds. We were able to identify three different putative sources for the flows in this area, these being: Young pillow mounds with up to 70 m relief that are covered by pillow tubes that have flowed down their flanks; Pillow lavas in the western part of the area that appear to have flowed from W to E, perhaps from the ridge axis; Old, heavily sedimented and manganese coated hackly lava that outcrops in deeper parts of the study area. All three of the flow types are fissured to a certain extent. Three large (10-30 m wide, 10-20 m deep) N-S trending fissures were discovered. The northernmost cut through pillows and was filled in at its northern end by pillows that had flowed down slope from the west. A second cut through pillows, and may possibly have been the site of eruption of pillows (in accord with camera tow observations from the area). The southernmost fissure was in the hackly flows, and had noticeably more talus and sediment in its base and less steep slopes than the other two large fissures, indicating that this fissure was older. This fissure was also filled in at its northern end, probably by pillows from the southern pillow mound. Small fissures and cracks (up to 1 m width) cut the youngest looking pillow mounds. Therefore, the youngest pillow mounds and flows from the W postdate the hackly flows and the formation of the large fissures. We were not able to determine a clear age relationship between the flows that came from the direction of the axis and the pillow mounds.

Dive 3971

This dive consisted of a W to E traverse east of the EPR axis, at ~9° 43.5'N, to follow a distinct lava channel and long eastward flowing lava. Main dive objectives were to: 1] examine the western head of the channel; 2] collect samples for chemical analysis to evaluate if the continuity of the long flow can be established geochemically, and; 3] examine a distinct linear

N-S feature observed in sonar side scan imagery. Western head of channel is discontinuous, eventually passing into a pillowed flow front and a heavily collapsed lobate flow. Eastward the channel is also discontinuous and surrounded by hackly-surfaced lava. Further eastward are one or more pillowed flow fronts trending ~ E-W overlying either hackly or lobate lava. The N-S linear features appear to be a fault. No scarp was found but N-S trending tension fractures were observed. This feature appears to have channeled one or more northerly flows southward and this may also be the related to the E-W flow fronts observed earlier. 10 samples were taken, which represent the volcanic terrain from the lava channel to the distal end of the long flow.

Dive 3972

Redeployment of the high temperature chemical data-logger at the base of P-vent was the primary objective of the dive. This was successfully accomplished. One of the low-temperature chemical data-loggers, deployed previously at a control site, was moved to the 100°C diffuse flow site near Bio9. This will be retrieved on a subsequent dive. Tica vent site was revisited to up-load the remaining low-temperature chemical data-logger and one of the basalt panels for the microbial study was repositioned. Once on board, the low-T data-logger recovered from Tica after 13 days revealed the effects of coexisting with complex biologic communities. In particular, several Paralvinella (sp) worms were observed inhabiting the electrode housing. The Imagenex system was turned on once on the seafloor. A route from Tica to "Q-vent" taking the submersible along the east wall of the ASC was selected. It is not clear at this point if this traverse resulted in the desired Imagenex data. Q-vent was sampled with major pairs, chemical sensors and gas-tight samplers. Time and power was insufficient to sample "M and Bio-vent", as initially planned. Efforts were made at Q-vent to deploy a device for chimney growth that was provided by Meg Tivey. These efforts were not successful and the device recovered for later deployment. Chimney samples were recovered from Q-vent for microbial studies. Difficulties with the port manipulator complicated, but did not prevent, sample recovery.

Dive 3973

The objectives of this dive were multidisciplinary. Mapping the lava channels that extend east from the axial summit trough (AST) near 9° 50'N (although they do not appear to connect to the AST) was the first objective. We landed on the northern limit of the channel where the 'RatCam', the elevatored camera system, had landed on a very folded sheet flow. The RatCam did not appear to be working, no flashes were evident so it was released to the surface (after inspection on board after the dive, the camera did work but the strobe cable was found to have flooded- a few quite dark photos of *Alvin* were taken). We traversed the channels doing a zig zag from north to south and back again; at the northern and southern edges of the channel there are lobate flows with some collapse. Imagenex data and down-looking digital imaging was done throughout the dive. The channel interiors were very flat and expansive, occasionally lineated parallel to the expected direction of flow. The margins of the channel were found to be more lineated with transitions to folded and jumbled lava. At the head of the channel, the lobate flow was budded and found to overlie the sheet flow. This relationship helps explain why no direct connection between the channels and the AST is evident in the sonar imagery. The dive proceeded towards the AST in order to collect Imagenex profiles across the trough at various locations near P and Bio9 vents. The latter part of the dive was dedicated to collection of the yellow chemical sensor from the Bio9 mushroom vent, and deployment and collection of settlement/incubation panels at Tica vent. Four lava samples were recovered from the sheet flow and overlying budded lobate flow.

Dive 3974

The dive objectives were to investigate the region to the west of the AST in the 9° 50'N portion of the ridge. Previous ABE coverage showed a series of four or more steep sinuous slopes in the bathymetry that appear to be flow fronts. The dive plan was to cross the axis from west to east documenting these features and recovering samples. At the end of the dive, the plan was to investigate a prominent collapse area that is perpendicular to the AST and to do a Imagenex survey of it.

The dive began about 2 km to the west of the axis at a depth of 2602m. The beginning of the dive was delayed for about 45 m because of some serious grounds that eventually went away. The down-looking camera however had to be turned off because of these electrical problems. The dive began in a relatively flat area covered with a mix of jumbled and hackly sheet flows and lobate flows that were only covered with a moderate to light amount of sediment. Traversing to the west led us to a steeper area that was comprised of well-formed pillows. This pillowed slope corresponded to the steep slope on the ABE bathymetric map and it is presumed that it represents a flow front. At the top of this slope there was a small ridge or mound of pillows and then the pillow lavas became transitional into flatter, more tubular pillows. In the shallow depression just east of the ridge/mound was characterized by a mix of sheet lavas. In some places it appeared the pillows lay above (were younger than) the sheet flows. The remainder of the dive traversed three of the slopes that were presumed to be flow fronts. In all cases the steep slopes (~10-15 m high) were comprised of well-formed pillows that transitioned to lobates and then hacky lavas in the flat areas immediately above them (see traverse ~17:52 to 18:20; Samples 2 and 3; also ~ 19:40- 19:50; 21:21 –21:28). The flatter platforms between flow fronts typically was dominated by folded and hackly sheets mixed with lobate flows. There were a few places where flat sheets formed channels in the hackly and lobate flows (~ 18:35). In at least one case, it appeared that the flat sheet and hackly lavas were flowing down a flow front slope. Clear contact relationships were documented at 20:01 to 20:30. Where the pillows were in contact with flat sheets they were clearly overlying them, but when there was a mix of pillows and hackly lavas it was often difficult to tell the relative age relationship. It was possible that some of the pillows may have been a late eruptive phase that extruded from the hackly flow unit. Over the second to last flow front (~20:34) the lavas predominantly become lobates that have a good glassy surfaces and are only lightly sediment covered. These look like the characteristic "Age 2 lobates" we described out of the AST during the AdVenture dive series. In area where there are mixed pillows and lobates, some of these lobates have "tortoise shell" surfaces that have cracked with gnarly-looking tubules of lava emanating from them.(21:27) Further upslope, in an area the appears very flat on the ABE bathymetry, the lobates become more extensive and have characteristic shallow collapse in them. The incubation experiment was set out on this field of lobates and a Sample 11 was taken at 21:55 just before power limitations ended the dive. The survey of the collapse area was not carried out because the dive ended early.

Dive 3975

The initial launch dive position requested was 9° 28.778'N and 104° 15.797'W located on the western flanks of the 9 28 ABE survey box. The primary objectives of the dive were to investigate the flow fronts that were imaged by ABE and DSL-120 in 2001, to take samples of these flow fronts, and to map the magnetic field of the flows for comparison with the ABE magnetic data. We landed somewhat east of our intended drop point so that we needed to drive west first to reach the older mound-like features seen in ABE and DSL120 sidescan at WP1. *Alvin* had a major ground problem upon landing and it wasn't until 17:00 GMT (10:00am

local) that we were able to locate and isolate the ground and start all the science sensors and videos etc. The Imagenex system unfortunately did not work properly for the rest of the dive. After taking a sample at the landing place (Sample 1) and deploying the in situ incubation experiments for Wolfgang Bach we drove west across a flow front from lobates into pillows and then almost immediately at the base of the scarp a young unsedimented hackly sheet flow. We sampled this flow (Sample 2). We then proceeded to the mound area, which was low-lying lobates and pillows (Sample 3). Turning around we head back east across the hackly sheet flow and then pillows at the toe of the scarp. We came across a small "run-out' of hackly sheets and sampled that at a small fissure near the summit (Sample 4). We then proceeded to climb a succession of lobates and pillows interspersed with channeled sheet areas until we reached the summit. Sample 5 was taken at this summit in lobate lava. We then drove across a mostly pillow and lobate plain for ~ 300 meters which towards the end began to show progressively more areas of collapse. A hackly flow and collapsed lobates were then observed. We stopped and sample a glassy lobate flow (Sample 6). After leaving the sample station we immediately entered into pillowed terrain, which corresponded to a scarp and presumably a flow front. On top the pillows gave way to lobate flow and we stopped and sampled the lobates (Sample 7). We turned to head directly east and started to see vent crabs and flat fluid-like lobates and large areas of collapsed lobates. We eventually reached the western trough after passing through areas of collapse and small lava pillars about 1 m high. The trough contained relatively unsedimented hackly and ropy sheet flow. We stopped to sample an orange stained pillar at the side of the channel (Sample 8) and then a white stained altered piece of basalt (Sample 9). The wall of the channel showed striking stratigraphy in cross-section. We then traversed south in the channel before coming across a small fissure in the eastern wall, which had a small colony of hydrothermal tube worms (Tevnia) growing in it. That was essentially the end of the dive as we had run out of power.

Dive 3976

The dive objectives were multidisciplinary and included: 1) searching in a sheet flow east of the AST where an *Alvin* HMI light head had been identified in the photographs taken on camera tow #11, 2) conducting Imagenex and down looking camera surveys over the sheet flow east of the AST near 9° 50'N and over vent sites in the AST, 3) recovery of the high temperature chemical logger at P vent and 4) chemical sensing using the Ghostbuster and fluid sampling at Bio9 vent. Despite searching for the light head for ~30 minutes, it was not located. Subsequent dives to this area should note the track of 3976 and search adjacent to it. The surveying of the sheet flow and axial trough and vent sites was accomplished. The recovery of the P vent high temperature logger was successful. However, the fluid sampling and chemical sensing was not successful because the dive as cut short because of a hydraulic failure in the port manipulator. The dive was curtailed by ~2 hours because of the hydraulic problem.

5. Towed Camera Surveys

Eighteen WHOI TowCam surveys were carried out during the cruise (Figure 11 and Table 4). Maps of each tow and summary sheets for each tow are provided in Appendix 9.2. A total of 135 kilometers of on-bottom coverage spanning ~121.5 hours of observations were provided by these largely night time surveys (Table 8). The camera was outfitted with 8 rock core winches with which samples could be recovered during each tow. This was one of the first extensive uses of the TowCam rock core winches and many lessons were learned regarding the tether line used and possible improvements to the geometry of the 'balls' to improve sample recovery. We experienced several problems losing balls, having dry hits (i.e. where the ball didn't seem to hit bottom and

obtain any sample), and once in awhile having the ball not rewind into its storage tube. We made several modifications which seemed to improve this situation, including: 1) using monofilament, which was more elastic and resilient, rather than fly-fishing leader, which is more static and abrades more easily; 2) using stainless steel shackles to attach the balls, rather than knots, which might have resulted in some balls becoming untied/detached; 3) using a tube as a template to wrap the monofilament around, and then taping (with masking tape) this stacked coil in place, rather than rubber banding loops, which resulted in the loops get tangled around and within themselves and the ball not dropping far enough. Still, once in a while we lost balls and had dry hits. Clearly it was hard to prevent losing balls that are hanging down and dragging along the seafloor (photographic forensics showed that pillows, fissures and collapses were the typical places where balls were lost). In this regard, it is always better to have the tether break when the sampler is stuck as opposed to ripping the motor off of the frame or damaging the gear mechanism, so a stronger tether is not the answer. In general, we used 100-200# test line. In the future, we plan to only use 100# test monofilament and to replace the line each time so that the resiliency of the line is optimized for each deployment. However, one possible modification, which could help to mitigate ball loss is to make it more streamlined (e.g. more elliptical or football shaped). Over the 18 camera tows, 91 samples were taken. The last tow did not include the samplers as we were cleaning and demobilizing them. Of a possible 136 samples that could have been returned, the percentage of recovery was 67% (91 balls recovered sample) with an approximate mean size of sample between 1/4 g and 1/2 g. 33 balls were lost to the lava flows, 12 were verified by the photographs not to have impacted the seafloor.

6. Preliminary Results

6.1. Near-bottom Magnetic Surveys

6.1.1. Alvin Near-bottom Magnetics

Data from five *Alvin* dives were suitable for off-axis analysis of the lava flow fronts and deposition of lava units (dives 3963, 3965, 3971, 3974, 3975). The dives in the AST near 9° 50'N ASC should also be useful for constructing a high-resolution magnetic map over the vent areas (3961, 3964, 3969, 3972, 3973, 3976). Preliminary analysis of the magnetic data from lava front dives show excellent correlation with the ABE magnetic maps both in the 9° 50'N area and the 9° 28'N areas, reinforcing the previous interpretation that the Central Anomaly Magnetization High (CAMH) can be related to the deposition centers for young lava from the axis.

For the example shown in Figure 22, on dive 3963, the magnetic edge of the CAMH can be correlated with the gentle flow front of a particular lava unit. This lava sequence and the underlying flow were sampled during the dive and should allow for U-series dating and paleointensity measurements. Interestingly further east the *Alvin* magnetics also correlate with a strong magnetic high that could potentially be attributed to the paleointensity high that precedes the Laschamps event minimum. Again, we have taken samples with *Alvin* to investigate this.

6.1.2 TowCam Near Bottom Magnetics

A total of 18 camera tows were surveyed across the axis of spreading of the EPR, all with magnetic field data collected (Figures 11, 23-24). Magnetic anomaly amplitudes vary up to several thousand nanotesla, which is typical of near bottom profiles over young ocean crust.

Camera Tow	Distance (km)	Time Start (Z)	Time End (Z)	Elapsed Time
1	2.54	9:14:52	12:01:23	2:46:31
2	6.21	6:15:29	11:02:19	4:46:50
3	7.67	0:00:14	7:11:44	7:11:30
4	8.13	13:51:21	21:22:22	7:31:01
5	8.2	4:19:40	11:47:56	7:28:16
6	6.97	3:46:04	10:20:49	6:34:45
7	7	4:36:18	11:03:48	6:27:30
8	7.47	5:53:22	12:45:52	6:52:30
9	8.61	0:02:53	7:57:24	7:54:31
10	9.7	3:18:12	10:52:57	7:34:45
11	6.58	5:23:57	12:38:12	7:14:15
12	5.81	7:20:24	12:41:24	5:21:00
13	7.03	5:19:51	11:48:06	6:28:15
14	9.73	2:56:28	10:46:28	7:50:00
15	7.85	3:08:34	9:20:34	6:12:00
16	9.45	3:47:44	11:43:59	7:56:15
17	8.29	3:59:47	11:42:17	7:42:30
18	8.18	0:46:19	8:21:19	7:35:00

Table 8. Details of distance surveyed and times for TowCam surveys on AT11-7.

The minimum wavelength of the near-bottom signal is about 125 meters, which is confirmed by power spectral estimates that show a signal to noise transition near 100 meters wavelength (Figure 25). Strong “edge anomalies are observed on many profiles and these can be correlated over several kilometers in some cases. Several camera tows (10, 12, 17) were designed to retrace the multi-channel seismic (MCS) lines of the mid 1980’s surveys [Detrick et al., 1985]. These coincident profiles will allow for independent control of the thickness of layer 2A for future modeling of these magnetic profiles. A number of profiles were collected around the 9º 50’N area to help constrain the ABE magnetic field data collected on AT7-4 in 2001. Due to the low latitude of the study area the inversion of magnetic field data is somewhat unstable, amplifying the north-south trends more than east-west trends. It is crucial therefore to establish the continuation of various magnetic anomalies observed in the ABE 9º 50’N data. This is of particular importance to the CAMH anomaly, which shows a strong eastern linear magnetic boundary at 9º 50’N, that is apparently controlled by a partially buried near-axis fault. The camera tow magnetic data allows us to extend the extent of this anomaly, determine its north and south limits and helps in the inversion of the data for crustal magnetization.

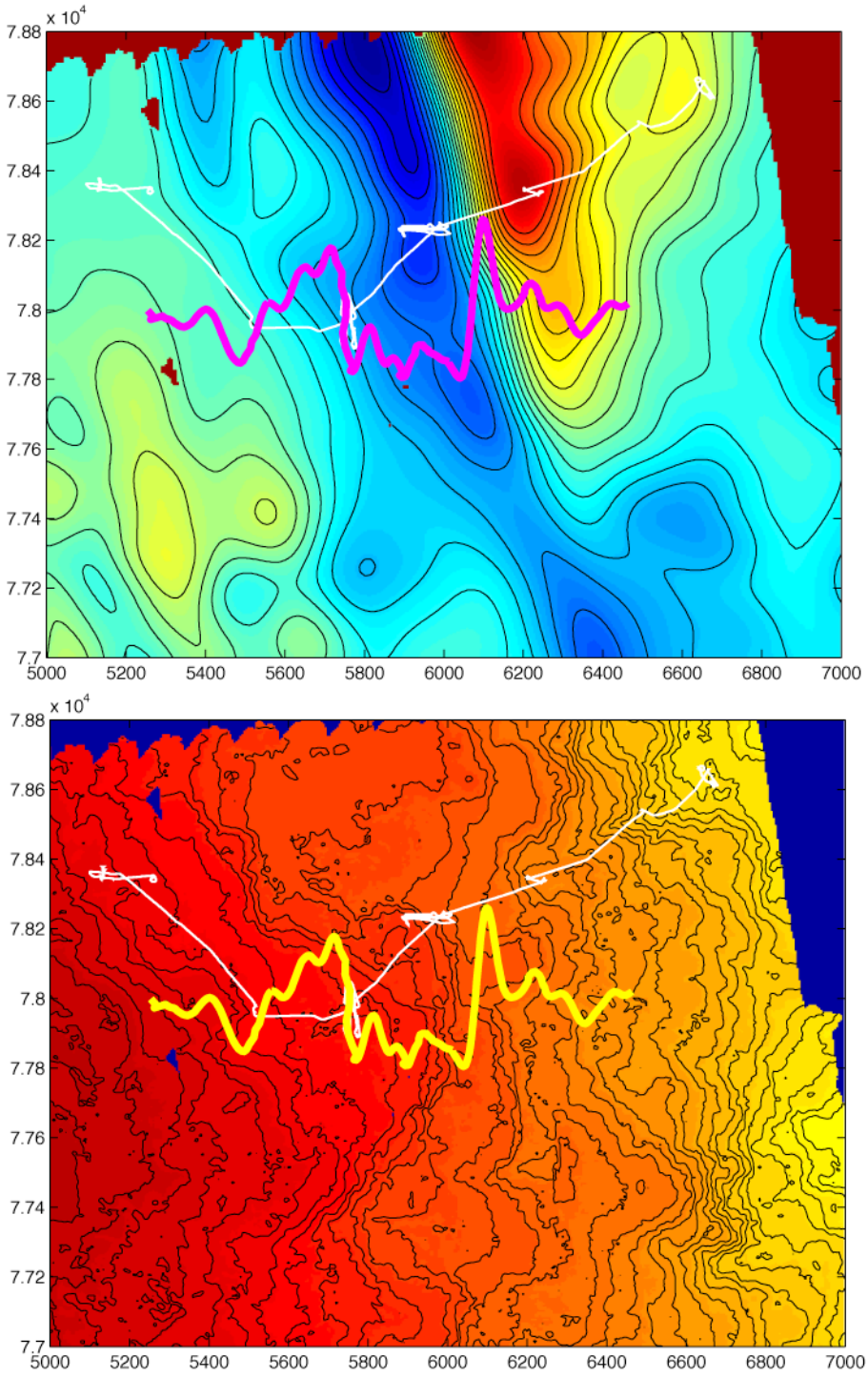

Figure 22. Bottom map shows ABE bathymetry (2 m contours) and *Alvin* dive 3963 in white. The yellow bold line is the magnetization inversion computed along the profile. Top map is the ABE magnetic map reduced to the pole with 200 nT contours and superimposed is the dive magnetization inversion (purple line) showing the excellent correlation between the magnetic low marking the eastern edge of the CAMH and the ABE map.

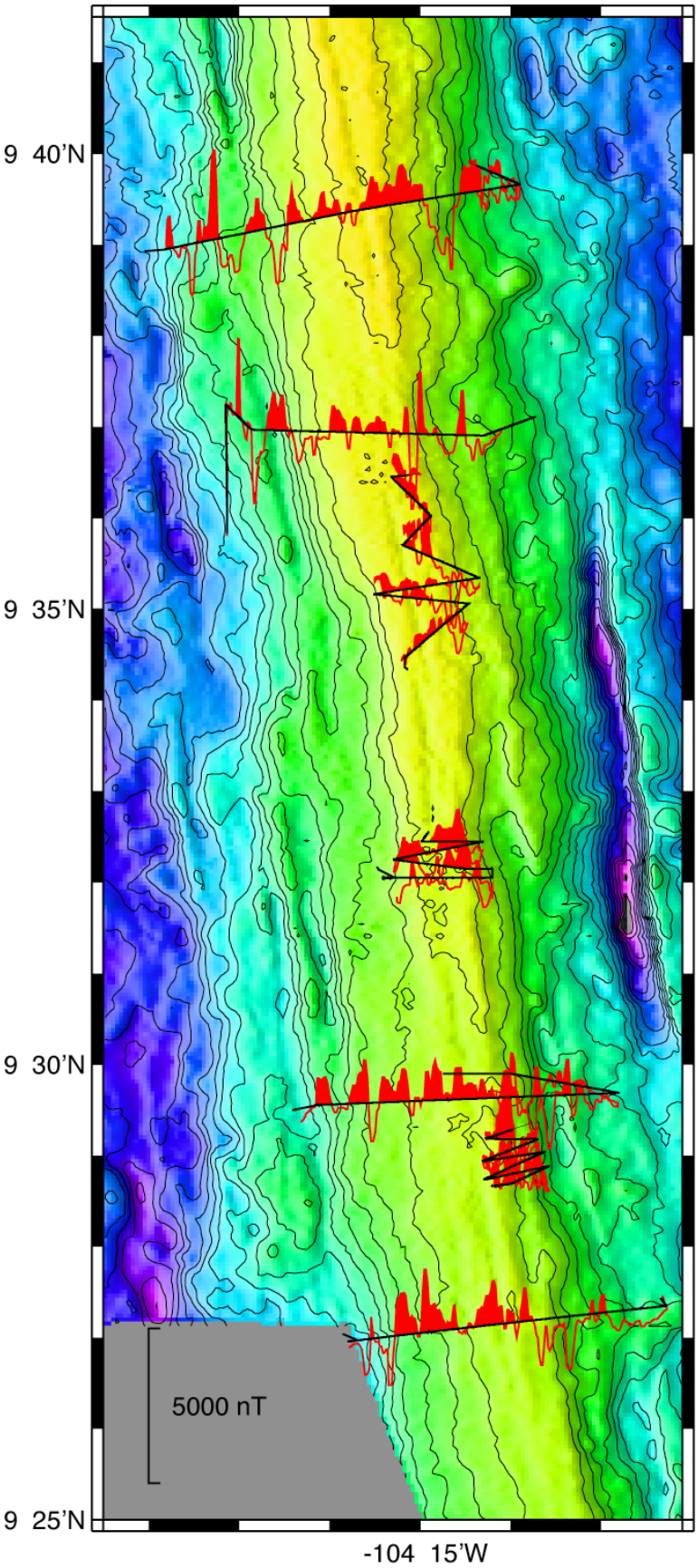

Figure 23. TowCam profiles showing magnetic anomaly measured along track for northern area of study overlain on SeaBeam bathymetry.

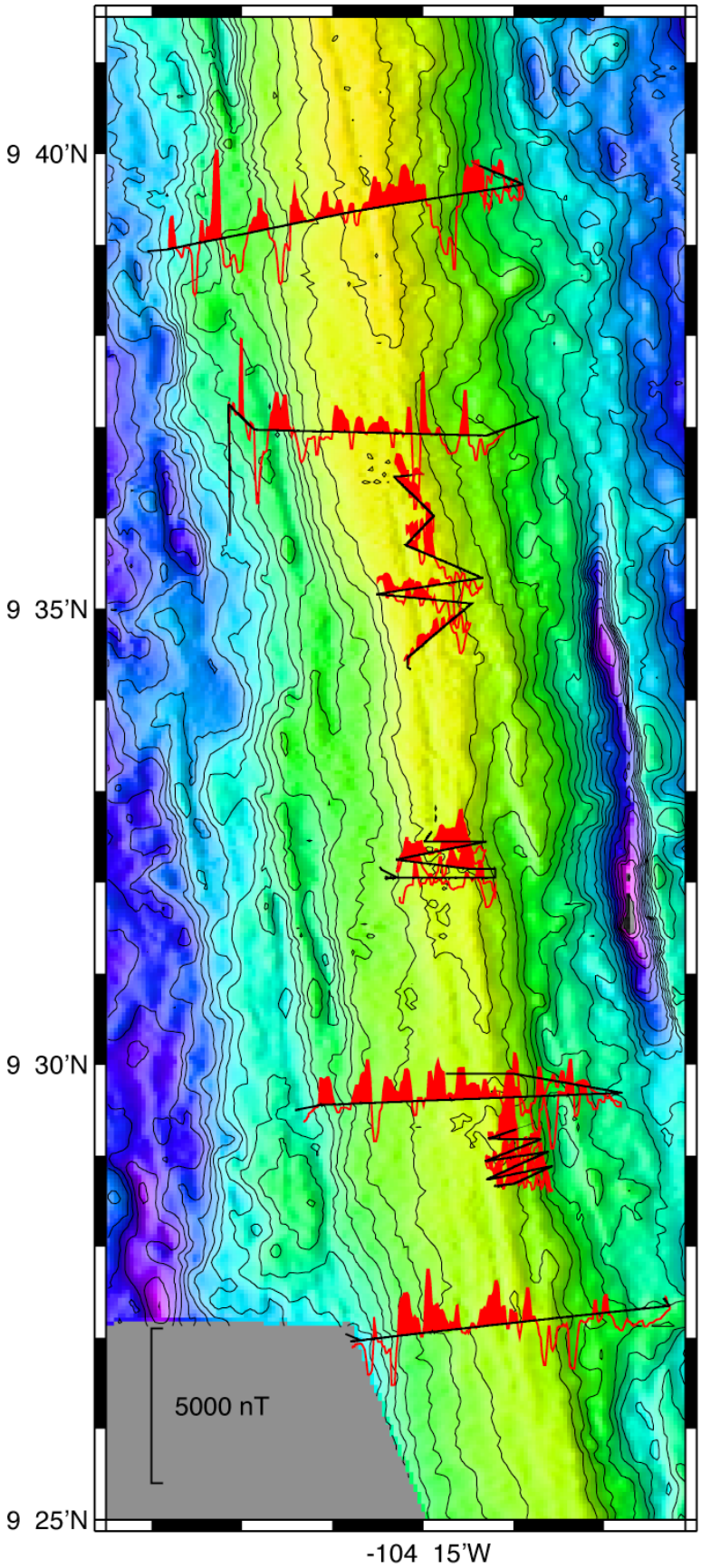

Figure 24. TowCam profiles showing magnetic anomaly measured along track for southern area of study overlain on SeaBeam bathymetry

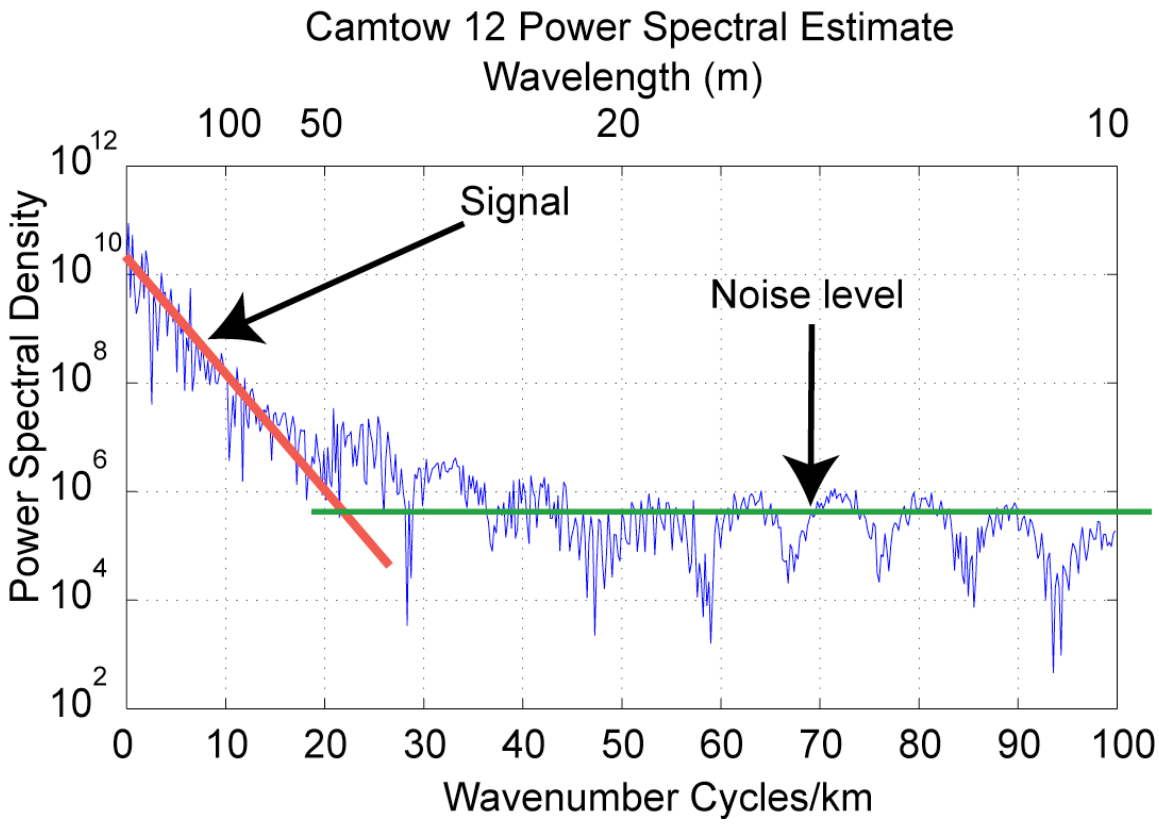

Figure 25. Power spectral density for TowCam #12 showing the signal to noise cutoff at ~50 meters wavelength.

6.2. Off-axis lava transport: Flow fronts and lava channels

The majority of volcanic eruptions at the EPR occur within or very near (<100 m) the axial summit trough (AST). These eruptions produce a carapace of young lava that can extend to ~3 km on either side of the axis. The distance from the axis to which an individual lava flow can extend is a function of lava cooling, volume erupted, eruption rate, and the topography it encounters. In general, short lived and small volume eruptions deposit much of their lava within the AST or near the axis (<1 km). During longer duration and larger volume eruptions it may be possible to transport lava across the EPR crestal plateau to distances of 1-4 km. We believe that deposits from both types of lava transport mechanisms are visible in sonar imagery and micro-bathymetry records collected during cruise AT7-4, in 2001. One goal of this cruise was to ground truth our interpretation of the sonar and micro-bathymetry records as well as document the mechanisms by which lavas are transported off axis.

6.2.1. Lava flow fronts

Along much of the ridge between 9° 25'N and 10°N, the near axis region is characterized in the sonar record by a shingled texture that appears to be overlapping lava flow lobes. They are identified by sonar-bright, distal flow margins that are scalloped over length scales of 100's of meters (Figure 26). We can confidently trace these margins along individual scallops or lobes, and in places it appears that margins can be traced along multiple scallops. We hypothesize that each of these margins represent the furthest down-flow and lateral extent of a flow lobe and through exploratory *Alvin* dives and towed camera imagery hoped to verify this and gain insight into the relationships between both laterally and vertically adjacent lobes.

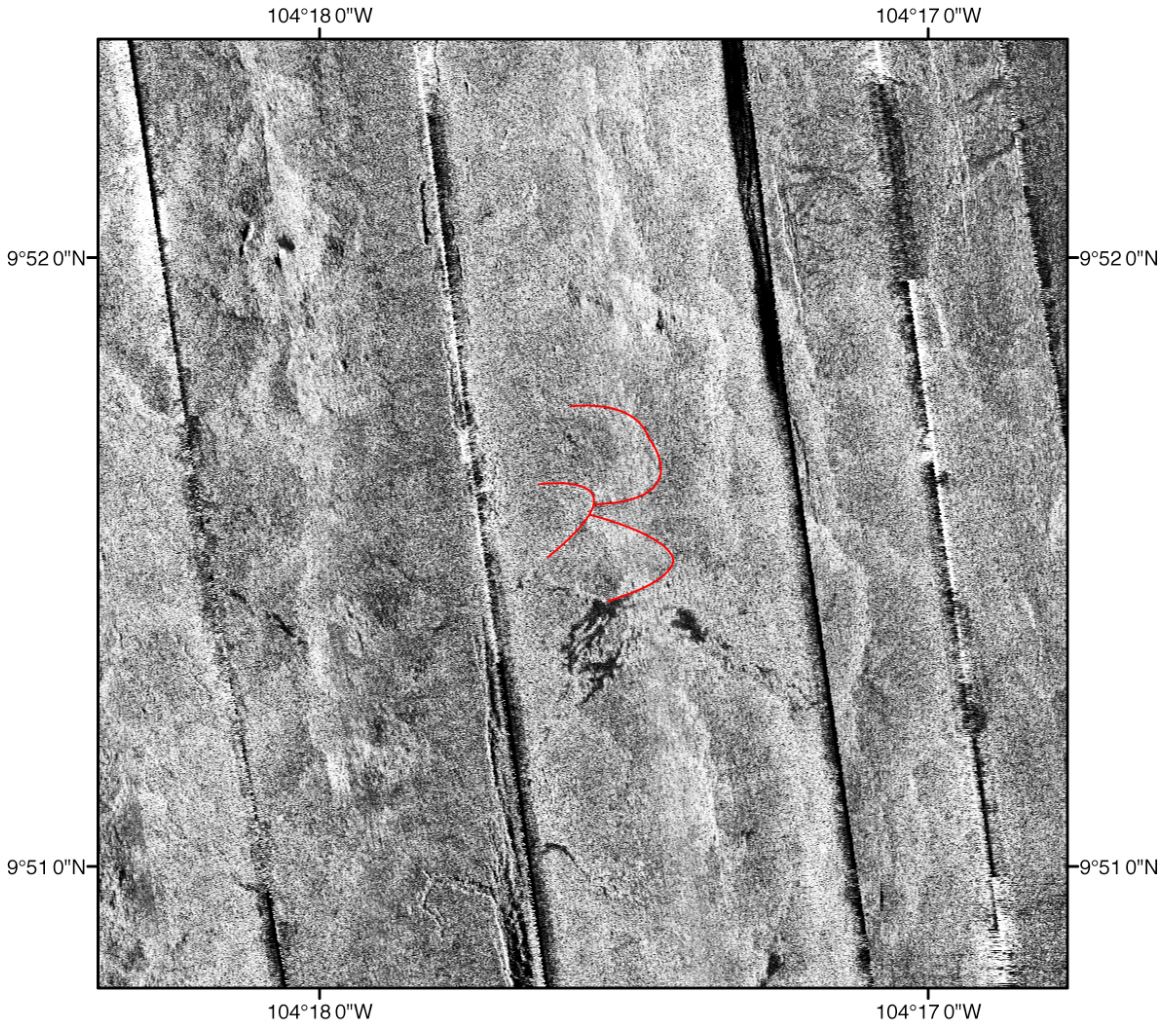

Figure 26. DSL-120A sonar imagery of the AST and EPR crestal plateau from 9˚ 51'-9˚ 52'N collected on cruise AT7-4. Overlapping flow fronts are visible on both sides of the AST; a few flow fronts have been highlighted in red. Linear, black (low backscatter) areas are lava channels. Northern terminus of the AST is seen along the middle of the bottom edge of the image.

6.2.2. Flow front descriptions

In contrast to most previous *Alvin* campaigns in this area, we began many dives off-axis and proceeded towards the axis in hopes of better identifying lava flow fronts. This method, along with planning dives to encounter flow fronts as detected from sonar and micro-bathymetry, proved successful and allowed observations and sample collection at >25 distinct lava flow fronts (Table 9). Flow fronts were encountered at distances from ~200-2000 m from the AST. In most cases we found that the margins identified in the sonar and micro-bathymetry records were readily identified in the field by both topographic and morphologic changes in the lavas. At many sites we were able to collect sample pairs of the flow front lava (pillows) and the underlying flow (lobates) as well as the lobates upslope from the flow fronts. At many of the sites we conducted Imagenex and photomosaic surveys.

Flow fronts range in height from 1.5-10 m and possess much steeper slopes (10°-45°) relative to the adjacent flow tops (0-4°) (Figure 27). Flow fronts are also identified by a morphologic transition from lobates and sheets on the top of the lobe to pillows on the flow front [e.g. Sinton et al., 2002]. Pillows are often elongate (tubular) or flattened on the upper reaches of the flow front and grade to equi-dimensional at the base. Very localized sheets that

cascade down the steepened pillow slope occasionally interrupt the otherwise monotonous pillow flow fronts.

Dive #	Lat	Long	Imagenex	Photo	Samples
3963	9.8436	-104.2734	Y	Y	N
3963	9.8424	-104.2753	Y	Y	3963-4,5,6
3963	9.8407	-104.2788	Y	Y	3963-7,8,9
3963	9.8383	-104.2831	N	N	3963-10
3965	9.8283	-104.2756	N	Y	3965-1, 2,6a,b
3973	9.8369	-104.2897	Y	Y	Y
3974	9.8372	-104.3050	N	N	Y
3971	9.8406	-104.2787	Y	Y	N
3970	9.5120	-104.2330	Y	N	3970-1,2

Table 9. Locations of some flow fronts examined during the AT11-7 cruise. See Figure 5 for dive locations.

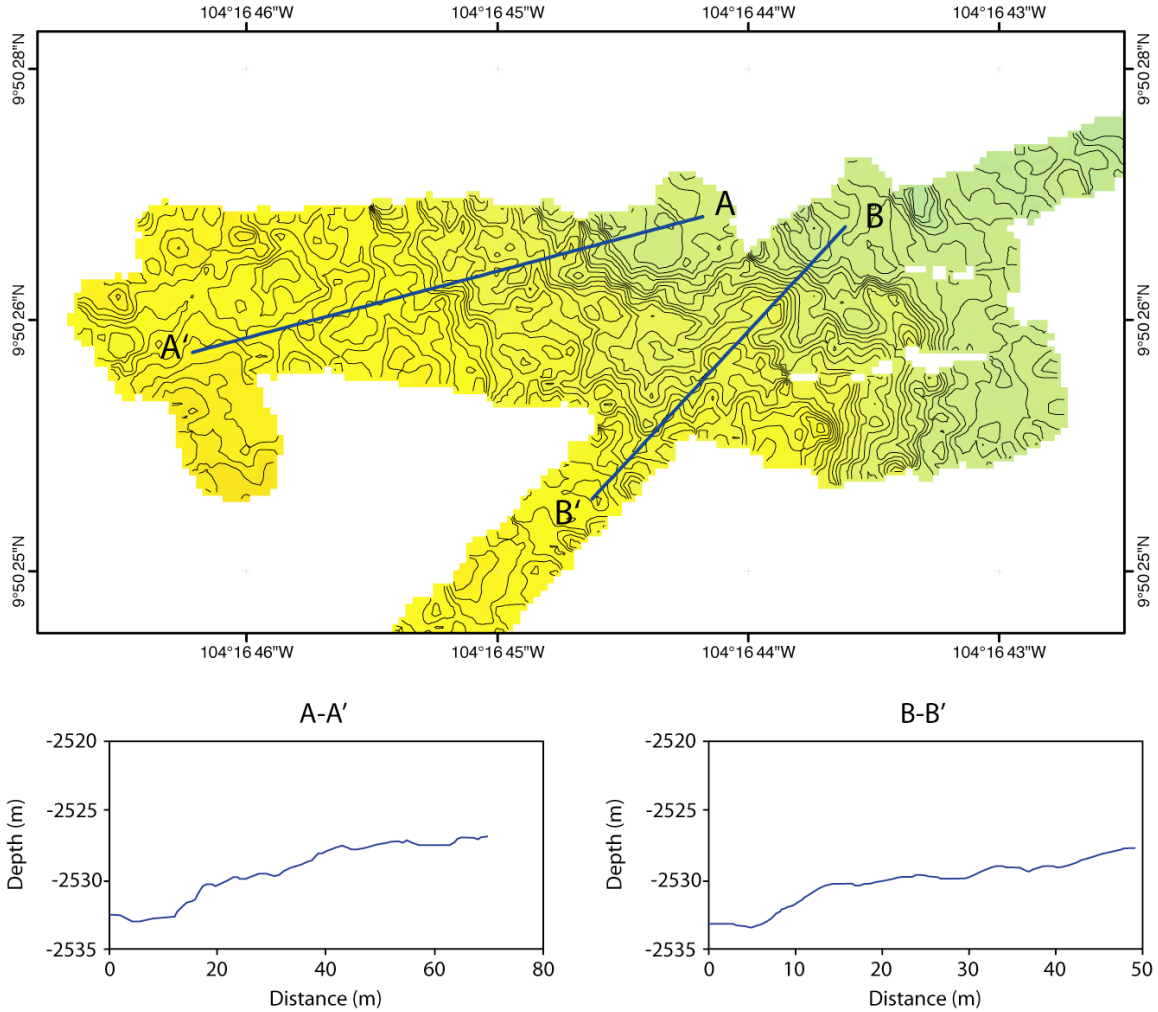

Figure 27. Imagenex bathymetry survey over a lava flow front near 9˚ 50.5'N, 104˚ 16.7'W collected on dive 3963. Profiles A-A' and B-B' cross the flow front at two locations and show the relative increase in slope at the pillowed front versus the adjacent lobate flows.

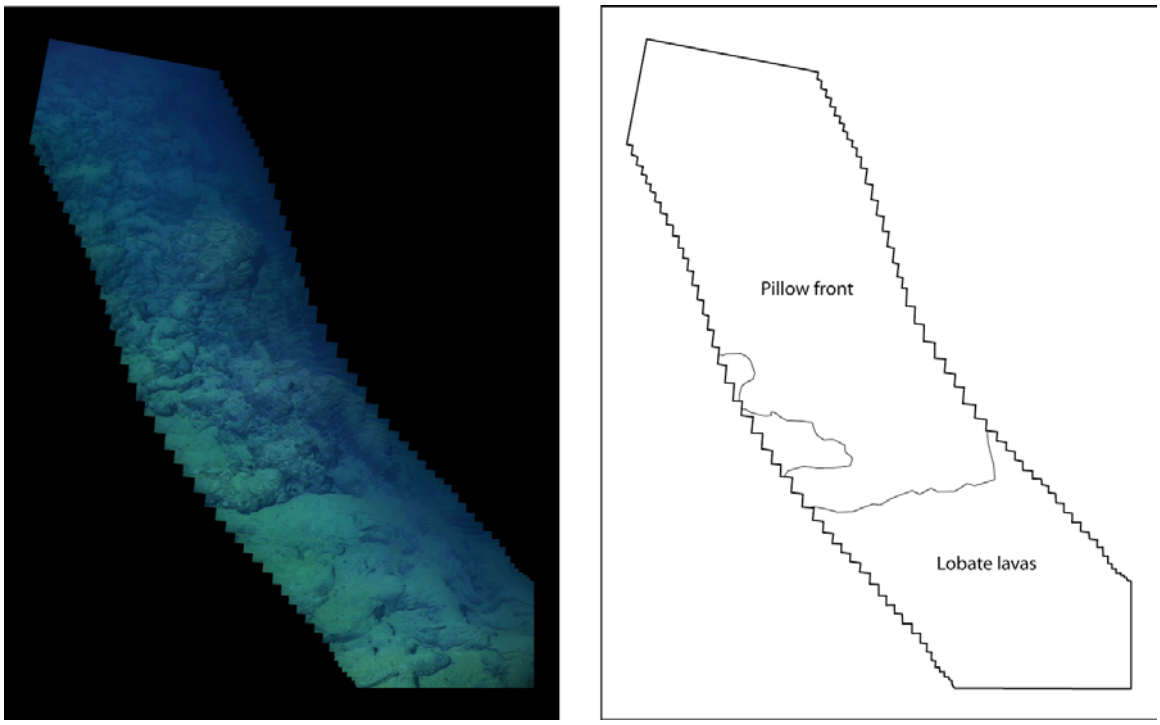

Figure 28. Photomosaic created from 3-chip digital video collected on dive 3963 showing a pillowed flow front overlying lobate lava from a previously emplaced flow lobe (see also Figure 19).

The relationship between the pillow lava at the front and the lobate and sheet lava upslope was, in most cases, unequivocal with lobes grading directly into pillows, indicating a temporal sequence of lobate advance followed by late stage pillow emplacement. There was generally a slightly thicker sediment cover on the lobate flows relative to the pillows that we attribute to the greater slope and surface roughness of the pillows preventing thick sediment accumulation. In some cases, the upper surface of the lobe contained a central channel that appeared to feed the flow front. The lobate flows bathymetrically below the flow front appear to be covered by the advancing pillow front (Figure 28) suggesting earlier deposition.

6.2.3. Lava Channels

Indirect evidence that off-axis lava transport is a common phenomenon on the EPR between 9°-10°N has come from several research avenues. Seismic imaging of the upper crust indicates a doubling of layer 2A, a low-velocity layer of extrusive volcanics, from 0 to 3 km away from the axis. Near-bottom magnetic data indicate a highly magnetized zone, believed to correlate with lavas erupted in the last 5 ka, that extends 1-2.5 km off-axis. Finally, isotopic concentrations (Sr, Nd, Hf, Pb, and U-series disequilibria) indicate ages of lavas up to 4 km off-axis much less than their predicted spreading age of 15-45 ka [Sims et al., 2003]. Based on examination of the sonar and micro-bathymetry records from AT7-4, we hypothesized that the ubiquitous dark (low-amplitude sonar backscatter) and linear trough-like features resolved in the micro-bathymetry represent lava channels that mark regions of focused, high-flux rate lava transport that could facilitate off-axis lava deposition (Figure 29). The aspect ratio (length:width) of these features is variable. We interpret the segments that are much longer than they are wide and are oriented (nearly) perpendicular to the AST to be lava channels. Others may be segments of channels, ponded lava flows, or collapse features floored by lava sheets. We have made detailed examinations of channels, i.e. Imagenex 675 kHz altimetric surveys, digital still photo and video documentation, and sampling, at seven different locations on 5 different channel systems (Table 10), and cursory examinations at a handful more sites.

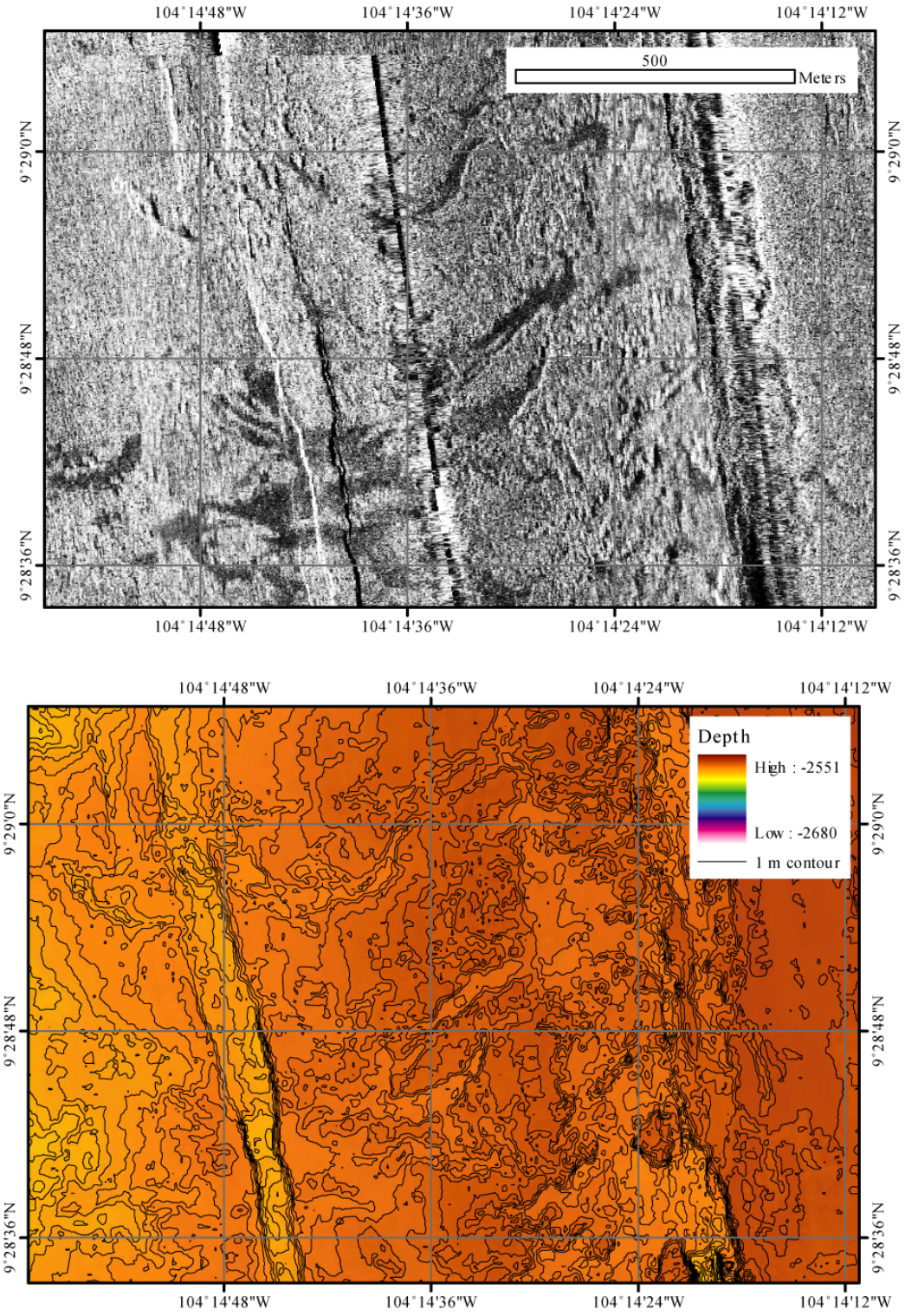

Figure 29. Sonar (top) and micro-bathymetry (bottom) showing several channels at 9° 28'N. Channels are identified as sinuous dark features in the sonar image and as linear depressions in the micro-bathymetry.

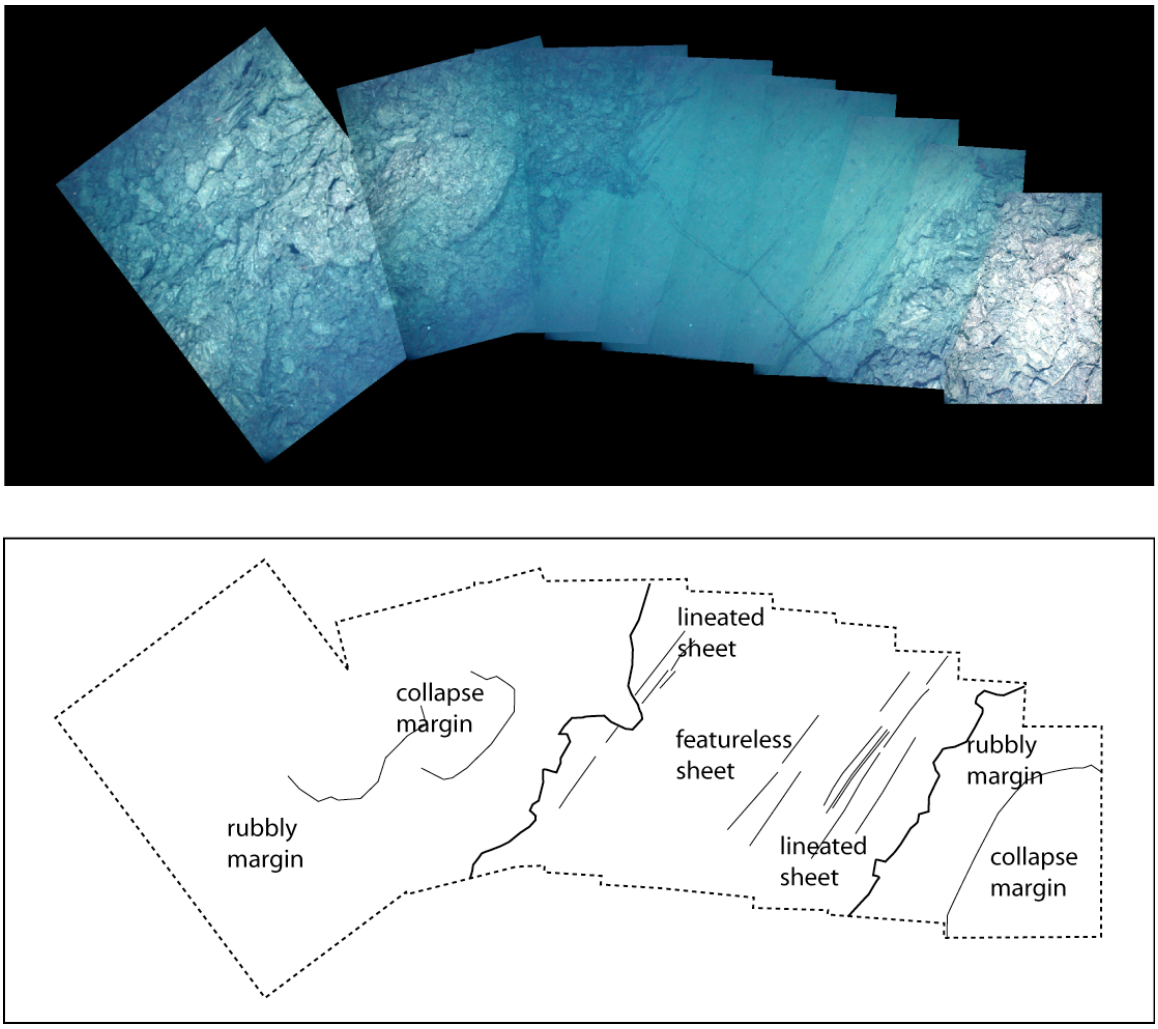

Figure 30. Mosaic across a channel created from down looking camera images collected on dive 3968. Below is a map of the image showing the distribution of surface morphologies across the channel. In this case, jumbled/hackly lava on the channel margins has spilled into the channel interior obscuring an unknown portion of the lineated and or folded flow.

6.2.3.1. Lava Channel Descriptions

The gross organization of lava surface morphologies within and surrounding the channel is similar at each of the sites examined with *Alvin* (Figure 30). The following description of surface morphologies within the channel will proceed from outside of the channel to its center. In most cases, the distribution of surface morphologies within the channel is nearly symmetrical around a presumed centerline. Channels are surrounded on both sides by lobate lava, that is often collapsed. The outer margins of the channel are composed of jumbled or hackly lavas (Figure 31) that appear as elongate strips parallel to the flow direction. The strips comprise from 5-20% of the total channel width. In each channel, the jumbled material is bathymetrically above the central portion of the channel and in one case appears to be bathymetrically above the surrounding lobate lava as well. At some sites we observe a band of folded lavas, again parallel to the overall channel orientation, adjacent and grading into the jumbled region. The folds in this region are chaotic and did not reflect a dominant flow direction (Figure 32). Where visible, this region comprises 5-10% of the total channel width. Where this region was not visible, there was some indication that the marginal, jumbled lavas had spilled onto the sheets and may have been obscuring the folded region. Further towards the

channel center we observe a region of lineated sheets. The lineations are parallel to the flow direction and appear to be continuous for many meters. Contrary to the model described by Chadwick et al. [1999], these lineations appear to be folds in the lava crust rather than scrapes produced by overlying crust as the lava was extruded. The folds appear to be recumbant with the hinge of the fold oriented parallel to the channel surface and the open end of the fold towards the channel margin. The folded regions comprise 15-40% of the total channel width and accommodated most of the relief of the channel often sloping at nearly 45˚ from the channel margin to the channel center. The folded region grades into the central portion of the channel that is characterized by nearly featureless sheet lavas that comprise 5-20% of the total channel width.

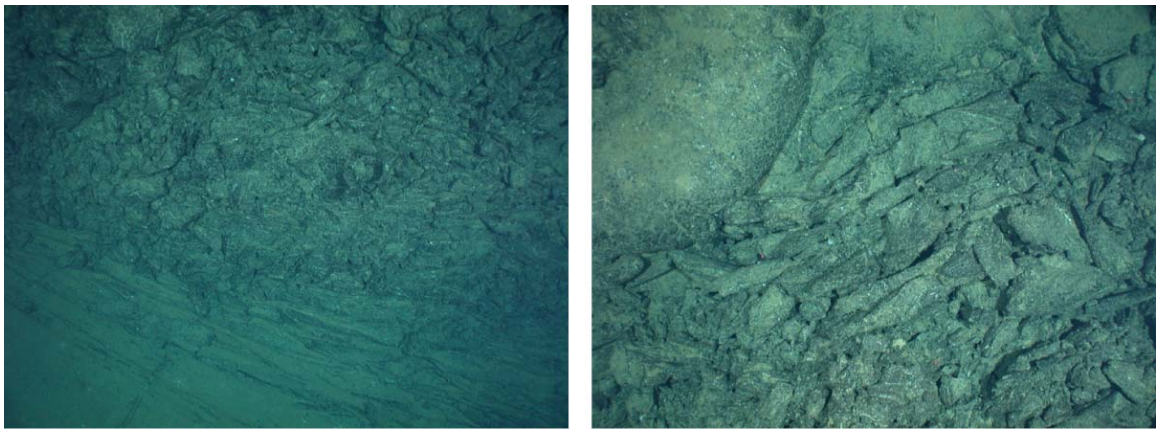

Figure 31. Consecutive down looking camera images collected on dive 3968 showing the transition from lineated sheet to jumbled sheet lava (left) as well as the intimate connection between the jumbled and lobate lava at the channel margin (right). Scale across left image is ~ 3m, and across right image is ~ 1.5 m.

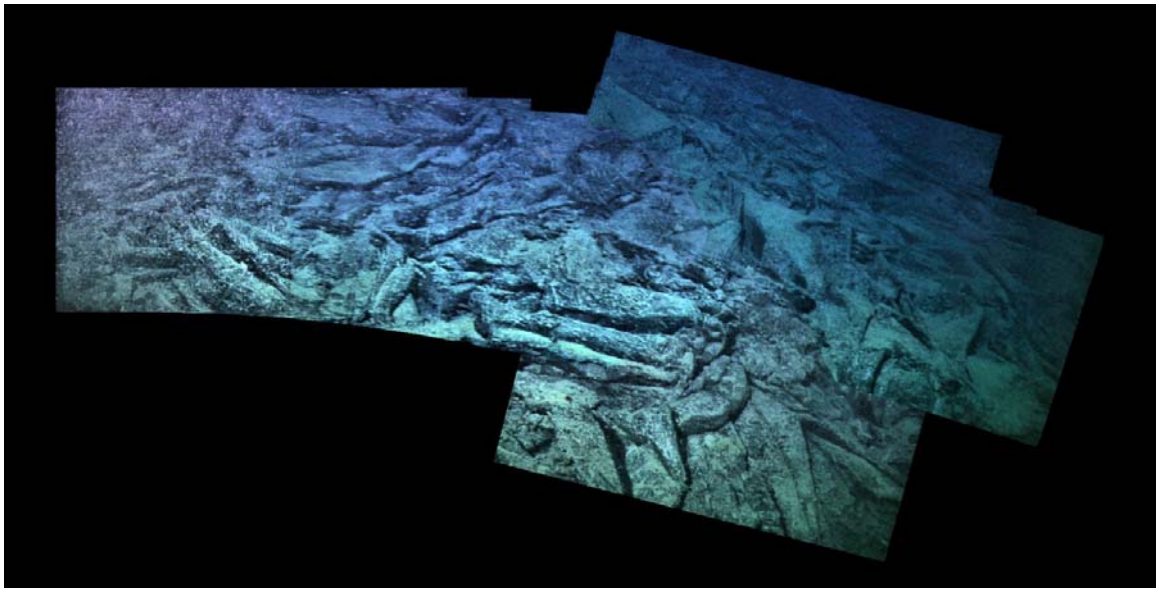

Figure 32. Mosaic of 3-chip digital video collected on dive 3968 shows the chaotic ropy folds between the lineated and hackly portions of the channel.

Dive #	Lat	Long	Imagenex	Photo	Samples
3968	9.4783	-104.2417	Yes	Yes	3978-2,3
3968	9.4825	-104.2433	Yes	Yes	3978-4,5,6
3968	9.4828	-104.2462	No	No	3978-8,9
3968	9.4853	-104.2419	N	Yes	3978-10
3973	9.8371	-104.2895	Y	Yes	none
3963	9.8383	-104.2808	Y	Yes	Yes
3966&3971	9.7233	-104.2592	Y	Yes	Yes

Table 10. Locations of detailed lava channel observations during AT11-7.

In the sonar record channel features are rarely continuous for >1 km. In addition, many channels appear to initiate some distance from the AST (200-500 m) despite the AST being the presumed lava source. We focused some of our observations on ascertaining the relationship of channels with surrounding lavas to address some of these feature characteristics from the sonar record. We find that in most cases, there is an unequivocal genetic link between the channel material and the surrounding lobates at the channel margin. There, lobate lavas grade directly into the hackly, jumbled margins of the channel (Figure 31). In several cases, the boundary between lobate lavas and the channel margin is one of collapse [Cormier et al., 2003]. Still, at these margins, the talus at the channel margins (or lack thereof over much of the channel surface) suggest that collapse occurred locally at the channel margin and after the emplacement of the channel.

The head of a lava channel was observed in two instances (9˚ 40'N- dive 3971 and 9˚ 50'N- dives 3973, 3976). In both cases, the channel initiated ~200 m from the AST, and in both cases the sheet lavas of the channel were covered by lobate and pillow lava (Figure 33). The timing of this relationship is clearly that the channels were formed first and later covered; however, it is not clear whether the later lavas are from a separate flow or represent the last stages of the eruption that produced the channelized flow. The distal ends of the channels were observed in two locations at distances of 750 m (9˚ 28'N, dive 3968) and 500 m (9˚ 50'N, dive 3976) from the axis. In the former, the channel is truncated by a fault at the E margin of the western graben (Figure 34) and in the latter (9˚ 50'N), it is covered by the same episode of lobates and pillow flows as is covering the channel head.

6.2.4. Lava Flow Front and Channel Discussion

In simple terms, the spectrum of surface morphologies observed on lava flows represent a balance between the competing forces of crustal formation, determined by cooling rate, and crustal disruption, determined by lava advection rate [e.g. Peterson and Tilling, 1980; Kilburn, 1981; Fink and Griffiths, 1990; Gregg and Fink, 1996]. Pillow lavas represent crustal formation dominating crustal disruption and featureless sheets represent crustal disruption dominating crustal formation. Lobate lavas and folded sheets lie between these two end members. Jumbled lavas likely represent a different mechanism of formation whereby folded sheets are further disrupted after the crust has developed causing the folds to break apart. We are able to infer something about the dynamics of lava transport from our observations of surface morphologies on lava flow fronts and in lava channels.

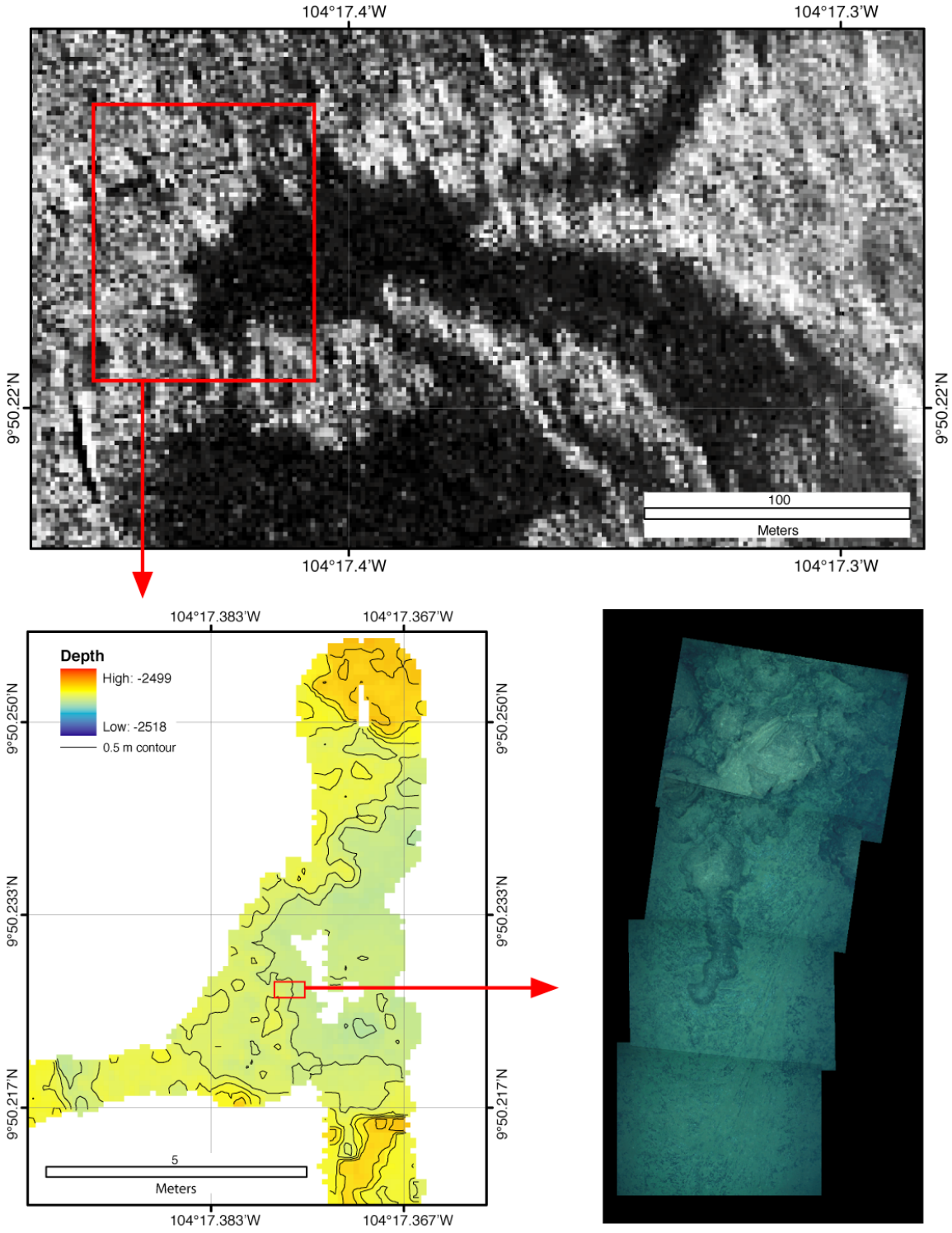

Figure 33. DSL 120 side scan sonar, Imagenex microbathymetry, and photomosaics show the head of a major channel system at 9˚ 50'N. The channel (sheets in photomosaic) appears to be overrun by a later pulse of lava characterized by lobates and pillows. Location boxes are approximate.

The lava flow fronts we examined represent lava transport over short distances. The bulk of each flow lobe is composed of lobate and sheet lavas suggesting that flux rates rapid enough to not produce pillows, but low enough not to channelize and produce sheet flows. At each flow front there is a transition to pillow lavas indicating considerably lower flux rates. The reason for the rapid decline in flux rate could be due to either 1) a cutoff of effusion at the source, or 2) the development of thickened crust that the lava must squeeze through. The implications of each model are important for understanding the construction of the ocean crust. The first model suggest that flow lengths are volume limited and that each flow lobe, or set of contiguous lobes, represents a discrete eruption and the second suggests flow lengths are cooling limited and that each eruption may produce any number of discrete flow lobes. As a note: we consider overflows from the AST at a single location to be a single eruption.

The fact that pillowed flow fronts occur at variable distances from the AST (200 m to 2 km) suggests that volume-limited model may be more appropriate. Assuming similar eruption temperatures, the rate of crustal growth should be equivalent thus cooling limited flows should be of similar length. The variability of flow thicknesses at the front implies that the crust has developed some confining strength, however, these differences are likely attributable to differing volumes of down-flow drainage after the volume at the source has been cut-off.

Lava channels represent regions of focused flow that often form within larger lava lobes or sheets of lava [Soule et al., 2004]. In addition, it is not uncommon in subaerial channels for flow velocities to be several times greater within the channel than at the flow front or in the surrounding lobe. It is generally accepted that in submarine lavas, sheet morphologies—as are observed within the channel—represent faster flowing lava than lobates—that are observed surrounding the channel [e.g. Gregg and Fink 1996]. Thus we conclude that submarine channels represent greater volume fluxes and flow velocities than the surrounding lava. Our observations suggest that the channels and surrounding lobates are intimately linked and most likely form during the same eruption. The down-dropped nature of each channel (Figure 35)—often manifested as collapse at channel margins—suggests that the channelized portion of the flow remains an active region of transport for long durations of the eruption and that after the lava supply has ceased the channel network can be preferentially drained and deflated relative to the surrounding lobate lavas.

Within the channels, we observe a transition in surface morphology from jumbled to folded to lineated to featureless sheets as we move from the margin to the interior. It is likely that this transition reflects changing rates of shear across the channel. Viscous fluid flowing in a channel will generally have a parabolic velocity profile with the greatest velocities in the center of the channel and the lowest velocities at the margin. This produces a shear rate profile across the channel that is highest at the margin and lowest at the center. It is likely that the distribution of surface morphologies we see across the channel surface reflects a similar distribution of shear rates. Here we propose processes that might cause the observed variation in surface morphology across the lava channels. At the margin of the flow, crust is disrupted soon after it forms. This process of making and breaking crust results in piles of jumbled and broken fragments that may even accumulate into levee-like constructions. It is also possible that some of this fragmental material is torn from the stagnant lobate crusts bounding the channel. Moving inward, the crust becomes chaotically folded and represents slightly lower rates of shear that are able to fold, but not fragment the crust. Further inward, the lava is lineated in the direction of flow. It appears that the some of the lineations are folds that have

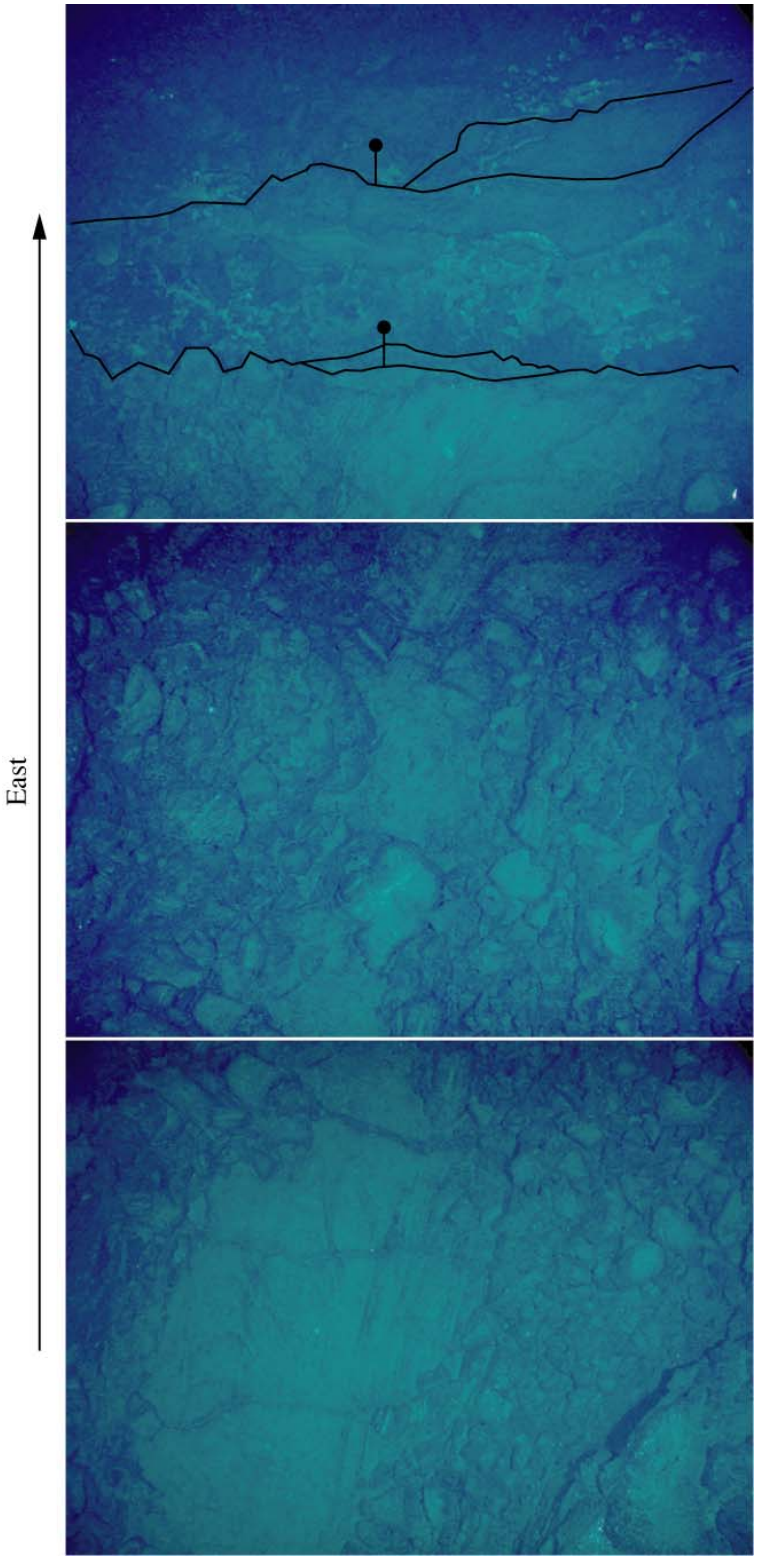

Figure 34. A series of consecutive *Alvin* down looking camera images from dive 3968 show a lava channel truncated by a normal fault at the eastern wall of the Western Graben identified from side scan sonar and microbathymetry collected on AT7-4. Photos are taken at 10 second intervals, are approximately 5 m across, and the series shows a track ~25 long. Black lines indicate fault steps, with the down dropped side shown by a black circle.

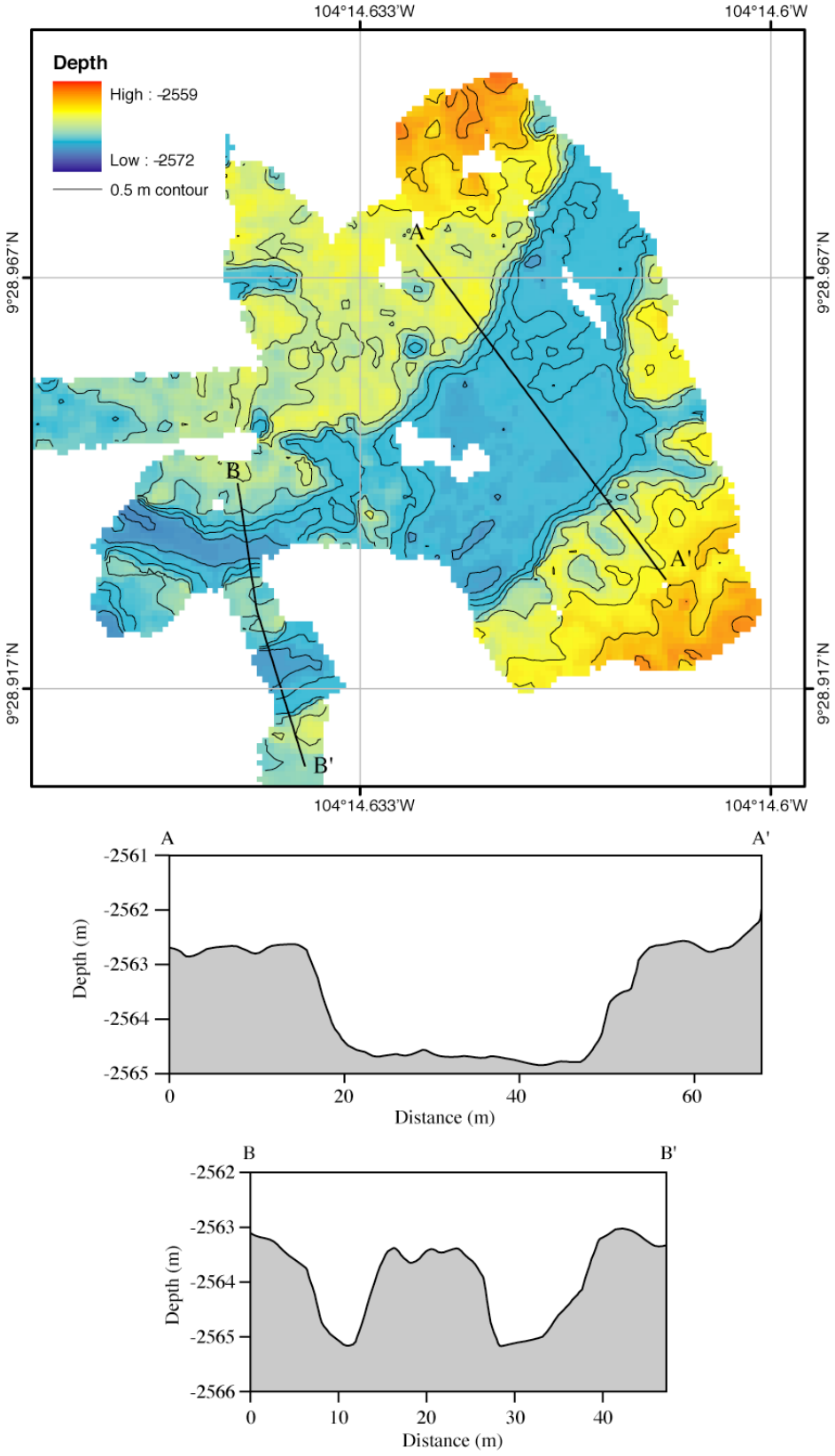

Figure 35. Imagenex bathymetry survey over a lava channel at 9˚ 28.95'N, 104˚ 14.625'W collected on Dive 3968. Profiles A-A' and B-B' cross the channel at two locations and show the down-dropped (i.e. deflated) topography. At A-A' the channel is ~25 m wide and 2.5 m deep. At B-B' the channel is split by a high standing central region that may reflect movement of the channel location, or an obstacle around which the lava flowed.

been sheared in the direction of flow. However, shear rates in this portion of the channel should be lower than at the margins where shear rates were clearly not large enough to shear out folds in the direction of flow. Instead, it appears that rates of crustal formation were lower in this portion of the channel. This could be due to a thermal gradient that reflects differences in flow velocity across the channel. Alternatively there could be lateral advection of the lava in the channel as has been observed in analog experiments. This would also explain the form of these elongate recumbent folds described above. In the central part of the channel, low shear rates and crustal growth rates lead to the featureless sheets that are present in the central portion of all the sheets examined (Figure 36).

The observation that channels are formed during submarine eruptions on the EPR [e.g. Cormier et al. 2003], and that they may represent regions of sustained high volume flux provides a mechanism to efficiently transport lava up to ~2 km off-axis. The fragmental nature of the lava within the channels and the overprinted heads and tails of each channel examined suggests that the full extent of these channel systems has yet to be observed. In addition, we have not observed any direct correlation between channels and the expected off-axis depocenters associated with them. Our observations of lava flow fronts, especially the transition in morphology from lobate to pillow lavas, suggest that near-axis lavas represent small volume short duration eruptions. Laboratory analyses of flow front samples will aid in our understanding of the genetic relationship between adjacent flow fronts and the processes of near-axis lava deposition.

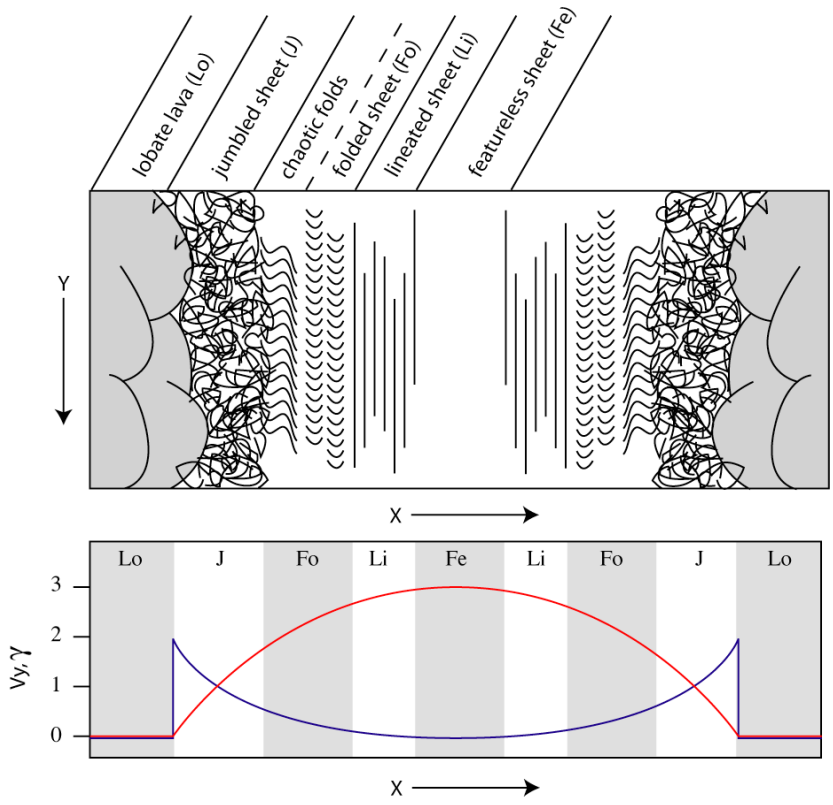

Figure 36. (Top) Schematic diagram of the plan view distribution of surface morphologies across a typical channel surface. Morphologies are distributed symmetrically around the channel axis and boundaries are gradational. (Bottom) Schematic plot of lava dynamics across the channel surface including: downflow velocity (Vy, red) and shear rate (g, blue). Morphology boundaries are shown by alternating grey and white bands and labeled in the shorthand defined in the plan view diagram.

6.3. Faults and Fissures

Tectonic deformation in the vicinity of the AST is scarce and characterized a) by fault scarps associated directly with the AST, b) by inward-facing faults with generally small vertical throw (<10m in general, reaching ~30 m or more off axis), and c) by fissures with little or no vertical displacement that are sub parallel to the AST. Near-axis fault are probably covered by lava flows owing to their small vertical throw. Locally and further off-axis (>1 km) some faults develop scarp heights sufficient to block, deviate, and control the emplacement of lava flows flowing off-axis. Sonar images provide information on the polarity, structure and length of faults in plan view, while bathymetry obtained from the camera tows provide constraints on fault scarp heights, tilt of blocks, and shape of the AST.

6.3.1. Faulting and the AST

Most of the AST is characterized by a collapse trough whose width varies between <50 and 150 m, with a vertical downdrop of up to 15 m. Locally the AST is almost entirely covered by lava flows. At 9° 32'N the axial zone shows a zone of deformation ~1 km wide, characterized by numerous normal faults en échelon and oblique to the AST direction (~10-20°), and extending several km along the axis. These faults define numerous tilted horst and graben blocks (Figure 37), and crosscut several lava sheet flows (dark areas in the sonar map below). High-resolution bathymetry from camera tow #13 shows that fault scarps in this area are typically 2-4 m (<10 m in all cases).

6.3.2. Normal Faulting

Normal faults are scarce or of small vertical throw in the area of recent lava flows (bright areas in sonar images), between the AST and the off-axis, sedimented seafloor. Most of the near-axis faults are inward-facing, with vertical throws 1-5 m (<10 m), and only develop throws of 20-30 m at distances of more than 2 km from the AST **(**Figures 37, 38). Lava flows extending off-axis from the AST bury small fault scarps and fissures. This is indicated by the total lack or scarcity of fault scarps over areas where the new lava flows have been emplaced recently (bright areas in sonar images, e.g. Figures 37 and 39), while fissures and faults are well developed over the older, sedimented terrain (gray in backscatter images).

Additional evidence of fault burial by lava flows is found at 9°28'N (Figure 40), where the ridge shows a highly asymmetric character. Lava flows erupted at the AST has flowed to the West, owing to the asymmetry on the height of the walls bounding the AST at this location. The East flank shows well-developed faults that define two off-axis grabens; later lava flows partially in filled the graben closer to the AST (Figure 40). On the West flank a graben ~50 m wide has developed ~500 m from the AST. The faults that define it are linear and continuous over several km, and crosscut a preexisting lava channel (dark areas in sonar mosaic, Figure 40). Portions of these younger scarps provide depth sections of the different lava units (Figure 40, bottom), showing a complex pile-up of pillow/lobate flows, sheet flows, and laminar, discontinuous slabs that may correspond to hackly lava flows. These observations suggest that tectonic strain is small, as frequent volcanic eruptions repave the seafloor in close proximity of the AST, burying preexisting faults. Larger faults (scarps >10 m high) are more common off-axis, and usually occur within sedimented terrain that has not been overprinted by lava flows derived at the axis or sourced by off-axis eruptions.

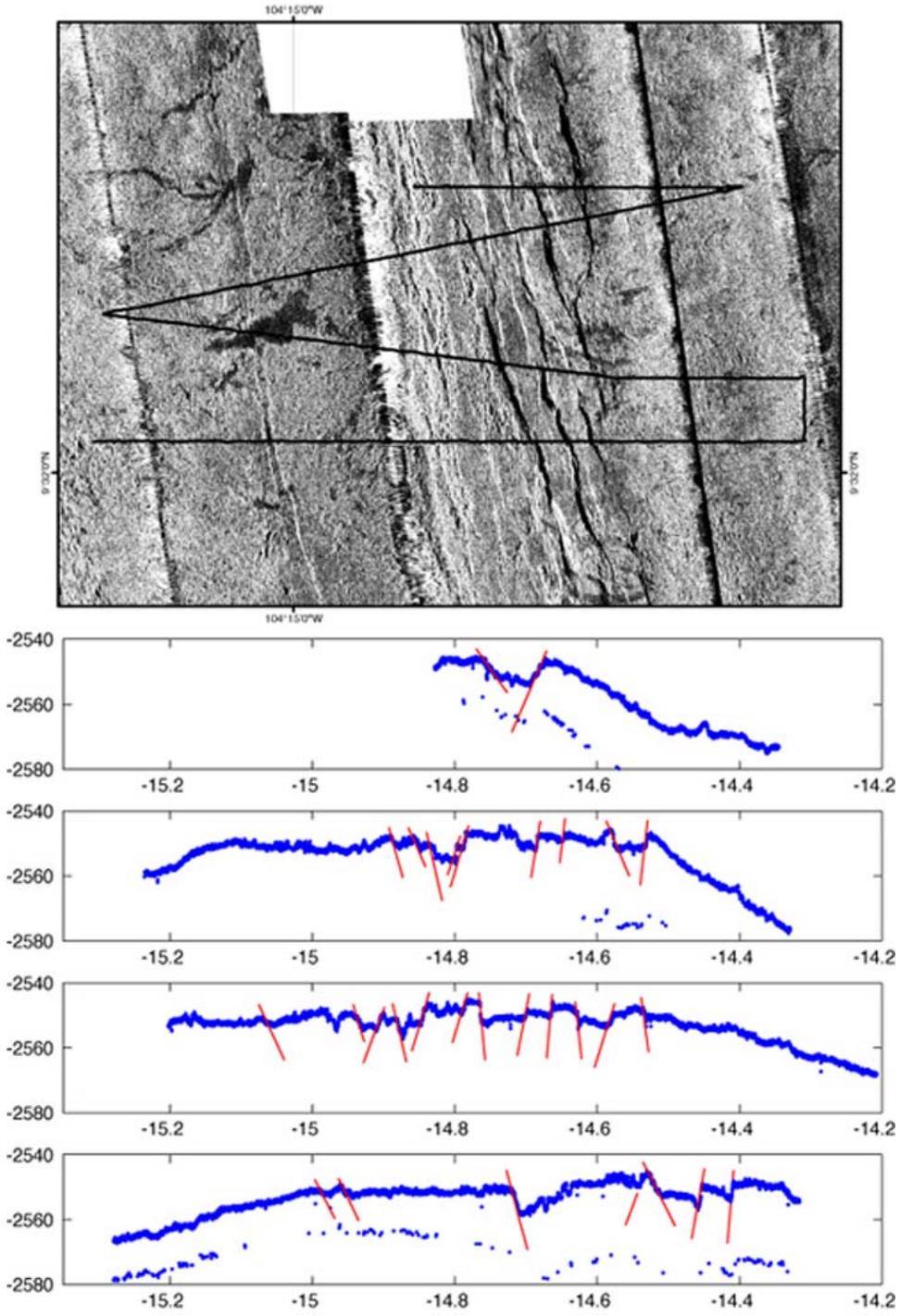

Figure 37. Across-axis bathymetry profiles (Camera Tow #13, bottom and corresponding sonar image with the TowCam track (black lines). Depth in meters along vertical axes. This section of the EPR shows a very wide axial area dominated by oblique faults (red lines) defining a complex series of horsts and grabens. Faults crosscut pre-existing lava channels and other young volcanic terrain.

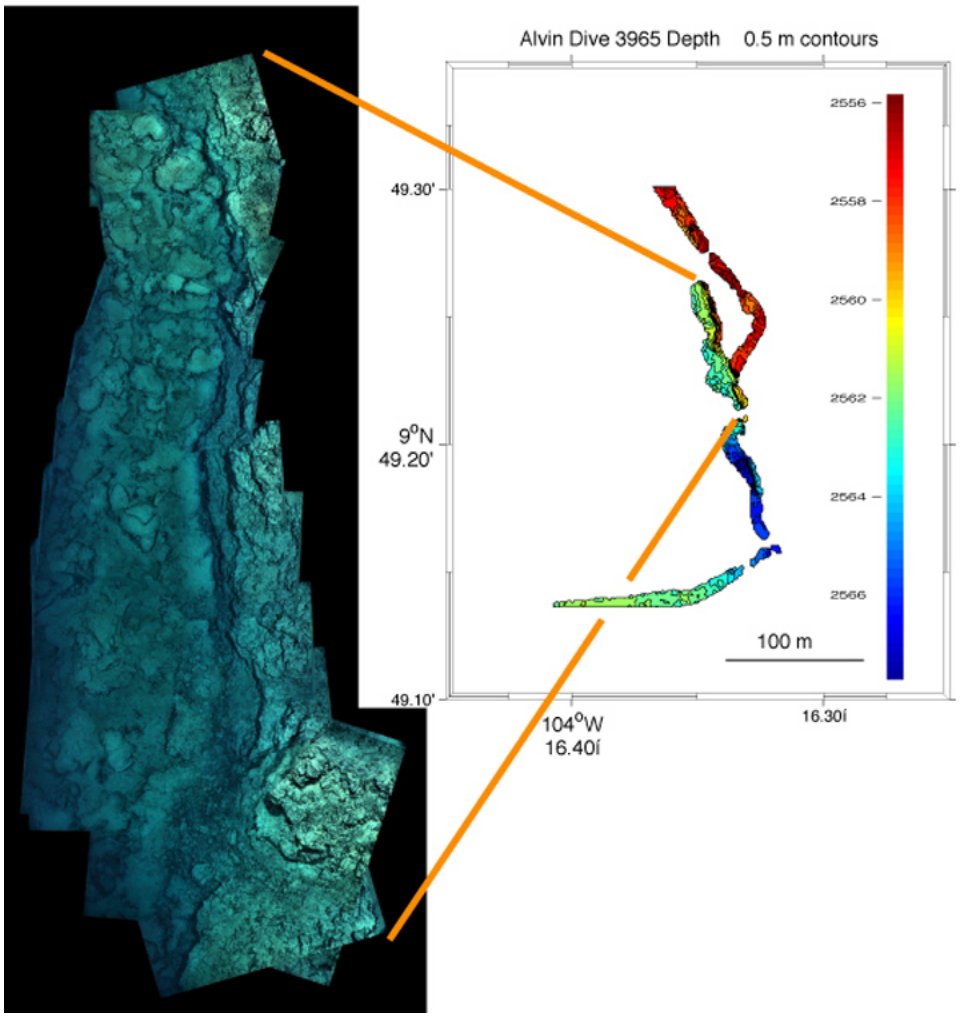

Figure 38. Normal fault scarp ~1.7 km east of the AST. Video mosaic of the fault scarp (left), and corresponding Imagenex micro-bathymetry (contour lines 0.5 m, *Alvin* dive 3965). The scarp shows a nearly vertical face with lobates and pillows but very little talus at the bottom, and has a vertical throw of ~8 m at this location.

6.3.3 Fissures

Fissures are most developed over old, sedimented terrain (gray areas in sonar maps, Figures 37, 39 and 41). While most fissures are sub-parallel to the AST trend, locally there are sets of fissures that fan radially or are highly oblique both to the AST and nearby faults (see yellow lines in Figure 39**)**. Spacing and width of fissures is highly variable. Heavily fissured terrain shows a close spacing of such structures of ~10-50 m, and the widths that vary from <1 m to >20 m. The lack of fissures near the AST indicates that these are covered by lava flows emanating from the AST and extending off-axis. In addition, we observe that pillow mounds are locally emplaced off-axis in several areas (e.g. near 9° 53'N and 9° 29'N) and cover previously fissured crust. Some of the pillow mounds are subsequently tectonized, with the development of new fissures sub parallel to those in surrounding areas.

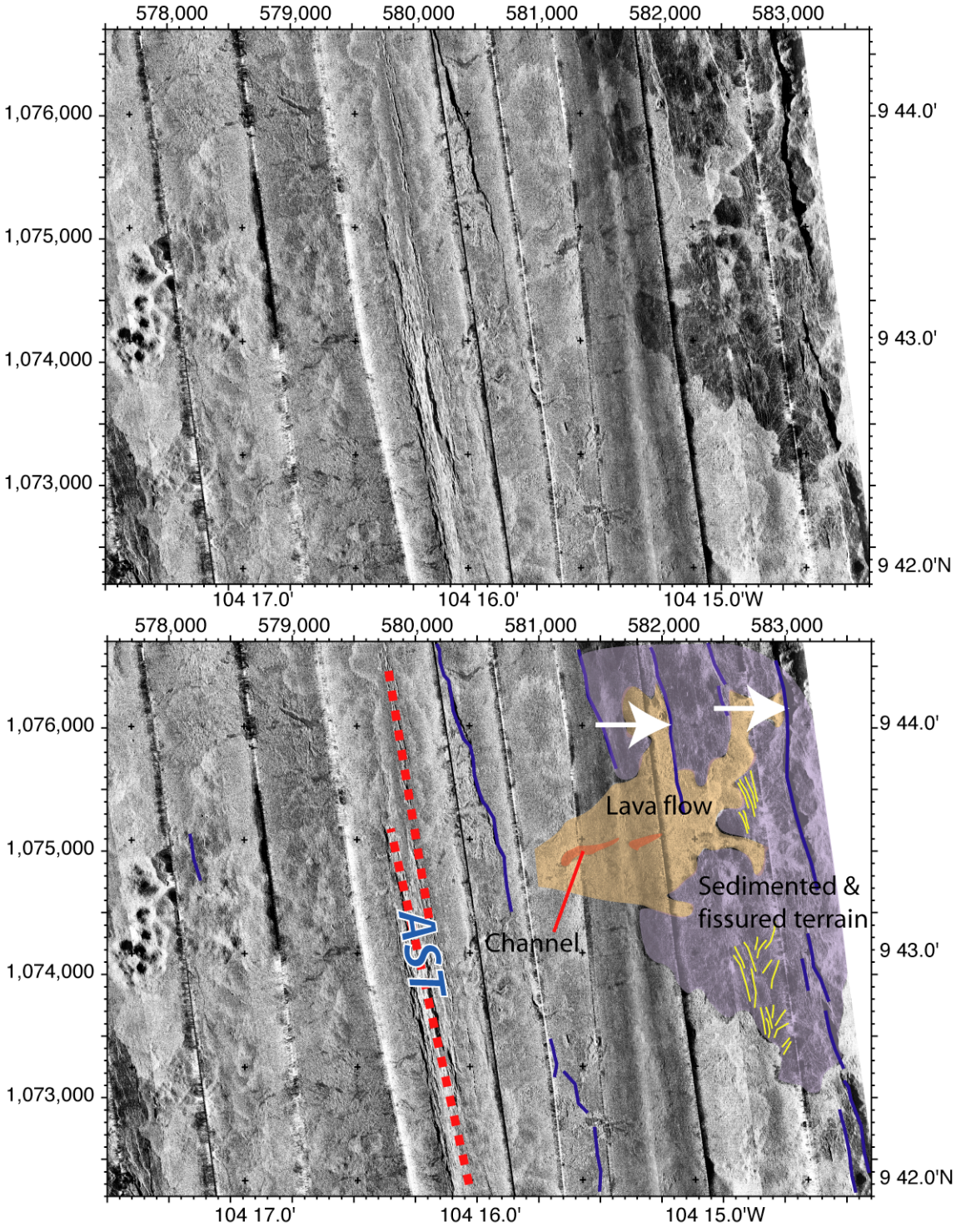

Figure 39. Lava flow that extends off axis ~2 km and crosses over older, sediment covered terrain is diverted by or ponds against off-axis fault scarps (white arrows). The sediment covered terrain is highly fissured (yellow lines); most fissures are axis-parallel, but locally they show curved traces highly oblique to the AST trend.

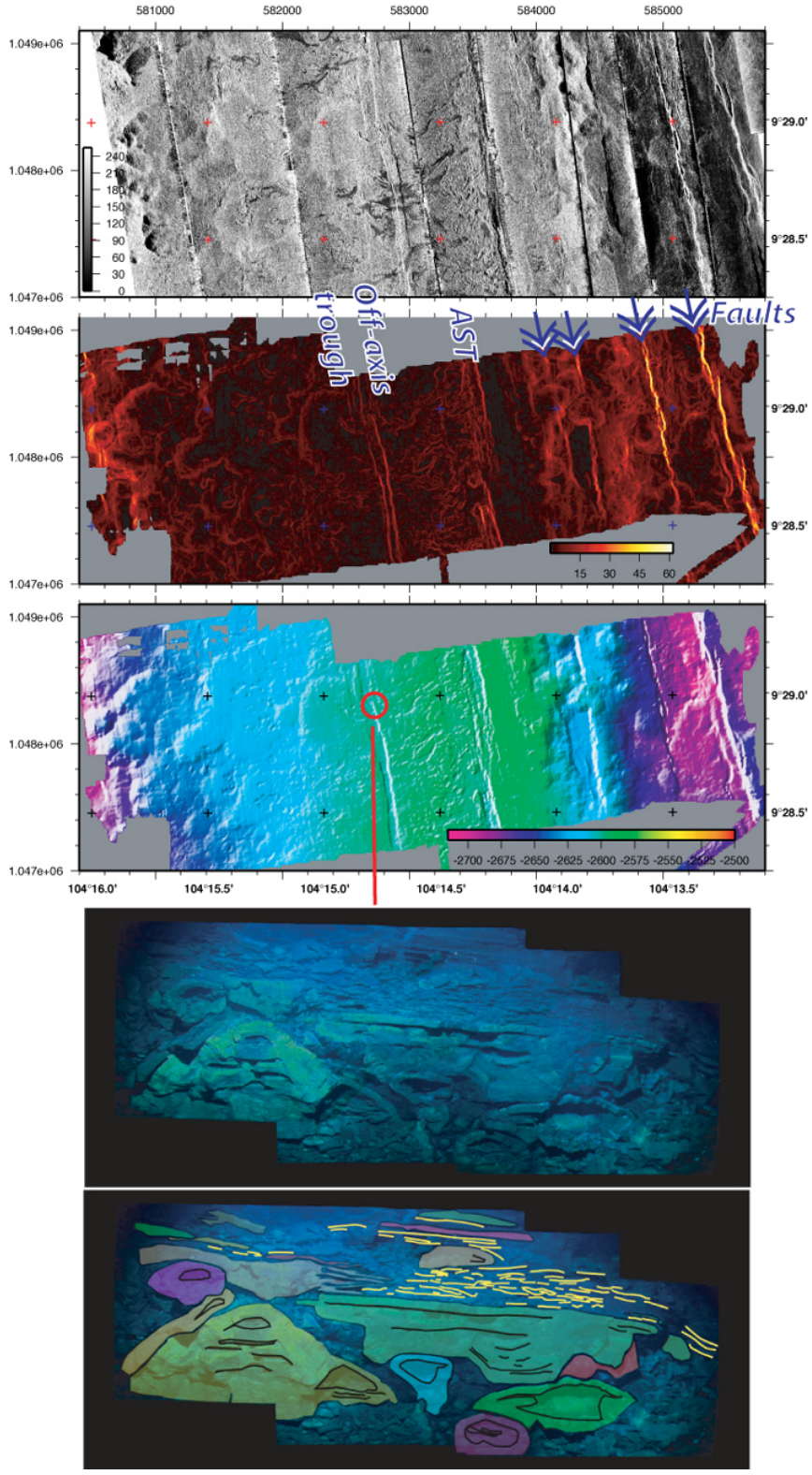

Figure 40. Top : Sonar, ABE bathymetry gradient and ABE bathymetry. Arrows indicate faults. Bottom: Video mosaic of an outward-facing fault scarp surface (location indicated by circle in ABE bathymetry). The volcanic stratigraphy shows a pile-up of pillow/lobate structures, flat-topped units (sheets?) and laminar slabs that are discontinuous and locally imbricated (yellow lines, selvages).

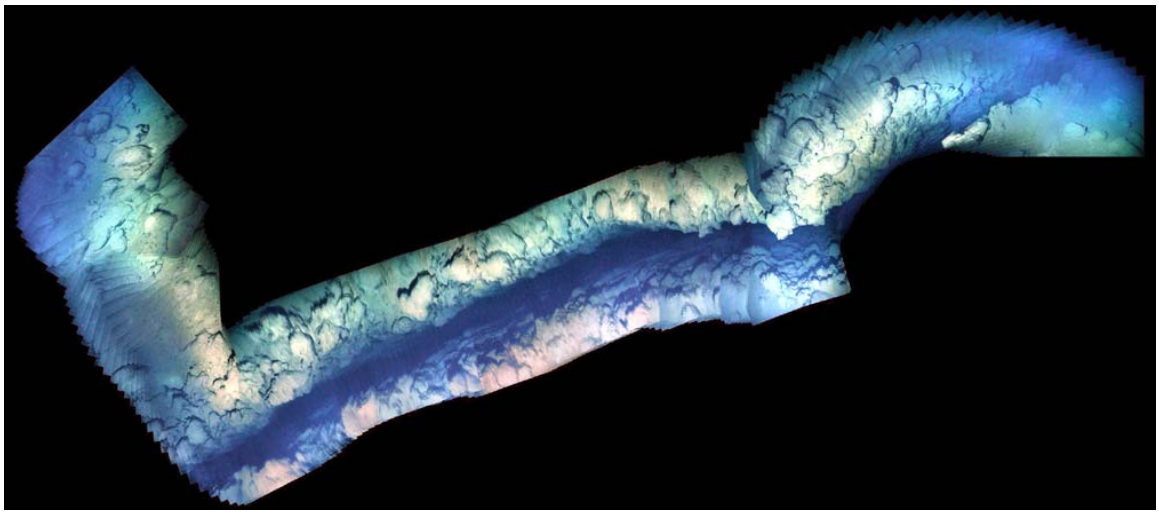

Figure 41. Fissure from *Alvin* dive 3970, ~2 km off-axis. The fissure is ~10 m wide and is sub-parallel to the AST.

6.4. Lava Samping and Petrology

6.4.1. Sampling Protocols

Ninety-five samples of lava (and one sulfide) were collected using *Alvin* (Appendix 9.3). Sampling of lava crusts was often difficult due to their extremely glassy nature so a "scoop" made with canvas netting on a steel frame was employed to pick up smaller fragments of some samples. Care was taken by the observers in conjunction with the pilot to ensure that the exact geologic and spatial setting for each sample was well documented. In addition, observers took images of the outcrop/flow where each sample was recovered. Times and locations (both geologically and in X-Y) for each sample station were noted in the divers' logs and checked against the times recorded on the video (frame grabs) overlays after the dives. Sample numbers correspond to individual dive numbers and specific places or stations on the seafloor (e.g. 3966-3 is the third station during dive 3966). Where multiple samples were recovered from the same feature/flow they were designated as "A", "B" etc. (e.g 3966-4A, 3966-4B). The final sample locations, based on time, were reconciled with the renavigated *Alvin* track positions (see section 3.3).

At the termination of each dive, samples of lava were carefully removed from *Alvin's* basket to ensure correct identification and to preserve the macroscopic features of each flow (e.g. glassy crusts, folding, Mn-coating). The sample location log and the basket map were used to ensure correct numbering of sample bags before samples were places on them. Before the samples were described and broken apart for sub-sampling, they were photographed using a digital camera. Multiple images of each sample are available as '.jpg' files in the cruise data compilation.

Most samples were large enough to show representative macroscopic features and textures. Typical sample weights were 1-3 kg but some were up to ~15 kg. Nearly all of the *Alvin* samples had ample amounts of glass that were separated for later chemical analyses. Samples that had no, or very thin, glass were designated as "WR" for whole rock. Care was taken to avoid contamination of the outer (surface that is upward facing) glass separates from the inner glass (surface downward facing that may have interacted with vapor). Where the two could be separated they were designated as distinct samples "o" and "i". Glass was removed by gently tapping the outer surfaces with a rock hammer or using steel chisels (where needed). Where sufficient quantities of glass existed, separates were put in whirlpacs in the following priority: 1. microprobe analysis (Probe), 2. other chemical analyses (Bulk), and 3.

paleointensity and U-series measurements (M-K) [e.g. Sims et al., 2003]. The greatest amounts were generally put in the Bulk packs. Probe and Bulk glasses were hand carried back to the Univeristy of Florida by M. Perfit; the M-K samples were hand carried by K. Sims to WHOI. A few samples of drips or inside glass were separated for analysis by SEM and were hand carried by I. Ridley. J. Maclennan hand carried some lava fragments that had crystal clots, micro-xenoliths, or phenocrysts for microprobe analysis. A listing of all of the samples recovered and their disposition is presented in Appendix 9.3. After each sample was described and sub-sampled it was placed in a labeled sample bag and put in a plastic bucket (each labeled with the sample numbers). All samples will be shipped to the Univerisity of Florida for curation and storage.

6.4.2. Sample Descriptions

Macroscopic and microscopic (using a hand lens) descriptions of each sample were recorded in a notebook that contains an image of the sample on the seafloor (taken from the *Alvin* framegrabs). The frame grabs associated with each sample locality have been compiled and will be linked to the Excel sample sheets. The descriptions include: approximate weight, degree of Mn-oxide coating (None, Light, Moderate, Heavy), thickness of outer glass, thickness of inner glass, presence of vapor-related features (e.g. drips, flanges, cusps, bubble walls), crystallinity and phases present in each lava sample, amount and distribution of vesicles, and any alteration that is present. A compilation of the sample locations, their field relations, and their descriptions is provided in Appendix 9.3.

6.4.3. Petrographic Features, Lava Morphologies and Macroscopic Features

Recovered samples were categorized into three basic types based on their gross morphologic features: pillow, sheet and lobate. Sheet lavas or sheet flows can further be categorized (in order of more deformation and disruption) as: flat, ropy, folded, jumbled, and hackly. Jumbled sheets are those where the folds and ropes so commonly seen on sheet flows are pushed together in piles but are still distinguishable as individual folds or ropes whereas in hackly flows, the sheets are so contorted and brecciated that individual folds are unrecognizable

Lava morphologies observed during this dive series conform to those previously described for this area since 1991 [Fornari et al., 1998; Kurras et al., 2000, Engels et al. 2003]. However, it is clear from our seafloor and subsequent shipboard observations of lava hand-samples that the standard distinctions between pillows, lobates and sheets are not as clear-cut as previously thought. There were many instances where we documented transitional changes in morphological characteristics from pillows into lobates, and lobates into sheets within what was presumed to be the same lava flow. The clearest changes occurred in the rapid transitions from flat sheets to ropy and folded sheets into jumbled and hackly samples. These often occurred at the margins of channels but were also observed in the middle of complex sheet/lobate terrain. Less clear transitions occurred between well-formed and textured pillows that became flattened, less textured and more tubular so that they looked like lobate flows. This commonly occurred where the steep slopes of pillow walls or mounds changed to flatter areas such as on the tops of flow fronts or pillow mounds. A few samples described as “pillows” based on observations from *Alvin* had features that looked like the crusts of typical lobate samples. Many of the pillow lavas observed during the dives had classic bread crust surface textures and were well decorated with glassy, knobs and fingers that commonly extruded from the base of the pillow. In regions with steep slopes (which may be flow fronts or side of pillow mounds/ridges) pillows formed long tubes that were elongated in a down slope direction.

Truncated pillows were also the most common lava form observed in fault scarps away from the AST.

Lobate flows appeared to transition into ropy sheets in some places and some samples of lobate crusts had folded glass surfaces identical to sheet lava. A major conclusion deduced from these observations was that individual flows or flow units likely have a variety of morphologic facies. At this point it is still unclear if pillows can be transitional to sheet or vice versa. Observations suggested the pillows commonly flowed over sheets but there were some indications (e.g. Dive 3966) that pillows may have been extruded from fractures in a hackly flow suggesting they might represent the final eruptive products of a flow unit.

In general flat, ropy and folded sheet flows tend to have low relief (<<1 m) whereas the jumbled and hackly facies of sheet flows can have relief of a meter or slightly more. This is a consequence of their formation by the deformation and accumulation of flatter sheets into chaotic piles, irregular ridges, and mounds. In some instances these piles resemble subaerial lava pressure ridges, levees, or tumuli. Inspection of individual hackly samples shows them to be complexly deformed with parts of samples being multiply folded – commonly containing large cm-sized open cavities or enveloping pockets of sediment and/or glass fragments (Figure 42).

Figure 42. Photos of textures and morphologies of lavas recovered by *Alvin*. A). Inside surface of lobate crust (see Figure 43) showing a variety of needle-like lava drips, cusps and runnels. The surface is microvesicular and only slightly glassy. B). Side view of lobate crust (inside surface is facing upwards) showing drips (right side) and cavities that formed by lava-vapor interaction. C). Folded sheet flow recoved from the floor of a collapsed lobate flow showing an open cavity filled with sediment and glass shards. D). Typical glassy lava bud that was a decoration recovered from a larger pillow.

Some portions of hackly basalts appear to have been deformed (folded and brecciated) when the flow was in a semi-solid state so that sections of a sample exhibit cataclastic textures formed from the fracturing of quenched glass and other sections will show smooth, stretched glass that was folded while still in a semi-molten, plastic state. Angular fragments of glass enclosed within folds commonly appear to have been hydrated or at least devitrified and were welded together. It is unclear if these angular glass fragments were epiclastic, formed from the mechanical break up of glass crusts- possibly as the host lava was deforming, or if they were formed by some type of hydrovolcanic explosion prior to their incorporation in the hackly flow. The incorporation of sediments in open pockets and folds indicate there was significant accumulation of sediment on the seafloor prior to the eruption of the host lava suggesting these lavas flowed over older terrain (Figure 42C). The open pockets have a physical appearance very similar to the smooth and cuspate inner surfaces of sheet and lobate flows that formed by interaction with a vapor phase [Perfit et al., 2003].

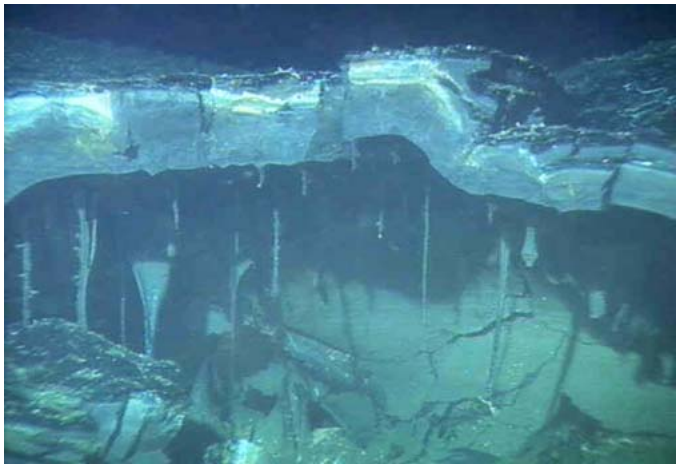

Figure 43. Lava drips on the underside of a lobate crust photographed on dive 3967. Crust thickness is ~7 cm, longest drips are ~12 cm.

Other textural/structural features that are very common on the lobate and sheet lavas we recovered are drips (Figure 43), flanges, ridges, bubble walls, and cuspate forms that exist on the inside (down-facing) surfaces of the flows (Figure 42A,B). All of these features are likely related to the interaction of lava with seawater creating vapor bubbles at near magmatic temperatures that accumulate below the quenched glassy crusts in lobate and sheet flows [Perfit et al. 2003]. It also appears that these vapor-filled pockets may get trapped in the folds of jumbled and hackly lavas to create elongate cavities and open tubes (Figure 43C). Although these features have previously been reported from this segment of the ridge [Engels et al., 2003], they appear to have been more frequently in this dive series compared to previous cruises. In part, this may have been because we were more aware of their existence and importance. Previous understanding of these vapor-related structures was hampered by only limited observation and documentation of their distribution on the seafloor. During this dive series we documented the presence of drip structures on the underside of a lobate flow just outside of the AST (Figure 43) and were able to recover a piece of this lobate crust (Figure 42A). The lava drips are as great as 4 cm in length. The image of the cavity *in situ* indicates these cavities can be more than 10 cm high and as much as a meter in diameter. This sample will be studied in detail to provide greater constraints on how and when such features form and what influence this process might have on the dynamics of lava flow and the chemistry of lavas.

Additional samples with drips and cusps were recovered during other dives. Most exist on the insides of lobate crusts and some suggest that differential vapor pressure may have influenced the direction of magma flow within the cavities (Figure 44) as there were places where it appeared that magma was being extruded from one cavity into another on a few samples. The undersides of these lavas typically have rough-textured, microvesicular surfaces that extend a few mm into the crystalline rock. Commonly this microcrystalline surface is transitional along horizontal surfaces to a thin, glassy layer with a waxy patina. Different types of drips were identified: some are cylindrically symmetrical, about 1 cm diameter base and 1-2 cm long whereas others that form on flanges or cusps have elliptical bases ~ 0.5 cm by 1.5 cm, 1-2 cm long (Figures 42, 43 and 45). Needle-like drips (0.4 cm diameter and up to 5 cm long) seem to form where one end of a cusp is detaching from the surface. All of these features attest to the fluidity of magma and dynamic nature of the vapor-lava interaction during eruptions.

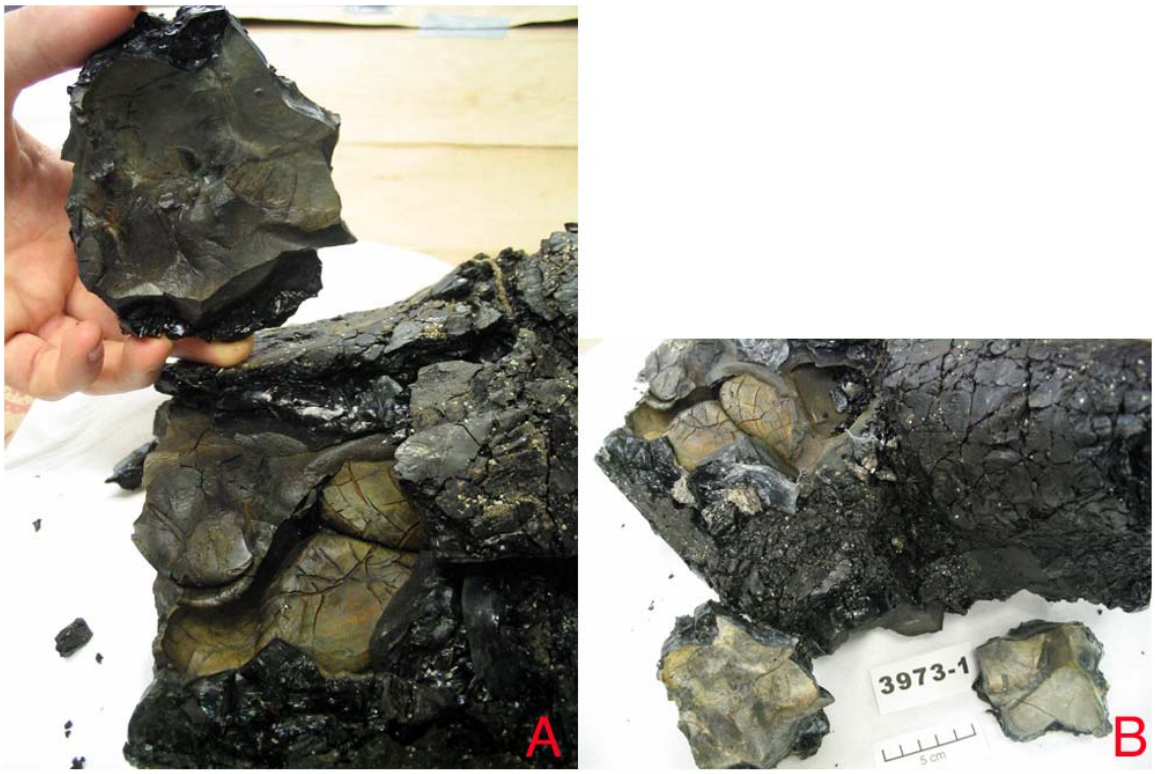

Figure 44. A. Upper surface of a folded to jumbled sheet flow recovered on Dive 3973. Just under the glassy outer crust is an open pocket that had lava intruded into it forming a lava bubble below the quenched crust at some time before the lava was entirely solidified. The piece being held in A. fits on to the top surface of the flow directly below it. B. Another view of the cavity found below the exterior surface. The inner surface has a waxy patina and only thin glass.

6.4.4. Petrography

Although we sampled a wide variety of lava types/morphologies that range from cm-thick sheet flows comprised almost entirely of glass to large pillows with thick, crystalline interiors, few samples contain more that a few percent phenocrysts (typically less than 1%). Crystallites and microphenocrysts of plagioclase are the most common phase followed by olivine and rare clinopyroxene (?) and spinel (?). Crystal clots of plagioclase ± olivine are

Figure 45. Dive 3967, sample #3 photographs showing details of drip structures and surface folds on interior of lobate lava crust and delicate, needle-like lava drip. A-B lobate crust in *Alvin's* basket; milk crate and wire mesh grid is ~2.5 cm squares. C- Mike Perfit holding the lobate crust sample upside down. Delicate needle-like drip is visible in middle of the sample. D-F- close up views of the needle-like drip on sample 3967-3.

relatively common (but << than 1% by volume) in some areas, as are trails of small plagioclase crystals. Some clots of plagioclase appear to contain vesicles and when they occur near glass, the glass seems to have been drawn down into the interstices between the crystals. Equally low crystal contents were detected in samples recovered from the proximal and distal ends of flows. This suggests that either the lavas did not cool sufficiently (or quenched too quickly) during emplacement to allow phenocrysts to form or that there is some efficient mechanism to separate crystals from liquid during flow.

Chemical analyses of what appear to be a single flow near 9° 43.3'N will provide some constraints on this problem. Given the great range in compositions that are known to occur in this region, and the dominant role of fractional crystallization in generating this compositional range (Perfit et al. 1994, Perfit and Chadwick, 1998, Smith et al., 2000, Perfit et al., in prep.), it seems incongruous that so few phenocrysts exist in these lavas. It points to a hypothesis that suggests cooling, crystallization and mixing are efficient in the subaxial magma chambers.

6.5. Vent Fluid Chemistry

6.5.1. Electrochemical Experiments

The overall object of the vent fluid study carried out on this cruise was to obtain in-situ chemical sensor measurements from low and high temperature hydrothermal fluids issuing from vents and seeps at 9° 50N' EPR (Figure 2). The electrochemical array in each of the chemical sensor packages developed at the University of Minnesota permits determination of pH, dissolved H_2 and dissolved H_2S, as well as temperature. In addition to direct measurements at vents using a sensor probe mounted on the *Alvin's* starboard manipulator (Figure 46A-D) that displays and records data in real-time to a laptop in the sphere, self-contained chemical data-logging instruments were used for the first time during this cruise to quantify short-term time series trends in vent fluid chemistry. Accordingly, three electrochemical units were deployed at vent sites for times between 3 and 13 days (Figure 46E-F).

The low-temperature deployments, involving two chemical/temperature data-loggers, were conducted at Tica vent (see Figure 2 for vent location and Figure 46e-f for instrument configuration) in collaboration with Tim Shank and Stace Beaulieu of WHOI. The Riftia patch at Tica is unusually robust, which likely relates to the pH and redox chemistry of the low-temperature diffuse-flow fluids. These fluids mix with seawater in the shallow subsurface, before migrating to the seafloor and supporting the biologic communities. åPreliminary data indicate pH approximately 0.5 units less than seawater. Sensor data at Tica also indicate dissolved H_2S concentrations of between 10 and 100 µmol/kg, depending on temperature and time. The mean value of dissolved H_2S is approximately 20 µm/kg- in excellent agreement with that actually measured using conventional approaches. To our knowledge, these data are the first of their kind. During the course of our study the low-temperature sensors were moved to different sites, retrieved and re-deployed by *Alvin*. The chemical sensors proved to be highly mobile and performed very well during all deployment intervals. Thus, a major objective of or research was accomplished.

Our research objectives were also focused on high-temperature deployments of robust in-situ sensor packages. Accordingly, one of the chemical data-loggers was deployed at P-vent for two five-day periods on two different occasions (retrieval and re-deployment) (Figure 46C). Temperature data indicate 366 ±2°C, while in-situ chemical data reveal a pH of 4.85. During both deployments, however, chimney growth above the sensor was on the order of ten inches, which is very significant considering the limited deployment time. These observations demonstrate that chemical sensors can be used at high temperatures for relatively long time intervals and still provide excellent temperature and chemical data. The concentric growth of the chimney around the sensor suggests that a sensor designed with multiple electrode arrays situated variable distances from the vent orifice may provide an effective means to investigate geochemical and microbial processes within the walls of actively growing chimney structures.

Consistent with our research objectives, we also sampled fluids from the instrumented vents using both major pairs and gas-tight samplers. The gas-tight samplers developed by Jeff Seewald at WHOI offered many advantages over the major water bottles in that they provided more accurate temperature control during sampling and allowed dissolved gases to be

determined immediately after each dive using a gas chromatograph. Shipboard knowledge of gas chemistry of vent fluid samples had a tangible effect on our in-situ sensor deployment strategy.

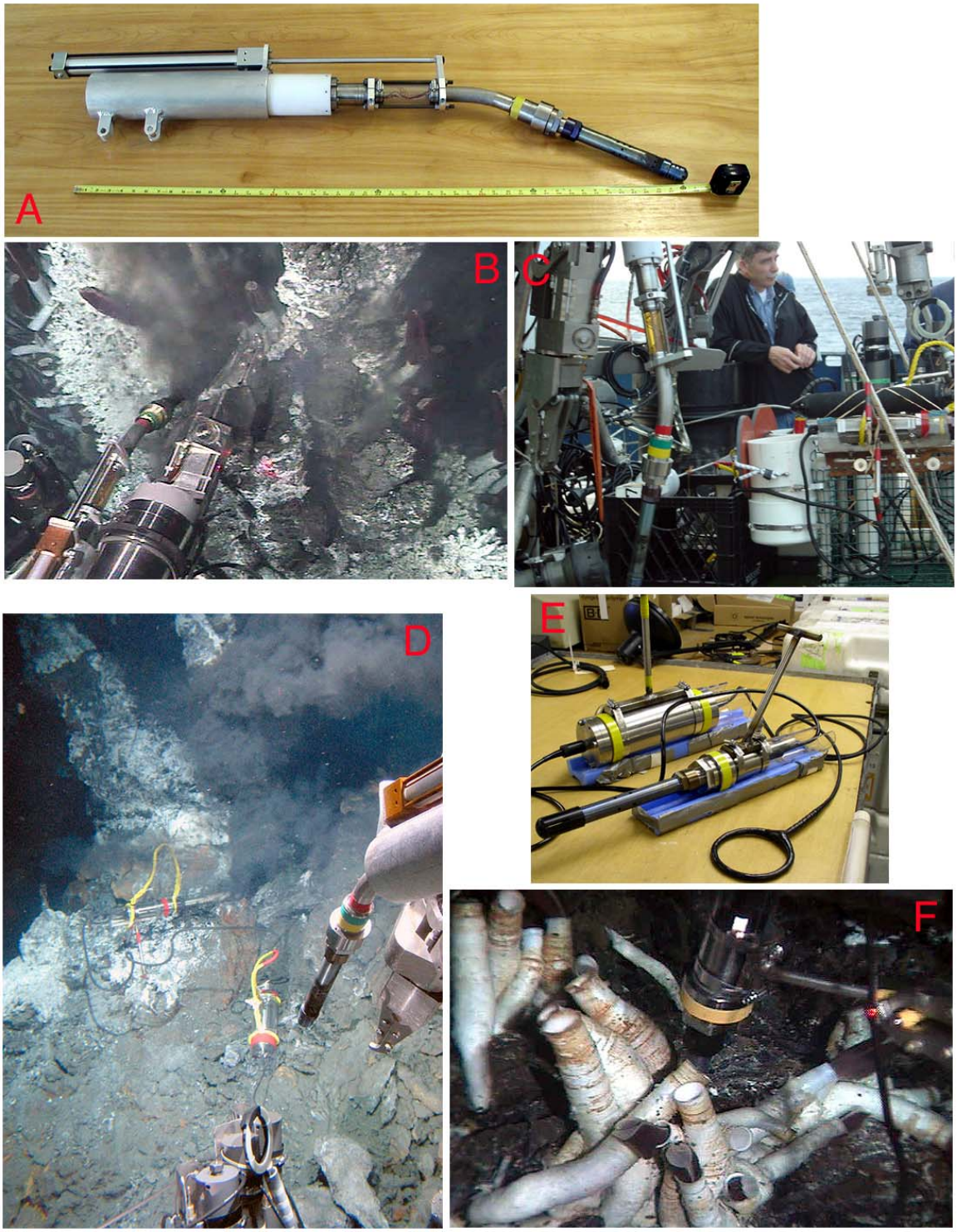

Figure 46. A- 'Ghostbuster' chemical probe showing hydraulic mount that fits on *Alvin's* starboard manipulator. B- Ghostbuster probe sampling at Tica vent. C- Bill Seyfried a *Alvin's* basket the Ghostbuster probe is at left on the starboard manipulator. D- The high-T self recording sensor as deployed at P vent; the Ghostbuster mounted on the starboard manipulator is at right. E- Off-load self

recording sensor package- low temperature model developed by the Univ. Minnesota group. F-Sampling with the low temperature off-load package in tubeworms at Bio9 vent.

Another objective involved sampling chimney material at the same vent sites at which in-situ sensors were deployed. Chimney mineralogy provides indirect, yet potentially useful information as a means of constraining redox and pH of coexisting vent fluids, especially involving phases (sulfides, oxides) that line the inner chimney wall and which are more closely linked in time and space to the actively vent fluids.

6.5.2. Abiotic Organic Synthesis in Basalt-hosted Hydrothermal Systems

Abiotic organic synthesis in basalt-hosted hydrothermal systems may have played a critical role in generating organic precursor compounds necessary to establish life on early Earth. In present day hydrothermal systems abiotic synthesis represents a potential source of organic compounds for organoheterotrophic microbes that rely on organic matter as a source of chemical energy and carbon. Despite the importance of organic matter to the creation and maintenance of life in unsedimented ridge-crest hydrothermal systems, little is known about the composition of and abundance of individual organic species present in vent fluids. The primary objective of this project was to collect high and low temperature hydrothermal fluids from the 9°50'N area of the EPR for organic chemical characterization. Samples will be used to identify organic species present and the development of appropriate analytical methodologies necessary for quantitative determination of abundances. Results of this study will provide data necessary for a preliminary assessment of the extent of abiotic organic processes in axial hot-springs.

Eight fluid samples were collected using isobaric gas-tight fluid samplers in addition to 14 samples collected using conventional major samplers. Sampling locations included high temperature focused flow from Bio9', Bio9", P, Q, and Tica vents and two low temperature diffuse flow in the vicinity of Bio9 and Tica (Figure 2). Samples collected in gas-tight samplers were analyzed onboard ship for the abundance of H_2, CH_4, CO, H_2S, and pH. A major accomplishment during the cruise was the development of an analytical procedure for the gas chromatographic determination of CO using a helium ionization detector. Aliquots of fluid were packaged in evacuated gas-tight containers for shore-based isotopic and chemical analyses of organic compounds. Fluid samples were also prepared for shore-based determination of inorganic species. The comprehensive analytical program used to characterize the organic, inorganic, and volatile chemistry of these fluids will allow thermodynamic and kinetic constraints to be placed on geochemical processes that regulate the generation and stability of organic species in ridge-crest hydrothermal systems.

6.6. Incubation Experiment - Microbiology of seafloor weathering

In order to assess the role of microbial activity in controlling the rates of seafloor weathering, samples were taken for geomicrobiological studies and in situ incubation chambers were deployed to examine the initial colonization of mineral surfaces by microorganisms.

6.6.1.Sampling

Seafloor samples were collected in discrete bio-boxes attached to *Alvin's* basket to avoid cross contamination and minimize exposure to surface sea water. Once on board, samples were wrapped in sterile aluminum foil and transferred to the laboratory. Sterile tools were used at all times to remove weathered surfaces from the rock samples. Sterile chisels and a mortar and pestle were used to break up large, coherent pieces of rock. Sterilization was achieved by spraying with ethanol and subsequent flaming, as well as autoclaving.

Samples were collected for DNA extractions in 2 ml sterile plastic vials and kept frozen at –70ºC and DNA extractions were performed as soon as possible using a MoBio Soil DNA Extraction Kit. Samples for geochemical studies were also frozen at –70ºC to inhibit alteration of $\delta^{56}Fe$ and $\delta^{18}O(PO_4)$ by microbial activity after sampling. Samples for shore-based fluorescent in situ hybridization microscopy (FISH) studies were fixed in 4% paraformaldehyde solution at room temperature for 4 hours, then rinsed with 1:1 phosphate-buffer-solution:ethanol (PBS-ethanol) several times and stored in PBS-ethanol at -20ºC.

The following enrichment cultures were started immediately following sampling: heterotrophic and autotrophic Fe-oxidizers in gradient tubes, heterotrophic and autotrophic micro-organisms in the presence of crushed EPR basalt glass and pyrite in 15 ml centrifuge tubes, heterotrophic Fe and S reducing micro-organisms in anaerobic serum bottles that were purged with N_2 gas after inoculation. The gradient tubes for culturing of Fe-oxidizing bacteria were designed to allow dissolved oxygen in solution to vary from atmosphere-saturated at the top to pyrrhotite-pyrite buffered at the interface with the FeS plug at the bottom. A list of the samples taken and cultures started during the cruise is reported in Appendix 9.4.

6.6.2. In situ incubation experiments

Polished slides of basalt glass, microcrystalline basalt, dunite, labradorite, hematite/pyrite, pyrite, marcasite, goethite, steel, Cu-coated steel, and window glass were deployed at the seafloor to examine bioalteration of minerals and biocorrosion of man-made materials (Figure 47). Four slides were attached to a perforated base plate in each basket using plastic crews. The baskets were labeled and brought to the seafloor in a bio box after sterilization in ethanol and soaking in Milli-Q water overnight. The bio box was filled with Milli-Q water and closed with a bungee cord to minimize contamination with surface seawater. Rock pebbles were used as a ballast to anchor the baskets on the seafloor. Some of the baskets will be recovered in November of 2004, while others will be left on the seafloor for several years. The locations of in situ incubation basket deployments and the arrangement of individual experiments are presented in Appendix 9.5.

A set of three baskets that was deployed near the *Riftia* patch at Tica vent during Dive 3961 was recovered after 13 days on the sea floor during Dive 3973. The slides did not show macroscopic oxidation or biofilm development; they were prepared and stored for shore-based DNA extraction and FISH analyses. Three baskets were left behind in an area of diffuse fluid discharge at Tica for recovery in November of 2004.

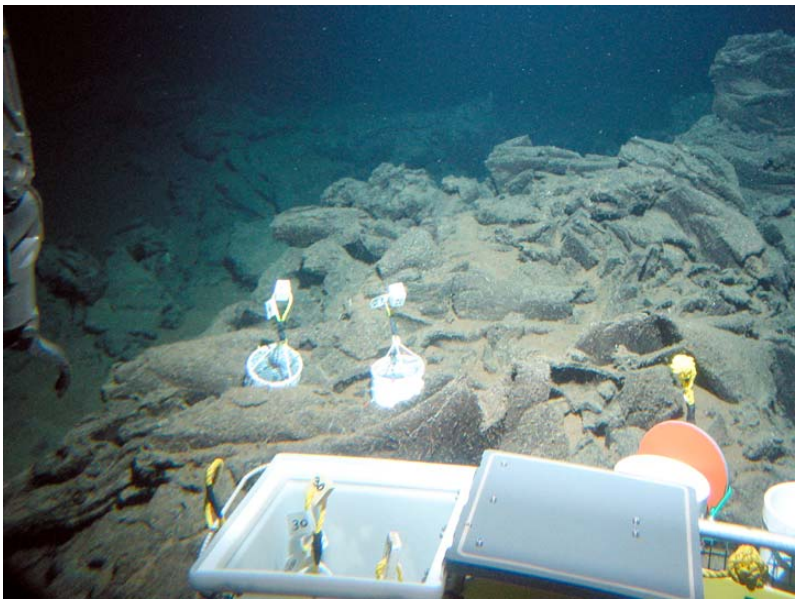

Figure 47. Photograph of deployment of one of the incubation experiments.

6.7. In situ Basalt Colonization Panel Experiment

The goal of this collaborative project (Tim Shank, Stefan Sievert, and Stace Beaulieu, all at WHOI, are the PIs of this experiment) was to gain insights into how hydrothermal fluid chemistry and microbial bio-films affect larval settlement on basalt substrates. Beaulieu was assisted in the field work by R. Waller. This project examines the first step in larval recruitment, and the ultimate development of megafaunal assemblages at vent sites. Our objective was to understand the biological/geochemical interactions during initial colonization of basalts at Tica Vent, and by analogy other vents at 9º 50'N, EPR (Figure 2). The specific approach for this cruise was to undertake a pilot study of microbial and invertebrate species colonization in conjunction with co-located, time-series detection of dissolved H_2, H_2S, pH, and temperature. We designed our experiment in conjunction with the time-series deployment of Seyfried and Ding's low-temperature chemical sensor data-loggers in a tubeworm (*Riftia* sp.) patch at Tica Vent. The general methods included deploying and recovering three sets of basalt settlement panels in close proximity to the chemical sensors for 4 to 13 day periods, examining recovered panels under a dissecting microscope to locate invertebrate colonists. Panels were also frozen (-70ºC) for the shore-based determination of microbial diversity, via 16S rDNA. A summary of activities related to this experiment follows.

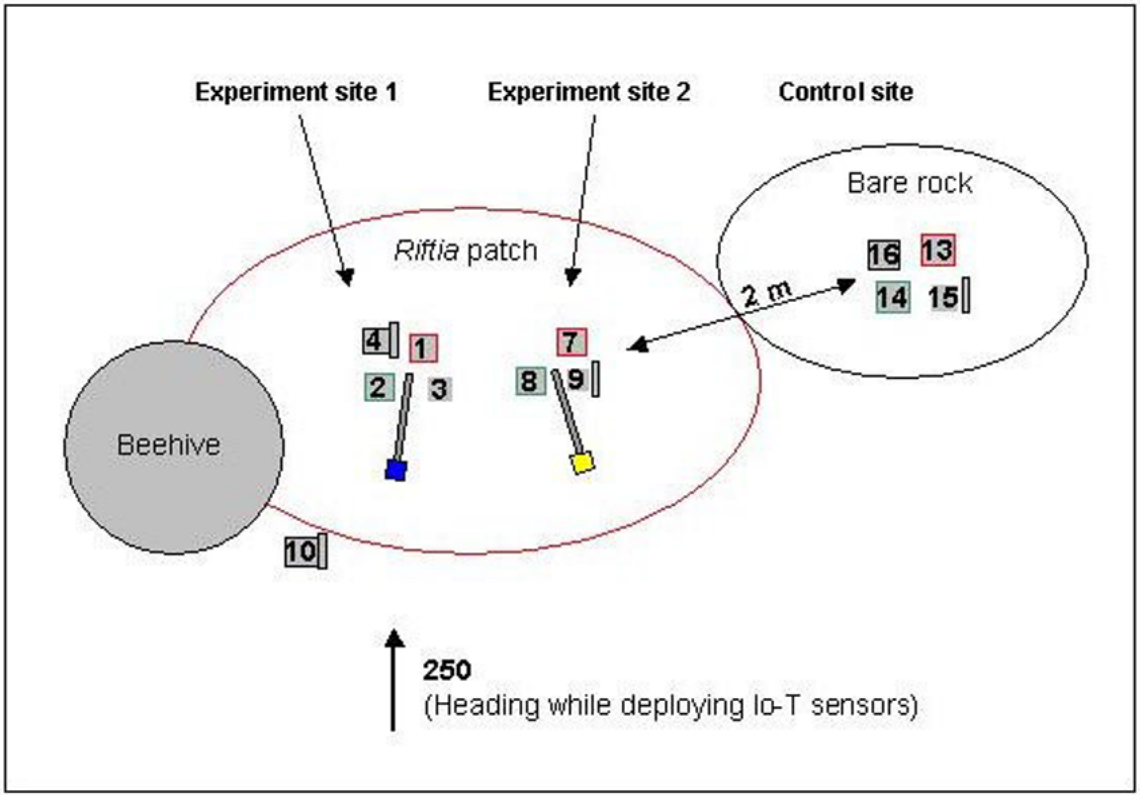

Figure 48 – Diagram showing the positions of basalt colonization panels, and Seyfried chemical sensors, within Tica Vent.

Dive 3961

Experiment deployment: We deployed 4 basalt panels at each of three sites-- two 'experiment' sites in a low-temperature vent and one 'control' site in a non-venting area (Figures 48-49). Four of the panels had VEMCO temperature sensors attached to the side. Both experiment sites 1 and 2 were clustered in the same *Riftia* patch, next to Seyfried's blue and yellow chemical sensors, respectively. The chemical sensors were approximately 0.5m apart. The control site (called the 'bare rock' site) was approximately 2m from the experiment sites. Fig. 2 shows the panels at experiment site 1 clustered around the blue chemical sensor. Panel #10 was accidentally hooked on the *Alvin* basket and dragged approximately 2m from its initial position.

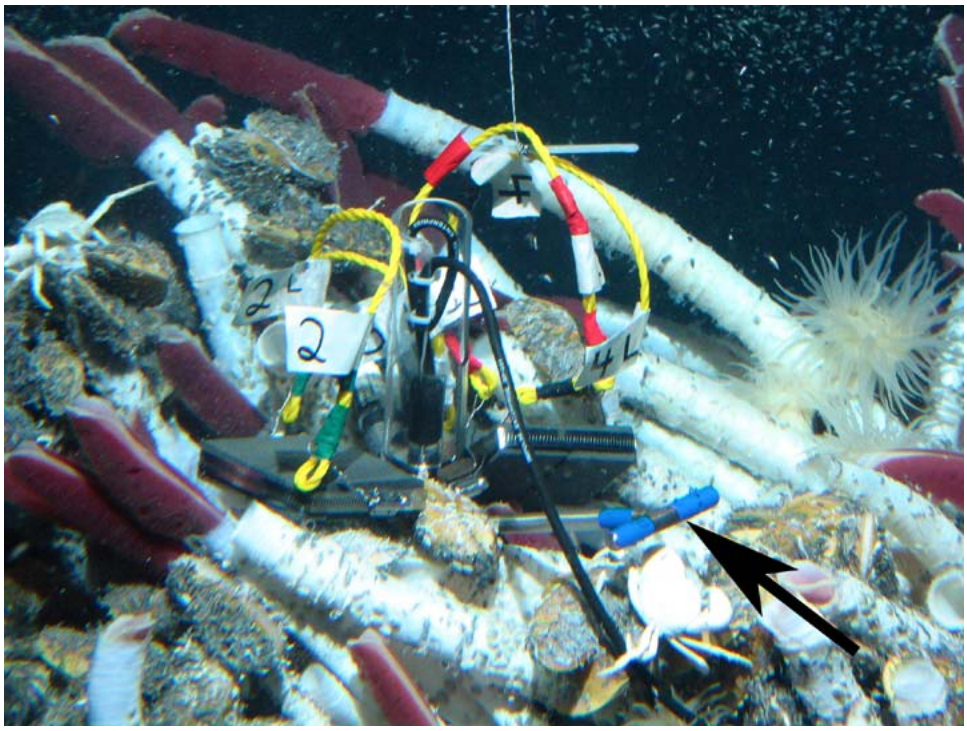

Figure 49. Digital still photograph of experiment site 1. Blue T-handle that can be seen in the center (shown by arrow) shows the location of the blue Seyfried chemical sensor

Dive 3964 (4 days later)
1st recovery and exchange of panels: During this dive, we recovered one panel from each of the three sites, and replaced these with a new panel. We measured the temperature near several panels at the control site and found no difference from ambient water. The yellow chemical sensor was also recovered on this dive.

Dive 3972 (12 days from start of experiment)
Re-positioned Panel #10: During this dive, Panel #10 was found and re-positioned to experiment site 1 (intended for experiment site 2). The blue chemical sensor was also recovered.

Dive 3973 (13 days from start of experiment)
2nd recovery and exchange of panels: We recovered two panels from each of the three sites, and deployed one new panel at each experiment site. Two of the recovered panels had VEMCO temperature sensors. The VEMCO from experiment site 1 had temperatures ranging from ambient to approximately 10ºC, while the VEMCO from the control site appeared to be at ambient 2ºC.

Overall, we collected 9 panels during this cruise (3 deployed for 4 days, 3 deployed for 9 days, and 3 deployed for 13 days). For each time period, we collected one panel from each site. We were not able to obtain a 3 x 4-day time series of panels from each site due to time constraints on Dive 3969. To the naked eye, most of the panels looked relatively bare. However, three of the panels had considerable 'bio-scum', marked with what appear to be limpet feeding tracks. Under the dissecting microscope, we took ~200 photographs of 'scum' patches, filaments and fuzz that appear to be microbial (Figure 50), as well as protozoan and

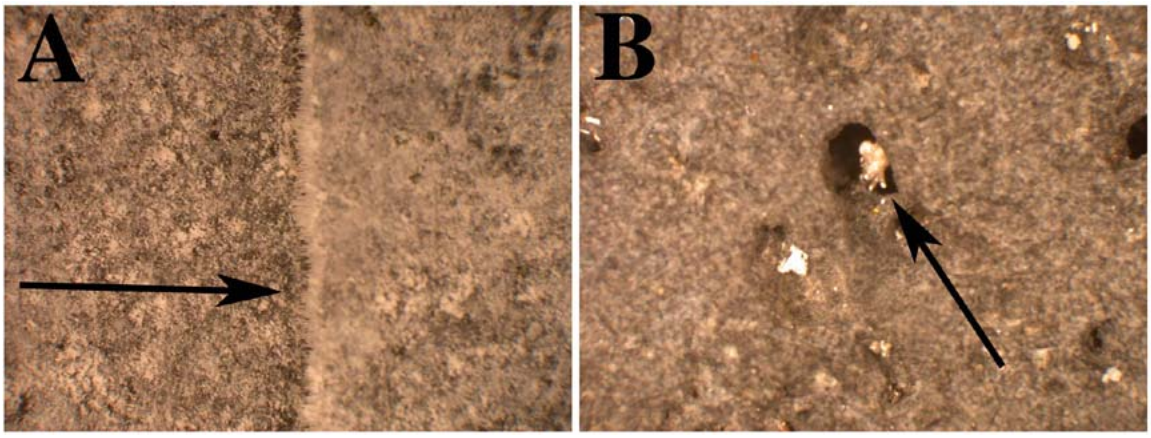

Figure 50. – A, Photograph taken under the microscope of 'bio-film' (shown by arrow) found on the basalt panels on recovery (magnification x200); B, Photograph of an ampharetid polychaete (shown by arrow) found within the pores of a basalt panel recovered (magnification x200).

metazoan colonists. The most abundant recognizable colonists appeared to be ampharetid polychaetes, often found deep in the tiny pores in the basalt panel surface (Figure 50). In addition to the small colonists that were frozen in sterile tubes for molecular identification, we collected many types of invertebrates from the biotube (weeble) washings (see AT11-7 SHANK FAUNA spreadsheet in Appendix 9.5). Many limpets and gastropods were associated with the panels, and amphipods were also found within the biotubes. Most of the basalt 'bricks' that were used to create the panels were frozen at –70ºC for microbial DNA analysis back at the laboratory. Also, for four of the panels, 1" bricks were preserved in glutaraldehyde for scanning electron microscopy back at the laboratory. Several panels were left in place to be collected by Shank in April 2004 (AT11-10) including: 4 at Experiment Site 1 (2 with syntactic floats), 2 at Experiment Site 2, and 2 at Control Site (near Marker UM1).

7. Acknowledgements

Our thanks to the *Alvin* pilots and at-sea operations group of the National Deep Submergence Facility at WHOI, and the shore based NDSF staff, and officers and crew of R/V Atlantis for their dedication and support of our field work. We also thank the WHOI Marine Operations office for logistical support. M. Swartz, S. Liberatore and A. Billings provided exceptional pre-cruise support for the TowCam system. P. Fucile's efforts at building the self recording magnetometer for the TowCam are greatly appreciated and resulted in a key data set. The science party of AT11-7 was one of the best we have ever sailed with and their dedication, expertise and good spirits made the cruise extremely productive and enjoyable.

8. References

Carbotte, S., and K.C. Macdonald, East Pacific Rise 8 degrees -10 degrees 30'N; evolution of ridge segments and discontinuities from SeaMarc II and three-dimensional magnetic studies, *J. Geophys. Res.*, 97, 6959-6982, 1992.

Chadwick, W., Gregg, T. and Embley, R., Submarine lineated sheet flows: a unique lava morphology formed on subsiding lava ponds. *Bulletin of Volcanology*, 61: 194-206, 1999.

Christeson, G.L., G.M. Kent, G.M. Purdy and R.S. Detrick, Extrusive thickness variability at the East Pacific Rise, 9° -10°N: Constraints from seismic techniques, *J. Geophys. Res.* 101, 2859-2873, 1996.

Christeson, G. L., G. M. Purdy, and G. J. Fryer, Seismic constraints on shallow crustal emplacement processes at the fast spreading East Pacific Rise, *J. Geophys. Res.* 99, 17,957-17,974, 1994a.

Christeson, G. L., W.S.D. Wilcock, and G.M. Purdy, , The shallow attenuation structure of the fast spreading East Pacific Rise near 9°30'N, *Geophys. Res. Lett.* 21, 321-324, 1994b.

Cochran, J. R., D. J. Fornari, B. J. Coakley, R. Herr, and M. A. Tivey, Continuous near-bottom gravity measurements made with a BGM-3 gravimeter in DSV *Alvin* on the East Pacific Rise crest near 9°30'N and 9°50'N, *J. Geophys. Res.,* 104, 10841-10861, 1999.

Cormier, M.H. et al., Waxing and waning volcanism along the East Pacific Rise on a millennium time scale. *Geology*, 31(7): 633-636, 2003.

Crawford, W.C., and S.C. Webb, Variations in the distribution of magma in the lower crust and at the Moho beneath the East Pacific Rise at 9°-10°N, *Earth and Planet. Sci. Lett.*, *203*, 117-130, 2002.

Detrick, R.S., P. Buhl, E.E. Vera, J.C. Mutter, J.A. Orcutt, J.A. Madsen, and T.M. Brocher, Multi-channel seismic imaging of a crustal magma chamber along the East Pacific Rise, *Nature (London)*, *326* (6108), 35-41, 1987.

Engels, J.L., M.H. Edwards, D. J. Fornari, M. R. Perfit, J. R. Cann, A new model for submarine volcanic collapse formation, G^3, 4, 1077, paper number 2002GC000483, 2003.

Edwards, K.J., McCollom, T.M., Konishi, H. and Buseck, P.R., Seafloor bioalteration of sulfide minerals: results from in situ incubation studies. *Geochimica et Cosmochimica Acta*, 67(15): 2843-2856, 2003.

Fink, J.H. and G., Ross W., Radial spreading of viscous-gravity currents with solidifying crust. *J. of Fluid Mechanics*, 221: 485-509, 1990.

Fornari, D.J., Haymon, R. M., Perfit, M. R., Gregg, T.K.P., Edwards, M. H., Geological Characteristics and Evolution of the Axial Zone on Fast Spreading Mid-Ocean Ridges: Formation of an Axial Summit Trough along the East Pacific Rise, 9°-10° N, *J. Geophys. Res.,* 103, 9827-9855, 1998a.

Fornari, D.J., T. Shank, K.L. Von Damm, T.K.P. Gregg, M. Lilley, G. Levai, A. Bray, R.M. Haymon, M.R. Perfit and R. Lutz, Time-Series Temperature Measurements at High-Temperature Hydrothermal Vents, East Pacific Rise 9° 49'-51'N: Monitoring a Crustal Cracking Event, *Earth Planet. Sci. Lett., 160, 419-431, 1998*b.

Fornari, D.J., M. Perfit, M. Tolstoy, D. Scheirer and Science Party, *AHA-Nemo2 Cruise Report* cruise data web site: http://science.whoi.edu/ahanemo2, 2001.

Fornari, D.J., A new deep-sea towed digital camera and multi-rock coring system, *EOS*, 84, 69&73, 2003.

Fornari, D.J, M. Tivey, H. Schouten, D. Yoerger, A. Bradley, M. R. Perfit, D. Scheirer, P. Johnson, K. Von Damm, R. Haymon, M. H. Edwards, Submarine Lava Flow Emplacement Processes: Implications for Fluid Circulation in the Upper Ocean Crust, *AGU Monograph; Thermal Structure of the Oceanic Crust & Dynamics of Hydrothermal Circulation*: eds. C.R. German, J. Lin and L.M. Parson, (in press), 2004.

Gregg, T.K. and Chadwick, W.W., Submarine lava flow inflation: a model for the formation of lava pillars. *Geology*, 24: 981-984, 1996.

Gregg, T.K.P., Fornari, D.J., Perfit,M.R., Haymon, R.M., and Fink, J.H., Rapid Emplacement of a Mid-Ocean Ridge Lava Flow: The East Pacific Rise at 9° 46'-51'N, *Earth Planet. Sci. Express Lett.*, *144*:, E1-E7, 1996.

Gregg, T.K.P., and J.H. Fink Quantification of submarine lava-flow morphology through analog experiments. *Geology* **23,** 73-76, 1995.

Gregg, T.K.P., D. J. Fornari, M.R. Perfit, W. I. Ridley and M.D. Kurz, Using submarine lava pillars to record mid-ocean ridge eruption dynamics, *Earth Planet. Sci. Lett*., 178, 195-214, 2000.

Gee, J., and D.V. Kent, Variations in layer 2A thickness and the origin of the central anomaly magnetic high, *Geophys. Res. Lett.,* 21, 297-300, 1994.

Guyodo, Y., and J.-P. Valet, Global changes in intensity of the Earth's magnetic field during the past 800 kyr, *Nature*, 399, 249-252, 1999.

Harding, A.J., G.M. Kent, and J.A. Orcutt, A multichannel seismic investigation of upper crustal structure at 9 degrees N on the East Pacific Rise; implications for crustal accretion, *J. Geophys. Res.*, *98*, 13,925-13,944, 1993.

Haymon, R.M., D.J. Fornari, K.L. Von Damm, M.D. Lilley, M.R. Perfit, and J.M. Edmond JM, Volcanic eruption of the mid-ocean ridge along the East Pacific Rise crest at 9 degree 45-52'N:

Direct submersible observations of seafloor phenomena associated with an eruption event in April, 1991. *Earth Planet. Sci. Lett.*, 119, 85-101, 1993.

Haymon, R.M., D.J. Fornari, M.H. Edwards, S. Carbotte, D. Wright and K.C. Macdonald, Hydrothermal vent distribution along the East Pacific Rise crest (9°09'-54'N) and its relationship to magmatic and tectonic processes on fast-spreading mid-ocean ridges, *Earth Planet. Sci. Lett,*. 104, 513-534, 1991.

Hooft, E.E., Schouten, H. and Detrick, R.S., Constraining crustal emplacement processes from the variation in seismic layer 2A thickness at the East Pacific Rise. *Earth and Planetary Sci. Lett.*, 142(3-4): 289-309, 1996.

Isezaki, N., A new shipboard three component magnetometer, *Geophys*., 51, 1,992-1,998, 1986.

Kent, G.M., A.J. Harding, and J.A. Orcutt, Evidence for a smaller magma chamber benearth the East Pacific Rise at 9°30'N, *Nature*, *412*, 145-149, 1990.

Kent, G.M., A.J. Harding, and J.A. Orcutt, Distribution of magma beneath the East Pacific Rise between the Clipperton Transform and the 9 degrees 17'N Deval from forward modeling of common depth point data, *J. Geophy. Res.*, *98*, 13,945-13,969, 1993a.

Kent, G.M., A.J. Harding, and J.A. Orcutt, Distribution of magma beneath the East Pacific Rise near the 9 degrees 03'N overlapping spreading center from forward modeling of common depth point data, *J. Geophy. Res., 98*, 13,971-13,995, 1993b.

Korenaga, J., Comprehensive analysis of marine magnetic vector anomalies, *J. Geophys. Res.,* 100 (B1), 365-378, 1995.

Kilburn, C.R., Pahoehoe and aa lavas: a discussion and continuation of the model of Peterson and Tilling. *J. of Volcan. and Geothermal Res.,* v. 11: p. 373-382, 1981.

Klitgord, K.D., S.P. Huestis, J.D. Mudie, and R.L. Parker, An analysis of near-bottom magnetic anomalies: Seafloor spreading and the magnetized layer, *Geophys. J. R. astr. Soc.,* 43, 387-424, 1975.

Klitgord, K.D., Sea-floor spreading: The central anomaly magnetization high, *Earth Planet. Sci. Lett.*, 29, 201-209, 1976.

Kurras, G., D.J. Fornari and M.H. Edwards, Volcanic morphology of the East Pacific Rise crest 9°49'-52'N: Implications for extrusion at fast spreading mid-ocean ridges, *Mar. Geophys. Res*., 21, 23-41, 2000.

Langmuir, C.H., J.F. Bender and R. Batiza, Petrologic and tectonic segmentation of the East Pacific Rise, 5°30'-14°30'N, *Nature*, *322,* 422-429, 1986.

Lee, S.-M., S.C. Solomon, M.A. Tivey, , Fine-scale crustal magnetization anomalies and segmentation of the East Pacific rise, 9°10'-9°50'N, *J. Geophys. Res.,* 101, 22,033-22,050, 1996.

Macdonald, K., J.-C. Sempere, and P.J. Fox, East Pacific Rise from Siqueiros to Orozco fracture zones; along-strike continuity of axial neovolcanic zone and structure and evolution of overlapping spreading centers, *J. Geophy. Res. 89*, 6049-6069, 1984.

Macdonald, K.C., P.J. Fox, S. Miller, S. Carbotte, M.H. Edwards, M. Eisen, D.J. Fornari, L. Perram, R. Pockalny, D. Scheirer, S. Tighe, C. Weiland and D. Wilson, The East Pacific Rise and its flanks 8-18°N: History of segmentation, propagation and spreading direction based on SeaMARC II and Sea Beam studies, *Mar. Geophys. Res.*, 14, 299-344, 1992.

Oosting, S.E. and K.L. von Damm, Bromide/chloride fractionation in seafloor hydrothermal fluids from 9-10°N East Pacific Rise, *Earth Planet. Sci. Lett.,* 144, 133-145, 1996.

Perfit, M.R., Fornari, D.J., Smith, M., Bender, J., Langmuir, C.H., Haymon, R.M., Across-axis spatial and temporal diversity of MORB on the crest of the East Pacific Rise between 9°30'-9°32'N, *Geology*, 22, 375-379, 1994.

Perfit, M.R., J.R. Cann, D.J. Fornari, J Engels, D.K. Smith, W.I. Ridley, M.H. Edwards Seawater-lava interaction during submarine eruptions at mid-ocean ridges, *Nature*, 426, 62-65, 2003.

Perfit, M.R, D.J. Fornari, W.I. Ridley, J.C. Maclennan, and K. Sims, High resolution geochemical and volcanological investigations of the East Pacific Rise (EPR) at 9°-10° N, EGS/AGU/EUG Joint Meeting, Nice, France, abstract EAE03-A-07269, 2003.

Perfit, M.R. and W.C. Chadwick, Magmatism at mid-ocean ridges: Constraints from volcanological and geochemical investigations, in: Faulting and magmatism at mid-ocean ridges, W.R. Buck, et al. (eds.), *Am. Geophys. U. Geophys. Monograph* 106, 59-116, 1998.

Peterson, D.W. and Tilling, R.I., Transition of basaltic lava from pahoehoe to a'a, Kilauea Volcano Hawaii: field observations and key factors. In: A.R. McBirney (Editor), *J. of Volcan. and Geothermal Res*. Gordon A. Macdonald Memorial Volume (special issue), pp. p. 271 -293. 1980.

Pockalny, R. A., P. J. Fox, D. J. Fornari, K. C. Macdonald, and M. R. Perfit, Tectonic reconstruction of the Clipperton and Siqueiros Fracture zones: Evidence and consequences of plate motion change for the last 3 Myr, *J. Geophys. Res.*, 102, 3167-3182, 1997.

Scheirer, D. S., D. J. Fornari, S.E. Humphris, and S. Lerner, High-Resolution Seafloor Mapping Using the DSL-120 Sonar System: Quantitative Assessment of Sidescan and Phase-Bathymetry Data from the Lucky Strike Segment of the Mid-Atlantic Ridge, *Mar. Geophys. Res*. 21, 121-142, 2000.

Schouten, H., M. Tivey, D. Fornari, D. Yoerger, A. Bradley, P. Johnson, M. Edwards, and T. Kurokawa, Lava Transport and Accumulation Processes on EPR 9 27'N to 10N: Interpretations Based on Recent Near-Bottom Sonar Imaging and Seafloor Observations Using ABE, *Alvin* and a new Digital Deep Sea Camera, *Eos Trans. AGU, 83(47),* Fall Meet. Suppl., Abstract T11C-1262, 2002.

Schouten, H., M.A. Tivey, D.J. Fornari, and J.R. Cochran, Central Anomaly Magnetization High: Constraints on the volcanic construction and architecture of seismic layer 2A at a fast-spreading Mid-Ocean Ridge, the EPR at 9˚30'-50'N, *Earth Planet. Sci. Lett.*, *169*, 37-50, 1999.

Shank, T.M., D.J. Fornari, K.L. Von Damm, M.D. Lilley, R.M. Haymon and R.A. Lutz, Temporal and spatial patterns of biological community development at nascent deep-sea hydrothermal vents along the East Pacific Rise, *Deep Sea Res. II* 45, 465-515, 1998.

Sims, K.E. et al., Aberrant youth: Chemical and isotopic constraints on the origin of off-axis lavas from the East Pacific Rise, 9˚-10˚ N. Geochemistry Geophysics Geosystems, 4(10): 27, 2003.

Sinton, J. et al., Volcanic eruptions on mid-ocean ridges: New evidence from the superfast spreading East Pacific Rise 17˚-19˚S. *J. Geophys. Res.,* 107(B6): 21, 2002.

Sohn R., D.J. Fornari, K.L. Von Damm, S. Webb, and J. Hildebrand, Seismic and hydrothermal evidence for a propagating cracking event on the East Pacific Rise crest at 9° 50'N, *Nature*, 396, 159-161, 1998.

Smith, M., M.R. Perfit, D.J. Fornari, W. Ridley, I., M.H. Edwards, G. Kurras, and K.L. Von Damm, Segmentation and Magmatic Processes at a Fast Spreading Mid-Ocean Ridge: Detailed Geochemistry and Mapping of the East Pacific Rise Crest at the 9° 37'N OSC, G^3, 2, paper #2000GC000134, 2001.

Soule, S.A., Cashman, K.V. and Kauahikaua, J.P., Examining flow emplacement through the surface morphology of three rapidly emplaced, solidified lava flows, Kilauea Volcano, Hawaii. *Bull. Volcan.,* 66: 1-14, 2004.

Tivey, M.A., The central anomaly magnetic high: Its source and implications for ocean crust construction and evolution, Ph.D. Thesis, School of Oceanography, University of Washington, Seattle, WA, pp. 131, 1988.

Tivey, M.A., A. Bradley, D. Yoerger, R. Catanach, A. Duester, S. Liberatore and H. Singh, Autonomous underwater vehicle maps seafloor, *EOS*, 78, 229-230, 1997.

Tivey, M.A., H.P. Johnson, A. Bradley, and D. Yoerger, Thickness measurements of submarine lava flows determined from near-bottom magnetic field mapping by autonomous underwater vehicle *Geophys. Res. Lett*., 25, 805-808, 1998.

Toomey, D.R., S.C. Solomon, and G.M. Purdy, Tomographic imaging of the shallow crustal structure of the East Pacific Rise at 9º30'N, *J. Geophy. Res*, *99*, 24,135-24,157, 1994.

Von Damm, K.L., S.E. Oosting, R. Kozlowski, L.G. Buttermore, D.C. Colodner, H.N. Edmonds, J.M. Edmond, and J.M. Grebmeier, Evolution of East Pacific Rise hydrothermal vent fluids following a volcanic eruption, *Nature, 375,* 47-50, 1995.

Von Damm KL, Buttermore LG, Oosting SE, Bray AM, Fornari DJ, Lilley MD, et al., Direct observation of the evolution of a seafloor 'black smoker' from vapor to brine. *Earth Planet. Sci. Lett.*, 149, 101-111, 1997.

Von Damm, K.L., Chemistry of hydrothermal vent fluids from 9-10°N, East Pacific Rise: "Time zero" the immediate post-eruptive period, *J. Geophys. Res.* 105, 11203-11222, 2000.

Von Damm, K.L., and M.D. Lilley, Diffuse Flow Hydrothermal Fluids from 9º50'N East Pacific Rise: Origin, Evolution, and Biogeochemical Controls, in: The Subsurface Biosphere at Mid-Ocean Ridges (AGU monograph -RIDGE Theoretical Institute), 2003.

Whitcomb, L.L., and J.C. Kinsey, DVLNAV homepage – An Integrated Interactive Navigation Program for Remotely Operated Underwater Vehicles and Inhabited Submersibles, http://robotics.me.jhu.edu/~llw/dvlnav/, 2002.

White S. M., R.M. Haymon, D.J. Fornari, K. C. Macdonald, and M.R. Perfit, Volcanic Structures and Lava Morphology of the East Pacific Rise, 9°-10°N: Constraints on Volcanic Segmentation and Eruptive Processes at Fast-Spreading Ridges, *Jour. Geophys. Res.,* 107, 10,1029, 2001JB000571, 2002.

Wright, D.J., Haymon, R.M., and D.J. Fornari, Crustal fissuring and its relationship to magmatic and hydrothermal processes on the East Pacific Rise crest (9°12'-54'N), *J. Geophys. Res.*, 100, 6097-6120, 1995a.

Wright, D.J., Haymon, R.M., and K.C. Macdonald, Breaking new ground: Estimates of crack depth along the axial zone of the East pacific Rise (9° 12-54'N), *Earth Planet. Sci. Lett.*, 134, 441-457, 1995b.

Wright, D.J., Formation and development of fissures at the East pacific Rise: Implications for faulting and magmatism at Mid-Ocean ridges, in: Faulting and magmatism at mid-ocean ridges, W.R. Buck, et al. (eds.), *Am. Geophys. U. Geophys. Monograph* 106, 137-151, 1998.

Yoerger, D., A. Bradley, R. Bachmayer, R. Catanach, A. Duester, S. Liberatore, H. Singh, B. Walden and M.A. Tivey, Near-bottom magnetic surveys of the Coaxial Ridge segment using the Autonomous Benthic Explorer survey vehicle, *RIDGE Events*, 7, 5-9, 1996.

Zhou, W., R. van der Voo, D.R. Peacor, D. Wang, and Y. Zhang, Low-temperature oxidation in MORB of titanomagnetite to titanomaghemite: A gradual process with implications for marine magnetic anomaly amplitudes, *J. Geophys. Res.,* 106 (B4), 6409-6421, 2001.

AT11-7 CRUISE REPORT

APPENDICES